A novel reduced-complexity approach for modelling ebullition in peatlands

Jorge Alberto Ramirez

Submitted in accordance with the requirements for the degree of
Doctor of Philosophy

The University of Leeds
School of Geography

September, 2013

The candidate confirms that the work submitted is his own and that appropriate credit has been given where reference has been made to the work of others.

Acknowledgements

I would like to thank the University of Leeds department of geography for waiving my tuition fee. I would like to thank supervisors, Andy Baird, Tom Coulthard, Mike Kirkby and Mike Waddington for their advice and feedback. Additionally I would like to thank the members of my RSG panel for their input.

I would like to thank my parents and my family for their moral support. Lastly and most importantly, I would like to thank my wife Chiara for her tremendous help, support and patience.

Abstract

Methane (CH_4) is a greenhouse gas with a global warming potential much greater than carbon dioxide, and one of the major sources of naturally occurring CH_4 are peatlands. Large amounts of CH_4 can be transported from peat to the atmosphere through bubbles (ebullition). The exact controls of ebullition remain uncertain, but evidence suggests that physical processes related to gas transport and storage within the peat structure is important. Although these processes are key to replicating ebullition, no computer models of ebullition contain a detailed spatial representation of the peat structure.

This thesis investigated the role of peat structure on CH_4 ebullition using computer and physical models. A computer model of ebullition was developed and tested against physical models of ebullition. The computer model contained a spatial representation of peat and rules to transport gas through the peat structure. Physical models consisted of i.) air injected into a simple porous medium, and ii.) a separate physical model with peat. Following a pattern oriented modelling approach, gas storage, bubble size, and bubble release (ebullition) were three patterns used to test the computer model. Overall the computer model was able to replicate the patterns generated from the physical models and this demonstrated that the computer model was useful for modelling CH_4 ebullition from peat. The results generated with the computer model confirmed our hypothesis: peat structure and subsequent gas storage were found to be important controls on ebullition timing location and quantity. From these results, we were able to make recommendations on sampling CH_4 ebullition from peat in the field.

Table of Contents

List of Tables

List of Figures

Chapter 1 Introduction

1.1. Background

Methane (CH_4) is a powerful greenhouse gas that has a global warming potential (GWP) 25 times more than carbon dioxide (CO_2) over a 100 year time-horizon [*Forster et al.*, 2007]. In the past 400,000 years quantities of atmospheric CH_4 have oscillated in tandem with warm and cold periods [*Chappellaz et al.*, 1993]. During cooler climates, atmospheric CH_4 concentrations have reached minimums of ~350 parts per billion (ppb), and doubled to ~700 ppb during warmer climates (Figure 1) [*Chappellaz et al.*, 1993; *Petit et al.*, 1999]. From preindustrial times (1700s) to the present day, CH_4 concentrations have increased 1000 ppb, representing the fastest change in 80,000 years [*Anderson et al.*, 2010], and reaching a 2009 value of ~1800 ppb [*Dlugokencky et al.*, 2009]. Most of the recent increase in atmospheric CH_4 can be traced back to anthropogenic sources, and ~40% have natural origins [*Heimann*, 2010], but much uncertainty exists over contributions by natural sources, with a growing number of studies finding sources previously underestimated or completely unaccounted for [*DelSontro et al.*, 2010; *Keppler et al.*, 2006; *Mastepanov et al.*, 2008; *Shakhova et al.*, 2010; *Solomon et al.*, 2009]. Moreover, it is not clear how natural sources of CH_4 will respond to climate change, but it is probable that some natural sources will produce a positive feedback on climate, whereby increasing temperatures cause the emission of more CH_4 [*Cao et al.*, 1996; *Davidson and Janssens*, 2006; *Isaksen et al.*, 2011; *Walter et al.*, 2006]. Thus, it is necessary to quantify future trends in CH_4 emissions from natural sources to reduce the uncertainty in climate predictions generated by

climate models that consider greenhouse gas feedbacks [*Gedney et al.*, 2004; *Torn and Harte*, 2006].

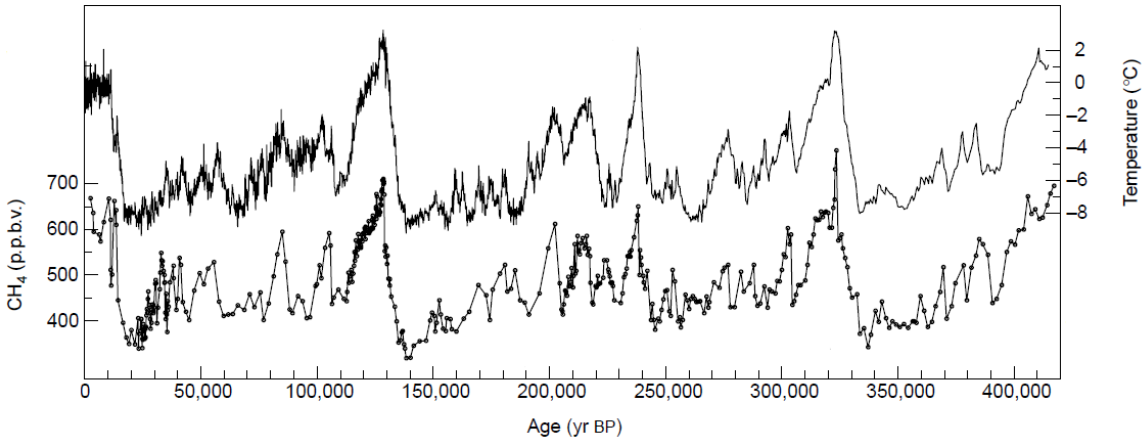

Figure 1. Vostok ice core time series.

Surface temperature changes from present temperature (black line), and atmospheric CH_4 concentrations (black line with circles) (taken from *Petit et al.* [1999]).

A major, naturally-occurring, source of CH_4 is peatlands [*Matthews and Fung*, 1987]. Peat is the accumulation of slowly decomposing plant and animal material that is mostly saturated with water. Peatlands are found throughout the world, but the majority of peat is found in the northern hemisphere, at latitudes >40°N. Overall, an estimated 3% of the Earth's land is covered in peat, with an approximate global extent of ~3.5 million km^2 [*Clymo*, 1984; *Gorham*, 1991]. Although this is a small proportion of land cover, peatlands store one-quarter (612 GtC, 1 gigatonne = 10^{15} g) of the global soil carbon (C) [*Jobbagy and Jackson*, 2000; *Yu et al.*, 2010]. Peatlands are both sinks and sources of greenhouse gases; they sequester CO_2 from the atmosphere and emit both CH_4 and CO_2. The oldest extant peatlands started forming after the last glacial period (12 ka) and contain a record (in the form of the peat and its sub-fossil components) of carbon exchange processes in the peatland when it first formed [*MacDonald et al.*, 2006; *Smith et al.*, 2004]. Peatland initiation during the early Holocene (~11 ka),

contributed to sharp increases in atmospheric CH_4 concentrations, and the storage of carbon in new peat growth produced a small reduction in atmospheric CO_2. This peatland expansion led to an initial warming effect caused by CH_4 emissions, but later switched to a net cooling effect as more CO_2 was sequestered [*Frolking and Roulet*, 2007]. Today, it is generally accepted that undisturbed peatlands are carbon sinks, and C balance studies confirm that net CO_2 uptake outweighs CH_4 emissions and export of waterborne C [*Roulet et al.*, 2007]. Thus, present day peatlands continue to have a cooling effect on climate, but given future changes in temperature and moisture, some peatlands may become C sources [*Arneth et al.*, 2010; *Strack et al.*, 2008].

Peat generally accumulates on flat landscapes to depths between 50 cm and several metres [*Rydin and Jeglum*, 2006]. Traditional conceptualizations of peatlands subdivide the peat into two layers according to the position of the water table. Below the drought water table exists a lower layer called the catotelm which lacks oxygen, contains relatively compact, highly decomposed material and constitutes the bulk of the peat profile. Within this layer anoxic conditions persist causing anaerobic decomposition resulting in the production of CH_4 by methanogenic archaea. Above the water table a peat layer <50 cm in thickness can exist called the acrotelm. This layer contains oxygen, consists of less decomposed material, and houses CH_4 consuming methanotrophic bacteria. The boundary between these layers is highly dependent on the position of the water table and the microtopography of the peatland landscape. The effect of elevation on these peat layers is apparent in topographic depressions (hollows) which can have a thin or sometimes non-existent acrotelm and mounds (hummocks or ridges)

which can have a acrotelm between 20 and 50 cm [*Rydin and Jeglum*, 2006]. More recently, *Morris et al.* [2011] have suggested that the two layer peat model is too simple to represent ecological, hydrological and/or biogeochemical processes within many peatland types and propose a conceptualization that can account for process heterogeneity within the peat profile. This newer model does not partition the peat using strict boundaries, but instead the profile is described by zones where ecological, hydrological and/or biogeochemical processes vary on a continuum.

CH_4 production increases with temperature, [*Dise et al.*, 1993; *Dunfield et al.*, 1993; *Yavitt et al.*, 1997] and is also dependent on the availability of plant material (i.e., roots, litter, and peat) that form substrate needed for methanogenesis [*Valentine et al.*, 1994]. A secondary source of CH_4 production originates from root structures themselves that can supply carbon compounds called exudates to methanogens. This form of production is dependent on the position of the water table that determines if root structures are in contact with methanogens in the anoxic, waterlogged peat [*Waddington et al.*, 1996]. Overall, the optimal conditions for CH_4 production occur below, but near, the water table where temperature fluctuations are relatively high, substrate is available, and rooting structures are waterlogged [*Clymo and Pearce*, 1995; *Sundh et al.*, 1994].

The consumption of CH_4 occurs above the water table within the oxic peat layer. The position of the water table determines the size of the oxic layer and, in part, regulates the quantity of CH_4 reaching the atmosphere. If the water table is near the peat surface the oxic layer is thin and CH_4 consumption is minimal, but if the

water table is below the peat surface the oxic layer can substantially reduce the amount of CH_4 emitted to the atmosphere [*Bubier and Moore*, 1994]. This relationship between low water table level and depressed CH_4 emissions has been observed in both laboratory and field observations [*Bubier et al.*, 1993b; *Moore and Roulet*, 1993; *Strack and Waddington*, 2007; *Yavitt et al.*, 1988]. Another mechanism that consumes CH_4 is the availability of oxygen below the water table at the location of root structures. It is known that the roots of certain plants can transport oxygen beneath the water table in a process called radial oxygen loss or rhizospheric oxidation, and the available oxygen is used by methanotrophs to convert CH_4 into CO_2 [*Joabsson et al.*, 1999].

1.2. CH_4 emissions from peatlands

Transport mechanisms deliver CH_4 from the source of production within the peat, through the oxic zone, and into the atmosphere. Depending on the transport mechanism, CH_4 residence time within the oxic zone can be long, with consequently high rates of CH_4 consumption; transport can also be fast, and bypass consumption. Three mechanisms are responsible for transport of CH_4 through and from peat: diffusion through water- and gas- filled pores, plant-mediated transport, and ebullition. The first process, diffusion, occurs along a CH_4-concentration gradient from sites of CH_4 production to the peatland surface and thence to the atmosphere. Diffusion is a slow process, and if an oxic peat layer is present, between 55 and 90% of CH_4 can be consumed by oxidizing bacteria [*Fechner and Hemond*, 1992; *Whalen and Reeburgh*, 2000]. *Roulet et al*. [1993] found that, when the water table dropped 25-30 cm below the peat surface, the oxic layer was sufficiently thick to suppress all diffusive CH_4 emissions from a

peatland. Likewise, *Bubier et al*. [1993b] noted that a water-table position 18-20 cm below the peat surface produced a substantial reduction in CH_4 emissions that could be explained by consumption.

Plant-mediated transport occurs within the stems of plants that serve as gas conduits delivering CH_4 from the roots to the atmosphere. Thus, CH_4 transported via this method can entirely bypass consumption in the oxic peat layer, causing high rates of CH_4 emission [*Frenzel and Rudolph*, 1998]. The importance of this mechanism is demonstrated in studies where gas venting species are removed and CH_4 emissions are measured. Using this technique *Shannon et al*. [1996] estimated that transport through plant stems accounted for 64-90% of CH_4 emissions. In a similar study, *Waddington et al*. [1996] observed a mean CH_4 emission of 42.3 mg m^{-2} d^{-1} from natural peat sites, and reduced emissions of 4.9 mg m^{-2} d^{-1} from sites where gas venting plants were removed. Although plant-mediated transport is an effective mechanism for CH_4 transport, it is dependent on the position of the water table, which determines if roots can access CH_4 within the anoxic layer [*Waddington et al.*, 1996].

Ebullition refers to the transport of CH_4 as gas bubbles that form in peat pore water. As the bubbles travel upward through the peat column they can accumulate behind existing bubbles lodged in pore necks [*Baird and Waldron*, 2003; *Kellner et al.*, 2006; *Strack et al.*, 2005] or underneath woody layers, or well-decomposed layers of peat [*Glaser et al.*, 2004; *Rosenberry et al.*, 2003]. Where gas bubbles are not trapped and the bubbles are emitted steadily, most of the CH_4 in them will be readily consumed above the water table within the oxic layer [*Rosenberry et al.*,

2006]. However, if bubbles accumulate and are released as pulses or bursts (i.e., cyclical or episodic releases), the CH_4 reaching the water table may advect rather than diffuse through the oxic zone and bypass methanotrophic consumption [*Coulthard et al.*, 2009]. Evidence has shown that emissions from large ebullition events could be larger than emissions produced by diffusive and plant-mediated transport. For example, *Glaser et al*. [2004] measured surface oscillations in a northern peatland and pore-water pressure within the peat profile. Rises in the peat surface and high pore water pressure were indicative of gas accumulation, while the converse was associated with degassing caused by ebullition. Throughout three months of measurements, ebullition was not steady and three large degassing events occurred, separated by 7-8 days. The estimated CH_4 release from these events was 136 g CH_4 m^2, and exceeded annual average diffusive flux by an order of magnitude. *Baird et al*. [2004] incubated near-surface peat samples within the laboratory for 125 days. Gas traps specifically designed to measure ebullition recorded daily fluxes, from 2.2 to 83.0 mg CH_4 m^{-2} day^{-1}, which were comparable to diffusive flux measurements in the field.

Although ebullition appears to be an important transport mechanism, its importance has only become apparent recently, with many previous studies only measuring diffusive or plant-mediated emissions. Methods to measure steady diffusive CH_4 flux from peatlands may have contributed to this belief. Traditionally, CH_4 flux was measured using closed chambers fitted to the peat surface. To measure CH_4 fluxes, the chambers are sealed, several gas samples are extracted over a short time period (20-30 min), and the samples are analyzed to determine CH_4 concentrations. Plotting CH_4 concentrations against time, CH_4 flux is calculated

from the slope of a linear regression [*Dise et al.*, 1993]. If the coefficient of determination (r^2) of the regression is less than 0.8, the samples are rejected and an error is assumed to have occurred during gas collection from the chamber. The procedure of estimating CH_4 flux from gas samples is repeated every one or two weeks to derive a series of fluxes for a season. The infrequent re-visiting of sites and short time period of gas collection mean it is possible that many ebullition events are missed [*Tokida et al.*, 2007], which may have led to the assumption by many workers that ebullition is unimportant as a transport mechanism [*Coulthard et al.*, 2009]. Also contributing to this belief was the discarding of gas samples that did not produce a linear relationship. In fact, assuming no error occurred in the collection of gas from the chamber, a non-linear accumulation of gas could only be explained by ebullition, and the use of the linear regression method will have systematically excluded these measurements. *Tokida et al*. [2007] noted this problem in CH_4 chamber measurements and modified the method by increasing the sampling frequency and retaining those gas data that exhibited non-linear increases in CH_4 concentrations. In their study, lasting four days, CH_4 emissions from a peatland were measured every 1.5-2 hours to produce a detailed record. The revised method successfully measured eight large ebullition events that were significantly greater than base flux and accounted for 50% of the total CH_4 flux (Figure 2).

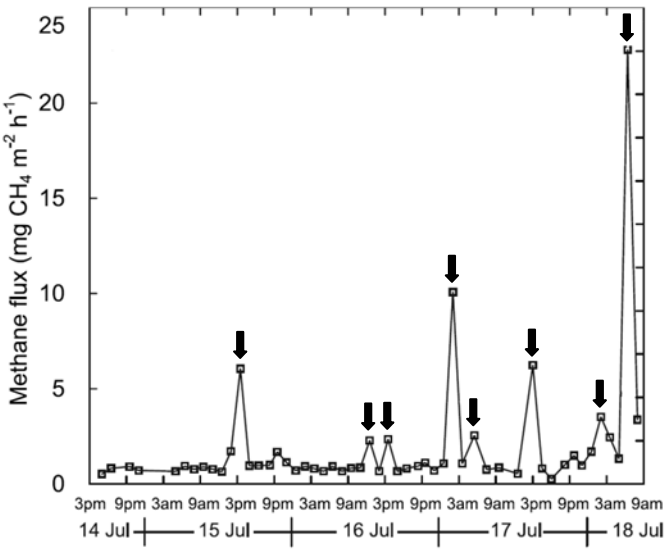

Figure 2. Ebullition field measurements.

High frequency chamber measurements record CH_4 ebullition (taken from *Tokida et al*. [2007]). Arrows indicate large ebullition events.

A growing number of studies have adopted techniques to measure ebullition, and are finding that ebullition is erratic and that large amounts of CH_4 can be released in a short period of time. As mentioned earlier, these large events are important because they can bypass oxidation and result in large amounts CH_4 reaching the atmosphere. The erratic or non-steady nature of ebullition can partly be explained by the inherent structure of peat which regulates the amount of bubbles that can be stored and released [*Baird et al.*, 2004]. Peat fibres or particles construct pore structures, with pores of variable size and density that result in bubble accumulation and release of varying magnitude [*Kettridge and Binley*, 2008; *Kettridge and Binley*, 2011]. Physical processes can also control the timing and size of ebullition [*Tokida et al.*, 2009]. For example, episodic ebullition has been correlated with decreasing atmospheric pressure, which increases gas volume and bubble buoyancy, and 'forces' gas to the peat surface [*Comas and Slater*, 2007;

Comas et al., 2011; *Fechner-Levy and Hemond*, 1996; *Tokida et al.*, 2005a; *Tokida et al.*, 2007]. For example *Waddington et al*. [2009] measured ebullition from laboratory peat cores for 172 days and found that 70% of ebullition events coincided with falling atmospheric pressure. *Comas and Slater* [2007] developed a method using transmitted electromagnetic waves to non-invasively estimate gas content within a laboratory block of peat. Reductions in gas content within the peat sample coincided with spikes in gas flux at the peat surface caused by ebullition. Time series analysis of the gas content found that fluctuations were non-random, and exhibited periodicity reflected in changes of atmospheric pressure.

1.3. Numerical modelling of CH_4 ebullition from peatlands

Numerical models have been developed to estimate the peatland contribution to the global CH_4 budget. The majority of CH_4 emission models represent ebullition as a threshold process between CH_4 dissolved in water and CH_4 as bubbles [*Frolking and Roulet*, 2007; *Lai*, 2009; *Zhuang et al.*, 2004]. An example of a threshold model is that of *Walter et al.* [1996]; it is a one-dimensional, process-based, CH_4 model that subdivides the soil profile into 1-cm layers with the water table dividing oxic from anoxic peat. In the model, ebullition commences when concentrations of dissolved CH_4 in the pore water are greater than 500 μM. When this threshold is exceeded the quantity of gaseous CH_4 available for transport via ebullition is calculated for each layer of peat within the profile, and transported directly to the water table, where it is added to the oxic-zone pool of CH_4 that may be transported to the peatland surface via diffusion. Consequently, if the water table is below the peat surface, the CH_4 must slowly diffuse through the oxic peat and may be consumed by model methanotrophs. The main problem of this model

is that it does not account for stored bubbles, and the possibility that stored bubbles can be released as ebullition in quantities large enough to overwhelm or bypass consumption within the oxic zone.

Kellner et al. [2006] developed a CH_4 ebullition model and compared model results to observations from peat cores incubated within the laboratory. In this study both temperature and atmospheric pressure, which affect bubble expansion and the solubility of gas, were included in a model to produce episodic ebullition. In the model a threshold method was applied on a pool of gas consisting of 60% CH_4, 12% CO_2, and 30% N_2. At every time step the effect of temperature and atmospheric pressure on gas volume was calculated for the three gasses separately. If the volume of the combined gases was greater than 15% of the total volume of the peat, gas, and water, ebullition occurred by removing the excess gas. Upon the next time step a fixed amount of gas representing production was added to the pool of gas, and the calculations were repeated. The model produced good agreement with observations of CH_4 flux from peat cores (r^2=0.66), but the authors noted that performance could be improved by including more complexity within the model by describing peat pore structures. Specifically pore size and location were highlighted as characteristics that affect the retention of gas throughout the peat profile. For example, small pores would cause gas to accumulate, and eventually build up to levels where buoyancy causes bubbles to be released upwards in large quantities. Larger pores would have less of an effect on gas retention, and allow gas to move freely through to shallower layers of peat.

1.4. Research aims and thesis structure

To date no CH_4 ebullition model has been able to re-produce the process of rapid/episodic CH_4 bubble loss from peat. What is needed is a better conceptualization of bubble accumulation, storage, and release within peat, and this requires the inclusion of a spatially-explicit representation of the peat pore structure within a model. Furthermore, the spatial heterogeneity of pore sizes at various depths, a property completely absent in previous models, should be represented to replicate variable amounts of storage at depth and bubble movement through peats. By including this level of detail, different rates of ebullition from peats with different pore structures can be investigated. Although this level of detail may appear excessive, it is necessary to model bubble storage and transfer at the pore scale, so that larger-scale ebullition patterns can emerge (e.g. episodic or cyclical degassing events). As such, the main aim of this study was to:

Replicate episodic ebullition from peat within a computer model by representing peat pore structure, and pore-level gas dynamics.

The following are sub-aims of the thesis that are addressed in the following chapters.

1) Investigate the role of pore structure on gas storage, bubble sizes, and bubble release (Chapters 2 and 3).
2) Investigate the effect of pore structure and bubble storage on ebullition from peat (Chapter 4).

3) Determine when environmental forcings are detectable in CH_4 ebullition emissions measured at the peat surface (Chapter 5).
4) Investigate the effect of sampling size and duration on ebullition estimates from peat (Chapter 6).

In Chapter 2 the state of the art in two-phase flow modelling is reviewed to identify the physical processes occurring during ebullition and highlight the limitations of current modellling methods if applied toward modelling ebullition in peat. Afterwards, a simple computer model of ebullition developed during this thesis is presented. This model includes a spatial representation of the pore structure, and pore-level gas dynamics (bubble accumulation, storage, and release). Next, patterns of CH_4 ebullition from peat are compiled from the literature and results reported of preliminary modelling work using the computer model to determine which patterns of bubble release, size, and storage emerge. From the preliminary computer model output it was possible to understand the role of pore structure on gas storage, bubble size, and bubble release (sub-aim 1).

Chapter 3 and 4 are dedicated to testing the computer model of ebullition with patterns of gas storage, bubble sizes, and bubble release generated from two physical models of ebullition operated in a laboratory. The first physical model was a direct analogue of the computer model developed in this thesis, and patterns from this physical model are directly compared to patterns produced by the computer model. This experiment provided confidence that the processes in the computer model are capable of simulating ebullition, and suggested that pore structure can influence gas storage, bubble size and bubble release (sub-aim 1).

The second physical model was based on real peat samples into which bubbles were injected to represent gas production. Patterns in rates of bubble loss and the size of the bubbles being lost from the peat samples were recorded. From this data, it was possible to provide further confirmation that the computer model is valid. Furthermore, this experiment provided evidence that differences in peat pore structure can affect gas storage and ebullition from peat (sub-aim 2).

In Chapter 5 a numerical exercise is performed using the computer model to investigate how environmental forcings like sun light or atmospheric pressure can drive the accumulation and release of CH_4 bubbles from peat. Scenarios comprising different pore structures and forcings of different magnitude were modelled. The output from these simulations suggests that peat pore structure determines when ebullition can be correlated to an environmental forcing (sub-aim 3).

A second numerical exercise was carried out in chapter 6 with the computer model of ebullition. In this chapter a large spatio-temporal scale (e.g. 1-10 m, 1-10 yr) simulation of ebullition from a structurally variable peatland was performed. The resulting ebullition from the simulated peatland was variable in space and time. Different amounts of spatial and temporal sampling effort were used to estimate the uncertainty in ebullition from the peatland (sub-aim 4).

Chapter 2 Numerical and physical modelling of ebullition

2.1. Introduction

Bubbles within porous media have an important role in mediating the Earth's climate [*Judd*, 2004; *MacDonald et al.*, 2006; *Shakhova et al.*, 2010; *Smith et al.*, 2004; *Walter et al.*, 2006], carbon dioxide storage [*Oldenburg and Lewicki*, 2006], recovering fossil fuels [*Sohrabi et al.*, 2008], environmental remediation [*McCray and Falta*, 1997], nuclear water disposal [*Bourgeat et al.*, 2009] and altering the flow of groundwater [*Baird and Waldron*, 2003]. Therefore, predicting bubble movement and emissions from porous media is necessary to understand present and future impacts on natural and industrial systems. Numerical modelling offers the possibility to quantitatively investigate these impacts, and much progress has been made in predicting bubble dynamics using modelling approaches with various levels of physical rigour, process complexity, and spatial scales [*Meakin and Tartakovsky*, 2009].

At the pore scale, models have been developed that provide detailed representations of porous structures and resolve bubble transport at the sub-pore level (μm), but due to their high computational demands these models have limited use in addressing plot and field scale questions relating to seasonal time scales. At present, coarser-scale models can provide large scale prediction (1-100 m) of bubble movement and emissions over long time periods (1-25 yr) [*Amos and Mayer*, 2006], but prediction uncertainty is high because the modelled spatial resolutions do not permit a detailed description of a porous medium and exclude

important structural features (e.g. fractures, impermeable layers) that significantly alter bubble transport [*Geiger et al.*, 2012; *Helmig et al.*, 2013; *Thomson and Johnson*, 2000]. Therefore, a major theoretical and computational challenge is to model bubble movement at large spatio-temporal scales, but explicitly represent the spatial heterogeneity of the porous medium in order to reduce model uncertainty. Several methods are making progress in modelling bubble transport in porous media, but none have been applied towards ebullition in peat. In the following section, these numerical methods will be examined and the possibility of applying them towards modelling large spatio-temporal scale (e.g. 1-10 m, 1-10 yr) ebullition from peatlands will be assessed.

2.2. Numerical modelling of bubbles in porous media

One approach to model bubble transport in porous media is to solve differential equations that explicitly describe the motion of individual bubbles [*Cihan and Corapcioglu*, 2008; *Corapcioglu et al.*, 2004]. These analytical approaches are advantageous because the equations clearly describe how variables within the model interact (e.g. pore size and bubble velocity), and the solution to these equations are computationally efficient. The major drawback of this approach is the number of simplifying assumptions that must be made to obtain a mathematical solution. Although in modelling it is always necessary to reduce the complexity of a system to its principal components and processes [*Mulligan and Wainwright*, 2013], analytical approaches can sometimes reduce the system to something that is unrealistic. For example, *Corapcioglu et al.* [2004] limited their study of bubble rise velocity to a single bubble within a homogenous porous medium, where the rising bubble did not come in contact with pore walls, could not sub-divide or

coalesce, and could only move in the vertical direction. Even though analytical methods are not able to model complicated bubble interactions in porous media like peat, these methods have provided much insight into the forces acting on a bubble moving in porous media. An analytical solution to bubble motion derived by *Cihan and Corapcioglu* [2008] found that bubble movement can be predicted by solving the equations governing the upward driving force of buoyancy, and opposing forces of drag and surface tension acting upon a bubble (Figure 3). In this model, drag force results from a bubble transferring momentum from itself to the surrounding liquid phase, and surface tension is the cohesive force located at the gas-liquid-solid interfaces. The findings of this study were that drag force is the dominant force opposing buoyancy when the bubble is rising and trapped bubbles within a pore cannot rise until the buoyant force is greater than surface tension force holding the bubble in place.

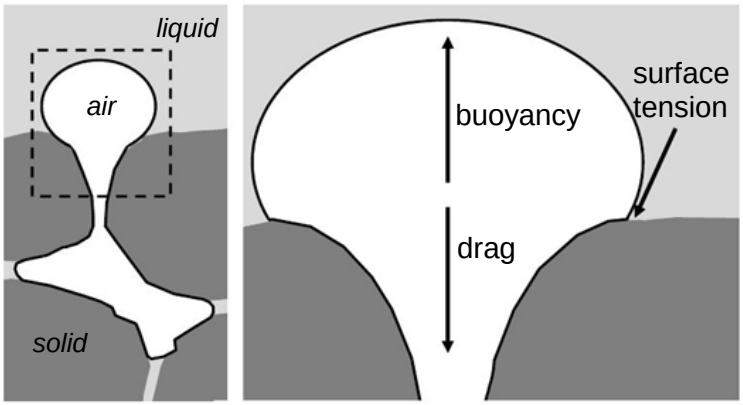

Figure 3. Forces acting on a bubble within a saturated porous media (based on *Corapcioglu et al.* [2004]).

Although figure depicts contact between air and solid phases the model of *Corapcioglu et al.* [2004] did not include this interaction, but instead assumed that a thin film of liquid existed between the air and solid phases.

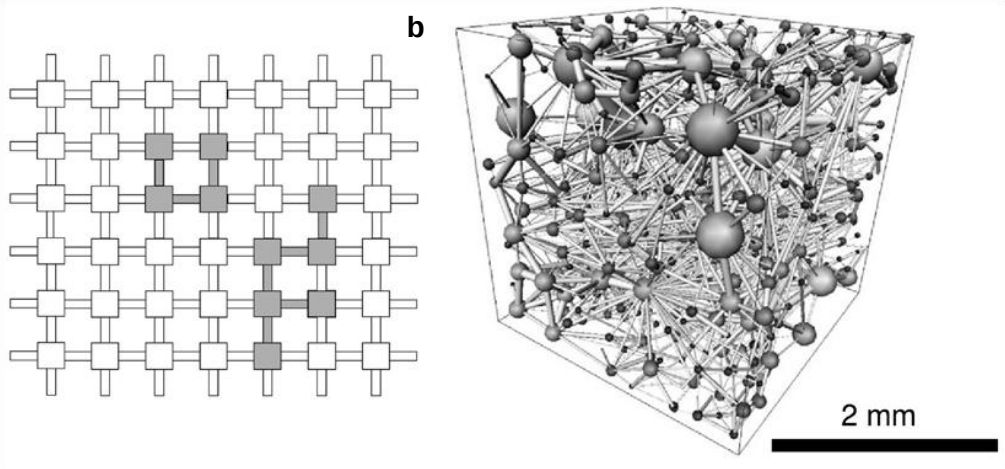

Figure 4. Pore network models.

(a) Two-dimensional pore network model where pores and throats are occupied with gas (in gray) and water (in white) (taken from *Zhao and Ioannidis* [2011]) . (b) Three-dimensional pore network extracted from quarry carbonate, where pores are represented by spheres and throats as cylinders (taken from *Blunt et al.* [2013]).

Other approaches to solve bubble movement in porous media are mechanistic models that simulate gas flow within a spatially explicit representation of the porous medium. For example, pore network models represent a porous medium as a regular or irregular set of pores connected by throats in two-dimensions (Figure 4a) or three-dimensions (Figure 4b). Models have been developed to calculate flow within pore network models for single phases (liquid), and multiple phases (liquid, gas, oil) [*Blunt et al.*, 2002]. An example of a simple pore network model is the invasion percolation model [*Birovljev et al.*, 1995], which represent a porous medium as a two-dimensional regular network of pores and throats saturated with water, with randomly assigned threshold values to determine when gas will invade or withdraw from a pore through a throat. Additionally, withdrawal thresholds for pore sites are influenced by the configuration of air/water occupancy in neighbouring pores, and buoyancy forces are modelled by reducing threshold values in the vertical direction. More physically-based pore network models go

beyond simple rule based approaches, and resolve multiphase flow within the network using simplified flow equations for gas and water [*Geiger et al.*, 2012].

A major limitation of pore network models is the computational expense of calculating multiphase flow within porous media that require a network containing a large amount of pores and throats. For example, a pore network model of a 729 mm^3 sample of Berea sandstone alone can contain 12,349 pores and 26,146 throats [*Rhodes et al.*, 2008]. For peat, examples of pore network models do not exist, but measurements of peat structures using x-ray tomography have found that small peat samples of 10 cm in length and 6 cm in diameter can contain 11,278 pores [*Quinton et al.*, 2009]. This suggests that the development and operation of a peat pore network model would most likely be limited to peat samples of this size.

A second mechanistic approach to modelling multiphase flow are lattice Boltzmann models (LBMs) [*Chen and Doolen*, 1998; *Rothman and Zaleski*, 2004] that are based on the simpler lattice gas models [*Frisch et al.*, 1986]. In lattice gas models individual fluid or gas particles move on a discrete lattice network and collide with other liquid or gas particles, or the solid objects representing the porous medium. During the collision stage the velocity and trajectory of each particle is calculated and momentum and mass are conserved. Due to the stochasticity of the lattice gas model, the resulting flow predictions are noisy and the lattice Boltzmann method was developed to average flow predictions [*Meakin and Tartakovsky*, 2009].

Although LBMs can simulate complex flows through spatially heterogeneous media, at present most methods can only predict multiphase flow for phases with similar densities and viscosities. At best, the majority of LBMs remain numerically stable when density ratios are less than 10 (density phase 1:density phase 2) [*Inamuro et al.*, 2004]. For ebullition in peat, this can present some difficulties for using LBMs because water is much denser than the combination of gases released from peat. Assuming that the gas emissions from peat are 60% CH_4, 12% CO_2, and 30% N_2 [*Kellner et al.*, 2006], the density ratio between water and the combined gases would be 960 (1000 kg/m^3:1.04 kg/m^3), and render most LBMs unsuitable for ebullition modelling in peat. Even though newer LBMs have been developed to accommodate density ratios of 1000 [*Bao and Schaefer*, 2013; *Inamuro and Ogata*, 2004; *Zheng et al.*, 2006], these models are still undergoing testing on individual bubbles rising in fluid, and have not been shown to work for more complicated cases like bubble movement in porous media.

A final mechanistic approach to consider for modelling multiphase flow in peat is computational fluid dynamic (CFD) methods. In CFD models, the modelled area of interest (e.g. peat) is discretized using a mesh, and the Navier-Stokes equations are solved to derive flow-field variables like velocity and pressure at each mesh location, for each phase [*Yeoh and Tu*, 2010]. A challenge of adopting CFD is the necessity of tracking the interface between phases (e.g. gas-liquid), and the need to model interface changes like bubble break-up and coalescence over time [*Meakin and Tartakovsky*, 2009]. Methods to track interfaces have existed for some time [*Hirt and Nichols*, 1981; *Sussman et al.*, 1994; *Unverdi and Tryggvason*, 1992], but CFDs with gas-liquid interfaces have not developed substantially

beyond the first benchmark simulations of bubble populations within a column of liquid [*Buwa and Ranade*, 2002; *Delnoij et al.*, 1999], and to date no CFD examples exist where gas and liquid phases interact with complex solid objects like peat. Moreover, if CFDs were to develop the capacity to model multiphase flow in complex structures, the high computational expense of these methods would limit their use to modelling gas flow within several connected peat pores. To highlight the computational expense of CFD, a 2D simulation of a micro-bubble (300 μm diameter) moving steadily within a straight micro-channel (width 100 μm, length 800 μm) can take 12 hr to complete on a computer with one processor, and simulations of a micro-bubble in 3D can take 200 hr to finish on a computer with eight processers operating in parallel [*Hoang et al.*, 2013].

2.3. Simple numerical model of ebullition in peat

In this section, a computer model of bubble movement in peat below the water table is described. The model contains a spatial representation of the porous medium, and can simulate ebullition emissions at the field scale (1-10 m), but does not adopt any of the existing modelling approaches for multiphase flow because of their computational demands. As previously mentioned, ebullition can occur as non-steady degassing events of various size. For this reason, a modelling approach that was flexible enough to generate the full spectrum of ebullition event sizes was required, and a suitable approach was found in a model of avalanching sand. The model adopted was first designed by *Bak et al.* [1987] to reproduce non-steady avalanching behaviour using rules dependent on slope angles. This model is akin to dropping grains of sand on a table from above at regular intervals. At the point of sand pile growth, the grains eventually achieve a maximum slope

which will produce an avalanche that moves sediment to neighbouring locations and can trigger more avalanches down slope if the adjusted slopes are too steep. Continuously adding grains of sand will cause avalanches of varying magnitude and frequency. According to the concept of self-organized criticality proposed by *Bak et al.* [1987], piles of sand grains will organize themselves into a critical state whereby the addition of a single grain of sand could produce no avalanche, localized avalanches, or a series of avalanches that cascade through the entire system. When this was implemented within a computer it was found that the occurrence of avalanches of different sizes could be described using a power law function. Essentially, small avalanches occur often, moderate avalanches less frequently, and large avalanches rarely. Following this finding, several studies have adopted the sand pile template to model non-steady phenomena including forest fires [*Albano*, 1995; *Drossel and Schwabl*, 1992], earthquakes [*Bak and Tang*, 1989; *Ito and Matsuzaki*, 1990], mass extinction [*Paczuski et al.*, 1996], air pollution [*Shi and Liu*, 2009], climate change [*Liu et al.*, 2013] and intraflagellar transport dynamics [*Ludington et al.*, 2013].

The simplicity and dynamics of the sand pile system motivated its adoption and modification as a model of CH_4 ebullition (Figure 5). This modified sand pile model was developed by Ramirez and co-authors in 2008 (see *Coulthard et al.* [2009]) and is called Model of Ebullition and Gas storAge (MEGA). The initial model was entirely developed by Ramirez and throughout the thesis further development, as documented in the Appendix, Section 1, was solely carried out by Ramirez. The aim of MEGA was to replicate non-steady (episodic/cyclical) release of CH_4 from peat into the atmosphere by addressing the point made by *Kellner et al.* [2006] that

a model of ebullition should have a heterogeneous spatial representation of peat pore structure. Furthermore, this variability in peat pore size should result in different amounts of accumulation and storage of gas within the peat, which, in turn, should give different types of bubble release behaviour. MEGA was implemented on a two dimensional cellular grid and represents a cross section of peat where cells can have three possible states: solid (peat fibres or particles), gas, or water (Figure 5 inset). Here, the individual shelf is equivalent to peat solids and the space underneath the shelf is a pore. The peat pore structure is represented by a series of shelves where the quantity and length of shelves can be set according to the physical characteristics of the peat (e.g. permeability or porosity). For example, open peat could be represented by relatively few small shelves (Figure 5a), whereas a closed or denser peat might require relatively larger shelves (Figure 5c).

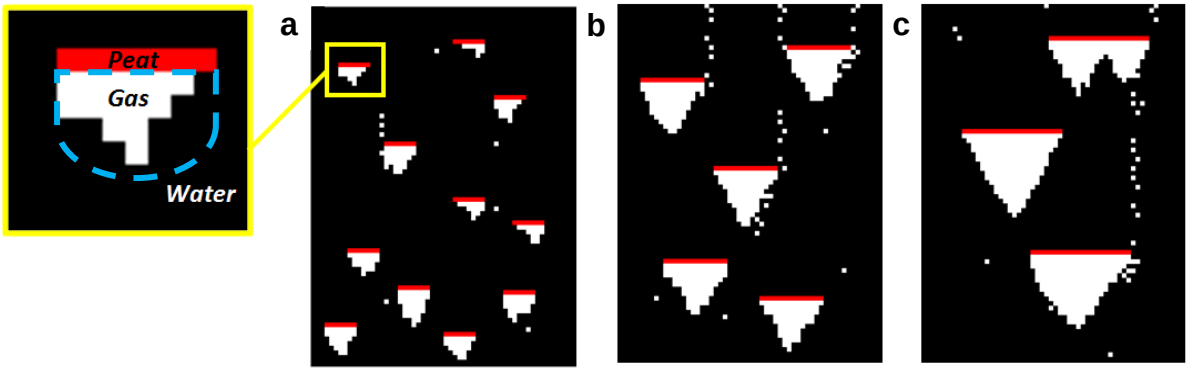

Figure 5. Shelf arrangements in MEGA.

Shelf arrangements representing (a) open, (b) intermediate, and (c) dense peat. Inset with three possible states in model: solid (peat fibres or particles), gas, or water. Pore space outlined in blue.

Within MEGA bubbles enter the shelf arrangement from below, at random or fixed locations, and at a constant volumetric rate representing production. This bubble input can be varied if required to reflect fluctuations in bubble production. The

location of random bubble input is bounded by the location of the leftmost shelf and rightmost shelf within the profile. Bounding the input of random bubbles prevents bubbles from moving through the profile along the edges without interacting with shelves. The movement of bubbles is governed by a set of rules that are executed as the shelf arrangement is scanned from top to bottom (Figure 6). Scanning is performed on the cellular grid across rows, and the direction of scanning, left-to-right or right-to-left, is randomly decided every model iteration.

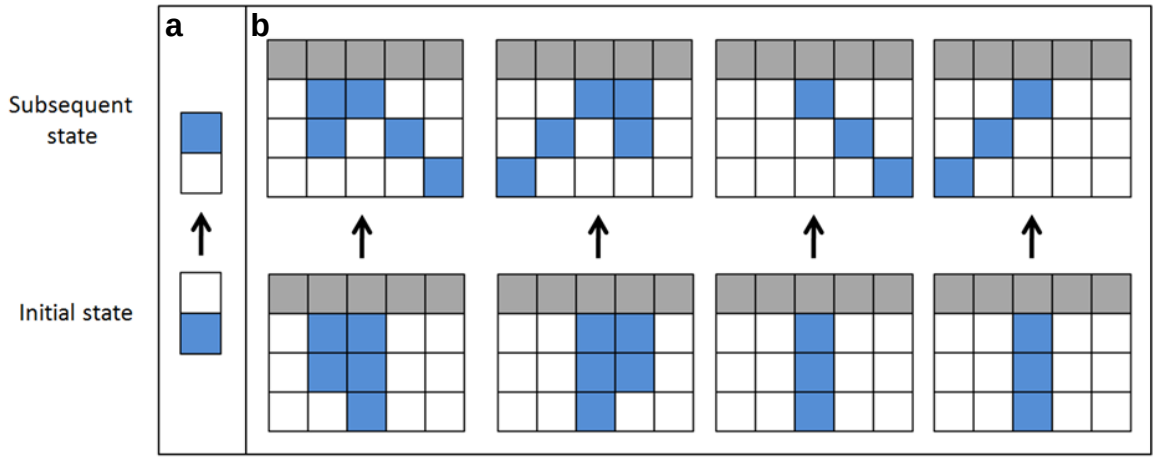

Figure 6. (a) Bubble movement and (b) toppling rules (gas = blue, peat = grey, and water = white).

During a simulation, the upward force of buoyancy acting on a single bubble is replicated by calling the bubble movement rule every model iteration until a bubble encounters a shelf (Figure 6a). If a shelf is vacant, the upward movement of the bubble will stop, and this is equivalent to a bubble moving into a vacant pore. By itself, a small bubble will remain trapped underneath the shelf, and this process is analogous to surface tension forces stopping bubble deformation that allows a bubble to pass through a pore throat created by peat fibres.

Another possibility is that a single bubble encounters a shelf with stored bubbles, and if this occurs the single bubble would coalesce with the stored bubbles. This process will increase bubble storage underneath a shelf until a critical state is approached and the resulting dynamic can cause bubbles to avalanche upwards to become trapped on shallower shelves (Figure 5c). Bubble avalanches are dependent on the height of bubble columns that topple according to a rule set (Figure 6b). For example, if three bubbles are stacked upon each other the column of bubbles will topple to the left or right according to which location is unoccupied (Figure 6b). Furthermore, the avalanching of a single column of bubbles can trigger multiple avalanches amongst the bubbles stored underneath a single shelf, and determines how much gas collectively is lost from that shelf. This avalanching at the pore level is analogous to buoyancy forces overwhelming surface tension forces that hold stored gas within peat pores. The buoyancy force acts to lift the bubble and causes it to deform as it moves into a pore throat.

The smallest bubble within MEGA is 1 mm in diameter and is equal to one cell in the 2D grid. Larger bubbles can develop as chains of connected one-cell bubbles separated by two or more consecutive non-bubble cells, and bubbles from different ‘sand’ piles can coalesce to from larger bubbles (Figure 7). Although bubbles in MEGA vary in size according to the length of bubble chains, individual one-cell bubbles that constitute larger bubbles are not 'aware' that they are part of a larger bubble. For this reason, it was not possible to have bubble rise velocity vary according to bubble size. As a compromise, a constant rise velocity is applied to all bubbles in the model regardless of size, and is equal to the rise velocity of a bubble of 1 mm in diameter. Bubble rise velocity is set at 282 mm s^{-1} after

measuring the terminal velocity of a rising 1 mm diameter bubble in clean water, and is comparable to published velocities [*Duineveld*, 1995]. Using this rise velocity, and modelling at 1 mm grid cell resolution, a time step was added to MEGA whereby one iteration, a scan of the peat profile, is equivalent to 1/282nd of a second.

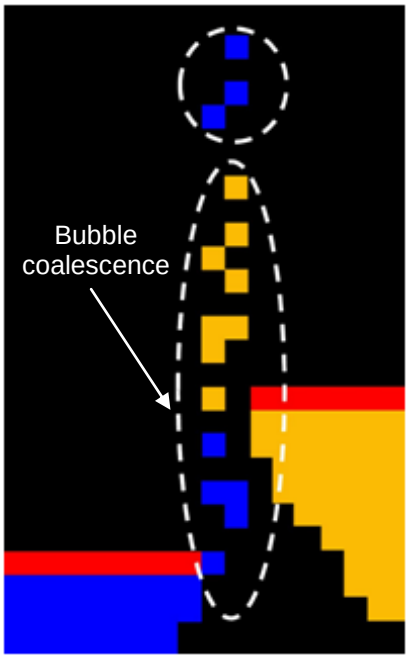

Figure 7. Bubble sizes and coalescence in numerical model.

Larger bubbles (encircled in dashed lines) represented as chains of bubbles (clusters of colour cells). Bubbles from two sand piles coalesce to from a larger bubble.

The primary 'data' or output collected from MEGA is bubble sizes. As mentioned earlier, bubbles consist of chains of bubble pixels, and bubble size was calculated by summing all the bubble pixels within a chain. Bubble sizes were collected continuously as bubbles exited the peat profile, and the model iteration when the bubble exits the profile is recorded. This information is supplied at the end of the simulation as a time series of bubble size in text file format. Knowing the number of iterations per second, this time series is post-processed to generate a secondary

dataset of volumetric rate of bubble release. Bubble release is the sum of the bubble sizes, as an area (mm^2), exiting the peat profile over a time interval (e.g. 1 second). Lastly, at the end of each simulation, the location, and number of bubble pixels within the peat profile is recorded to provide an estimate of bubble storage.

2.4. Model testing

The use of patterns to test if the structure of a model is valid is called Pattern Oriented Modelling (POM) [*Grimm et al.*, 2005], and this approach was adopted throughout this thesis to determine if MEGA 'captures' the key processes and properties to reproduce patterns observed in physical models including physical models using real peat samples. Patterns are discernable regularities found in nature or data collected from nature, and are the result of underlying processes [*Grimm et al.*, 1996]. The goal of POM is to produce the simplest model that can reproduce independent patterns produced by a phenomenon. As such, the decision to include a process in a model is made by evaluating whether this process contributes towards making an observed pattern. For example, if gas storage in peat were to exhibit a pattern, it would be necessary to include a spatial description of the peat in a model to store gas and the model should account for surface tension processes that trap gas.

The POM approach begins by identifying independent patterns produced by the system being modelled. These patterns can be found in the literature or observations collected in the field or laboratory. Next, the model construction is guided by the need to reproduce the identified patterns. In the final stage, patterns generated by the model are tested against observed patterns. In this section

patterns in bubble release, size, and storage from peat as reported in the literature are discussed. These patterns were used to construct MEGA. To test MEGA, an exploratory run of the model was performed and the patterns generated by the model were qualitatively compared against observations available in the literature.

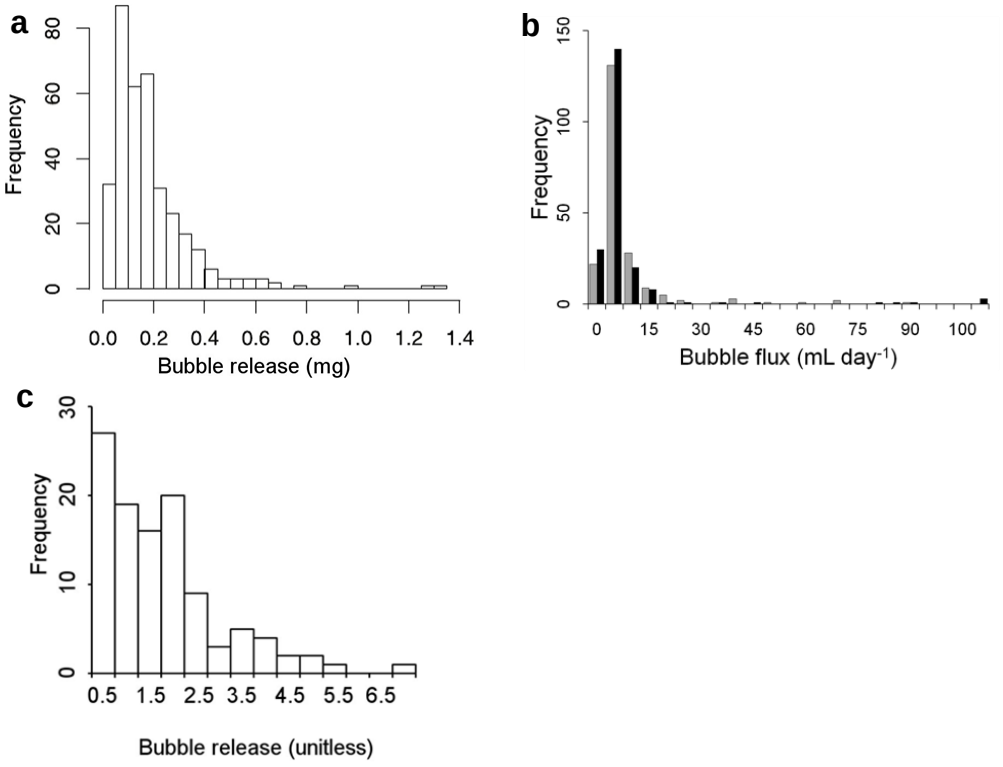

Figure 8. Observed ebullition from peatlands.

Histograms of observed CH_4 ebullition (bubble release) from peat in the (a,b) field and (c) laboratory. Plot 'a' taken from *Goodrich et al.* [2011], plot 'b' re-drawn from data used in *Stamp et al.* [2013]), and plot 'c', re-drawn from data used in *Kellner et al.* [2006].

Studies of CH_4 ebullition from peat are few, but these studies consistently report patterns in magnitude and frequency of bubble release that are characteristically non-normal with a strong positive skew (Figure 8). The shape of these distributions indicates that small ebullition events occur often, and extreme bubbling events rarely. Records of bubble sizes do not exist for CH_4 ebullition from peat, so no patterns are available as test data. Distributions of bubble size are

available for granular media like packed glass beads [*Meier et al.*, 2011], but this medium is structurally different from peat, and offers no insight on bubble sizes from peat. Although bubble sizes from peat do not exist, bubble size data from MEGA will be analysed to demonstrate the patterns that MEGA is capable of producing. This information will later be used to determine if bubble size patterns from peat experiments presented in Chapter 4 are similar to bubble size patterns from MEGA.

Field surveys of CH_4 gas storage within peatlands has been performed using methods like ground penetrating radar [*Comas et al.*, 2008; *Parsekian et al.*, 2012], changes in peat surface elevation [*Glaser et al.*, 2004] and direct sampling [*Tokida et al.*, 2005b]. These studies have proposed various explanations for the variability of stored gas within peat including variability in the availability of carbon for CH_4 production, variations in temperature regime within the peat profile, and variations in peat structure, but none of these processes/factors occur independently and it remains difficult to isolate the overriding cause for gas storage hotspots. Regardless of this uncertainty, a likely structural cause for increased gas storage within peat profiles is variability in peat porosity and permeability. Here, porosity is the amount of void space in the peat, and permeability is the ease in which gas can move through peat. A low porosity, low permeability peat would consist of small pores that have low connectivity. This peat structure would form a barrier within the peat, and trap large quantities of gas underneath this barrier [*Glaser et al.*, 2004; *Strack and Mierau*, 2010]. In contrast high porosity, high permeability peat would have large pores with high connectivity and allow gas to move freely through

the peat. This open peat structure would store low amounts of gas within the peat profile.

As previously mentioned, peat structure can vary according to alternating micro-topographic features (ridges and hollows), and it has been observed that peat forming ridges can have higher bulk density and smaller pore sizes than peat forming hollows [*Whittington and Price*, 2006]. As such, peat ridges should store more gas than hollows, and *Strack and Mierau* [2010] observed this pattern when measuring gas volumes in (i) ridges dominated by plant species such as *Sphagnum fuscum* that form low porosity, less permeable, peat, and (ii) hollows dominated by plant species such as *Sphagnum angustifolium* which form high porosity, higher-permeability peat (Figure 9). This field evidence suggests that gas storage is dependent on peat structure, particularly the permeability and porosity of the peat. Thus, a computer model of ebullition should produce a pattern that reflects increasing gas storage with decreasing peat permeability and porosity.

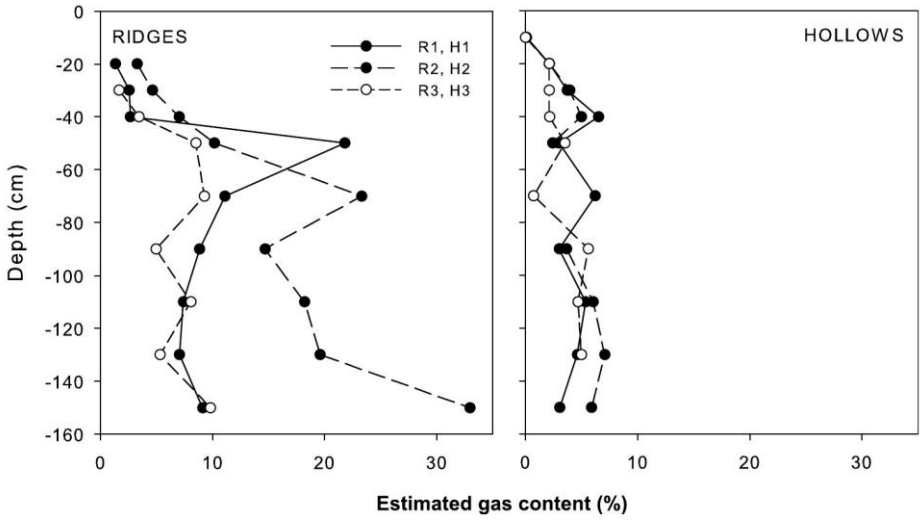

Figure 9. Gas storage in peat.

Depth profiles of gas volume estimated by direct sampling at (left) ridges and (right) hollows, plots taken from *Strack and Mierau* [2010].

These published patterns of bubble release and storage were compared with those produced by MEGA. To generate multiple examples of patterns from MEGA, a sensitivity analysis was performed to measure the effect of shelf length and quantity on bubble size, release rate, and storage. A parameter space was constructed to determine combinations of shelf length and quantity that would produce similar total shelf surface areas (Figure 10). For example, a simulation containing 360 shelves of length 6 mm (Figure 10, inset 1) would have the equivalent total shelf surface length as a simulation with 60 shelves of length 36 mm (Figure 10, inset 2). A total of 51 combinations of shelf quantity and length were simulated.

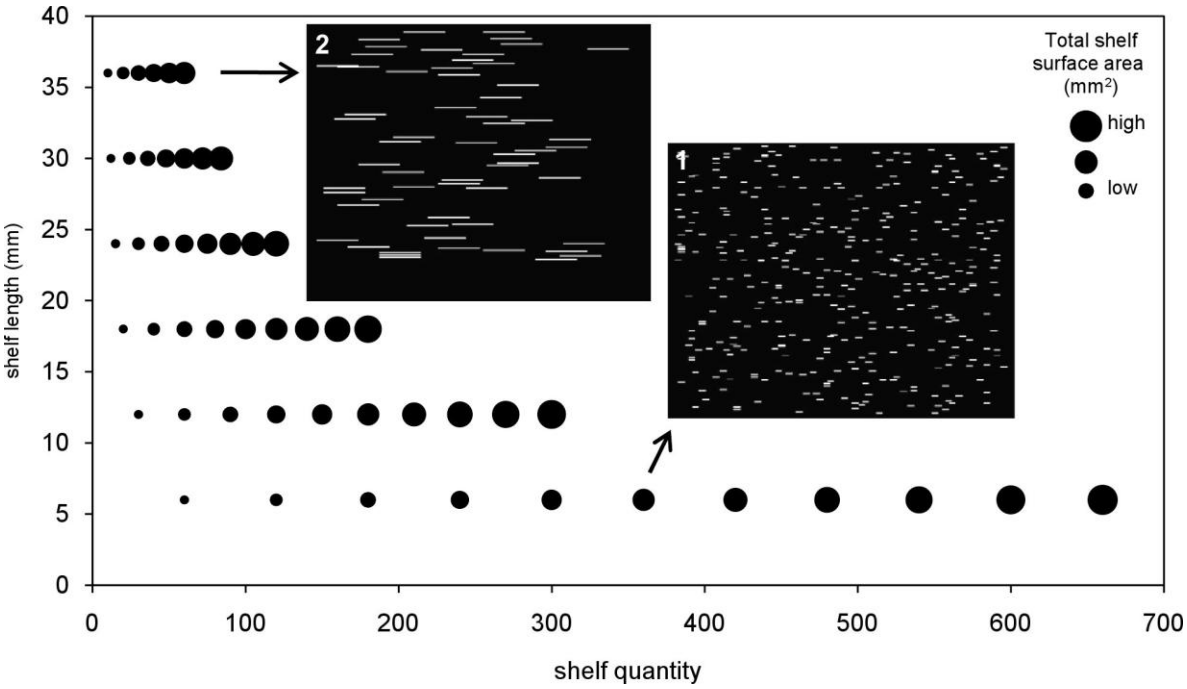

Figure 10. Combinations of shelf length and quantity.

Parameter space for shelf quantity and length, with plot symbols scaled according to total shelf surface area. Examples of randomly generated shelf arrangements for small (inset 1) and large shelves (inset 2).

Shelf locations were randomly generated on a gridded area 300 mm wide and a height of 250 mm. Two hundred and fifty millimetres of additional empty space

was added to the bottom of the profile to accommodate the build-up of large piles of bubbles. Prior to collecting output from MEGA, a simulation period, commonly called model spin-up, was executed where a predetermined amount of bubbles was added to the profile. During the model spin-up 'sand' piles were allowed to develop underneath shelves to create initial bubble storage conditions. To obtain an estimate for the amount of bubbles added to each profile, the maximum bubble capacity of a shelf was multiplied by the number of shelves created. Simulation duration was 18,000 s (5 hr), and 10 1-mm bubbles were added randomly at the base of the peat profile every 0.1 s. Bubble release was recorded every second, bubble sizes were recorded continuously, and total bubble storage within the shelf arrangement was calculated at the end of the simulation.

Bubble storage for each shelf arrangement were categorized by imposing breaks at the 0-25th, 25th-50th, 50th-75th, and 75th-100th percentiles of all the bubble storage records from each simulation. This categorization provides a means to distinguish between low, medium, and high amounts of bubble storage. A plot of bubble storage, against shelf length and shelf quantity reveals that for the same total length of shelf smaller shelves store fewer bubbles than larger shelves (Figure 11). The general explanation for this pattern is that larger shelves have a greater length which can store more bubbles and also have a greater likelihood of intercepting bubbles. More importantly, as shelves become larger there is the possibility that shelves can form dense shelf layers that restrict the passage of bubbles, and produce zones of bubble accumulation (Figure 11, inset 1). For example, maintaining total shelf area equal, but doubling shelf length from 6 mm (Figure 11,

inset 2) to 12 mm (Figure 11, inset 1) produces an 89% increase in storage due to dense shelf layers.

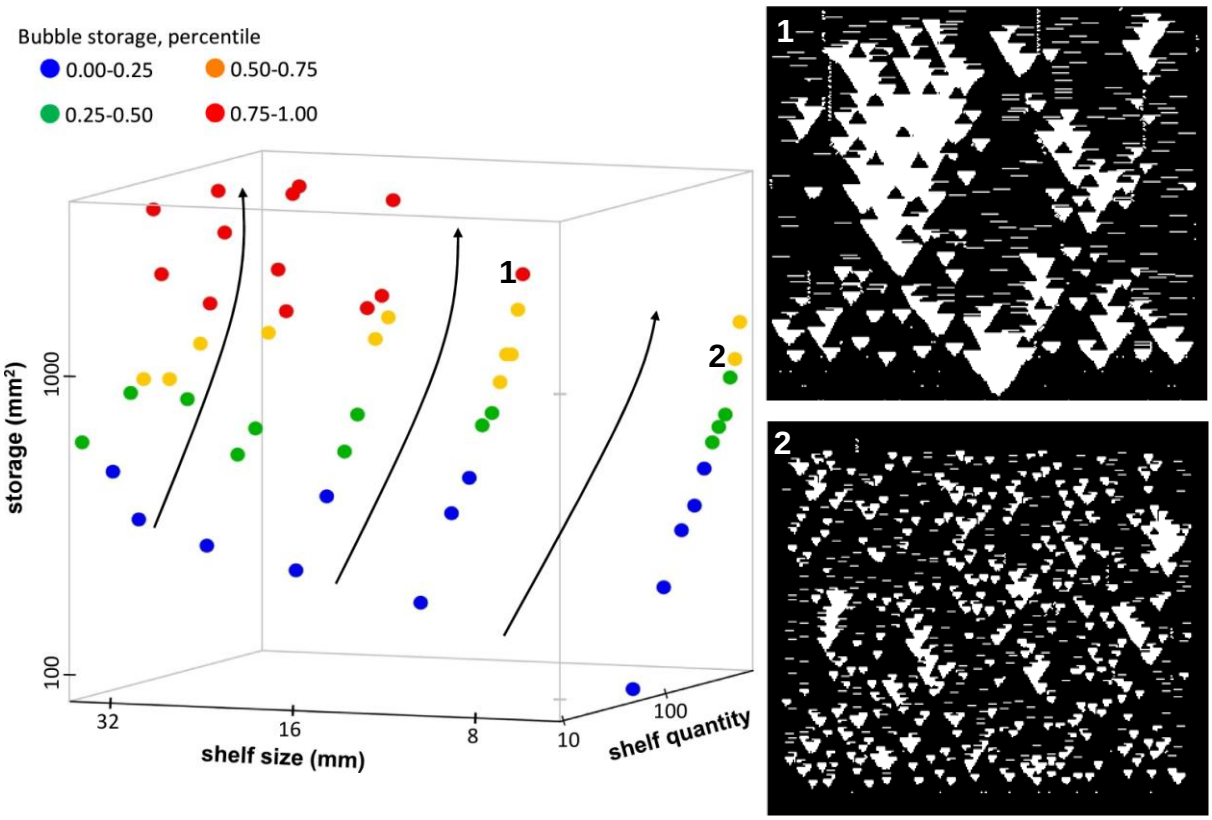

Figure 11. Relationship between bubble storage and shelf arrangement.

The storage of bubbles within shelf arrangements with different shelf lengths and shelf quantities. Points are coloured according to percentiles of all bubble storage records (note the logarithmic scale for shelf quantity, and storage). Insets 1 and 2 are shelf arrangements with the same total shelf length.

Previously, it was noted that observed patterns in gas storage indicate that greater amounts of stored gas coincide with locations of low-permeability or porosity peat that trap gas. In this sensitivity analysis MEGA is able to replicate this gas storage pattern. Shelf arrangements that consist of many large shelves represent low porosity/permeability peat, and shelf arrangements with few small shelves are high porosity/permeability peat. From the plot in Figure 11 the pattern between peat porosity/permeability and gas storage is evident; shelf arrangements with many

large shelves (low porosity/permeability) trap the greatest amount gas, whilst shelf arrangements with few small shelves (high porosity/permeability) trap the lowest amount gas.

2.4.1. Patterns in bubble sizes

Although bubble-size data for peat does not exist, MEGA's output for this variable were collected and analyzed to determine which patterns emerge. One of the characteristics of the original sand pile model, and many self-organized critical systems, are power-law distributions summarizing the magnitude and frequency of system events [*Turcotte*, 2001]. For the *Bak et al* [1987] sand pile model, the magnitude and frequency of avalanche sizes produced a power law distribution. Likewise, MEGA, consisting of inverted sand piles, also displays a power law relationship between frequency and bubble size. This relationship can be summarized by a power function (Eq. 1), where y is the frequency of a bubble size, a is a constant, x is the bubble size and b is the function's rate of decay (b<0).

$$y = ax^b \qquad (1)$$

A common way of checking whether a set of data conforms to a power law distribution is to produce a histogram using logarithmic scales for frequency (y-axis) and magnitude (x-axis). The nonlinear scaling of the log axes causes the power function to produce a straight line with a slope equal to the rate of decay (b) of Eq. 1. This method was selected to analyze the bubble size data for signs of power law distributions. Even though this method is not the most statistically rigorous [*Clauset et al.*, 2009], it is suitable for the purposes of this analysis, which is not to prove that bubble size strictly conforms to power laws, but to extract discernible patterns in the data.

For each shelf arrangement simulation, bubble size count data were binned using 10 equal intervals spanning the range of data values. Afterwards, the frequency of each bubble size interval was normalized between zero and one by dividing each frequency by the sum of all frequencies. To estimate the parameters of a power law, bubble size and normalized frequency were log transformed and a linear regression was preformed to derive the slope and y-intercept which, respectively, correspond to the rate of decay (*b*), and the constant (*a*) of a power function. To provide a goodness fit between the bubble size observations and the fitted power function an F-test was performed, with *p*-values adjusted for multiple comparisons [*Bland and Altman*, 1995]. At present, all bubble size frequencies from MEGA have displayed power law behaviour, but if future simulations produce bubble sizes that deviate from this pattern, other distributions for summarizing the data will be considered.

Applying this method to bubble size data from an example of small, medium, and large shelf types demonstrates that frequency distribution of bubble sizes from MEGA display power law patterns (Figure 12). This pattern reveals that small bubbles occur frequently, and larger bubbles occur less frequently. Interestingly, the three examples have similar rates of decay in bubble size (*b*), but markedly different maximum bubble sizes. Here the data suggests a secondary pattern that relates bubble storage to bubble size. The difference in bubble size between the shelf arrangements can be explained by the storage capacity of each shelf arrangement which is a product of shelf length and quantity. In general, shelf arrangements that have high storage capacity have a tendency to develop taller sand piles which can shed longer chains of bubbles (i.e., larger bubbles) from their

slopes (Figure 13 b,c), whereas shelf arrangements with low storage produce shorter sand piles, and smaller bubble chains (Figure 13a).

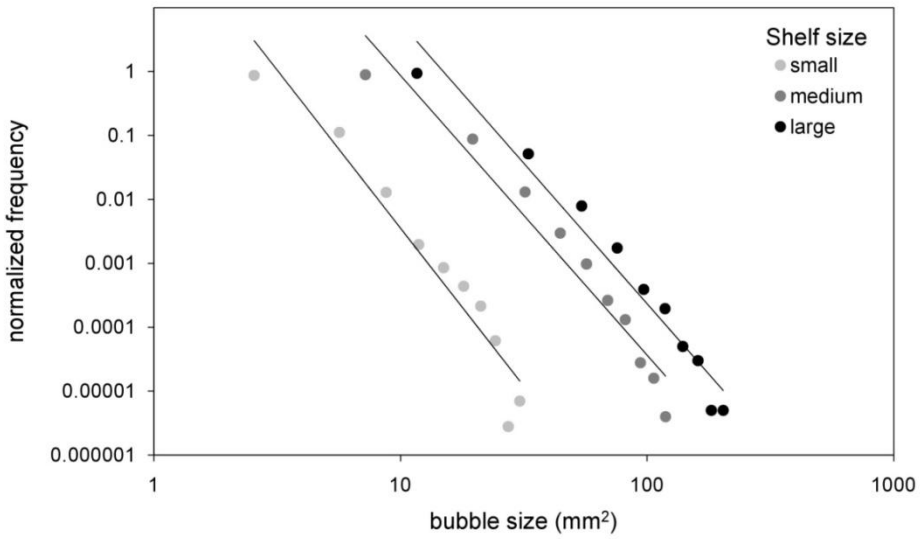

shelf type	shelf length, mm	quantity	*a*	*b*	bubble storage, mm^2	max bubble size, mm^2
Small	6	120	311	-4.9	1840	32
Medium	18	120	20589	-4.4	11008	125
Large	36	60	144021	-4.4	18066	214

Figure 12. Examples of bubble size distributions and corresponding power functions, and summary statistics.

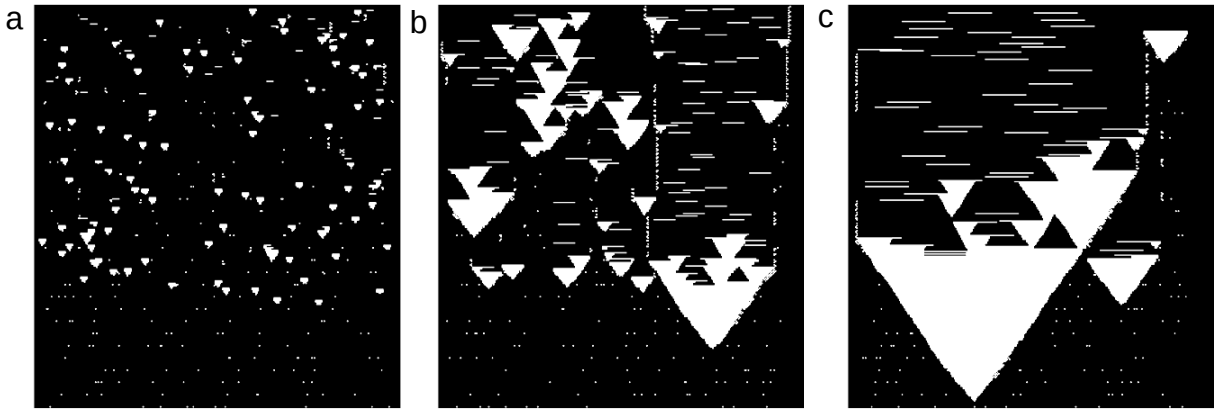

Figure 13. Storage of different shelf arrangements.

Shelf arrangements consisting of (a) 120 6-mm shelves, (b) 120 18-mm shelves, and (c) 60 36-mm shelves. (a) Low, (b) medium and (c) high storage , results in different sand pile heights, and different bubble sizes.

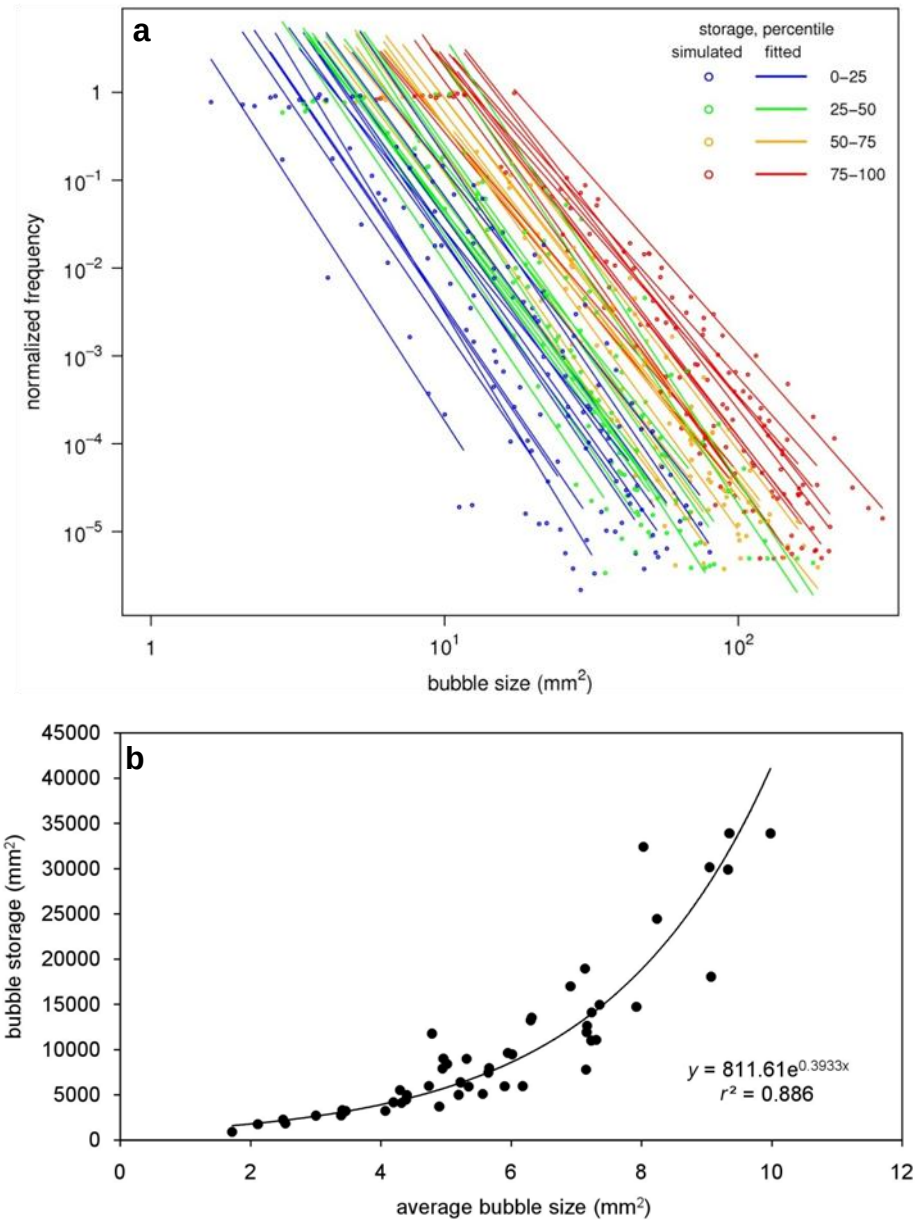

Figure 14. Patterns in bubble sizes from numerical model.

(a) Simulated bubble size magnitude and frequency with fitted power law distributions ($p < 0.05$) shaded according to percentile of bubble storage. (b) Exponential correlation between average bubble size and bubble storage.

In the following analysis a direct linkage between bubble storage and bubble size is made by colouring the fitted bubble size power laws from the sensitivity analysis simulations according to the previously defined percentile classes for bubble storage (0-25th, 25th-50th, 50th-75th, and 75th-100th percentiles) (Figure 14a). Here it

is possible to observe that all bubble size distributions follow a power law pattern (p<0.05).

Furthermore the rate of decrease in bubble size is fairly constant for all shelf arrangements ($\bar{x}$ slope = -4.5, σ slope = 0.4), but the effect of increasing bubble storage causes the bubble-size distributions to shift along the *x*-axis, and provides further evidence for the secondary pattern that shelf arrangements with high storage capacity produce larger bubbles than low storage capacity shelf arrangements. To test this hypothesis quantitatively, the average bubble size per arrangement was calculated and directly compared against total bubble storage (Figure 14b). The resulting relationship summarizes how average bubble size exponentially increases as bubble storage increases.

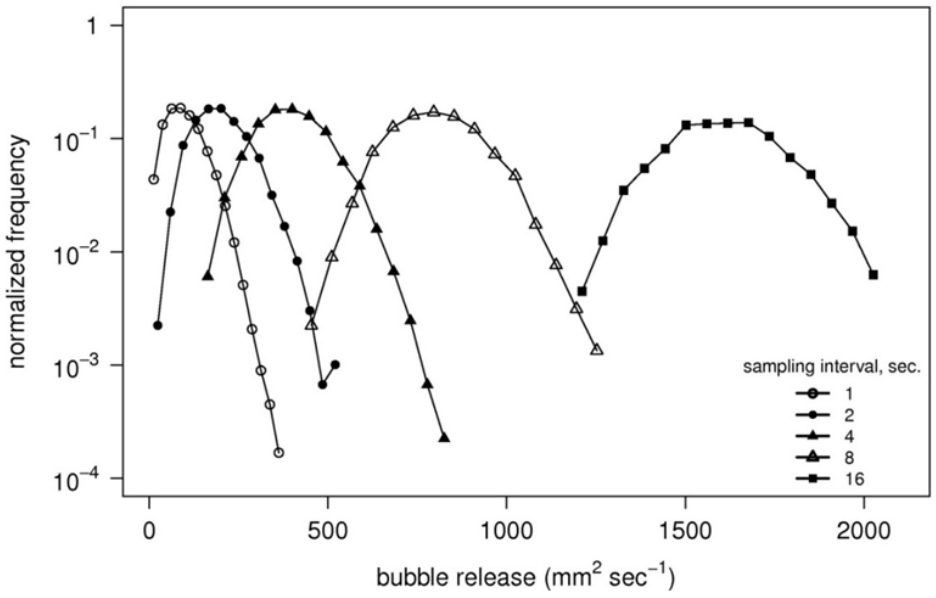

Figure 15. Effect of sampling interval of bubble release.

Frequency plot of bubble release sampled at increasing time intervals (points are connected with lines for clarity, no continuity should be inferred).

2.4.2. Patterns in bubble release

Observed patterns of bubble release magnitude and frequency from peat are characteristically non-normal and positively skewed. To test if MEGA can replicate this pattern, bubble release data were generated by summing the total amount of bubbles exiting each shelf arrangement over a time interval. Aware that the length of the sampling time interval chosen affects bubble release, a series of trial simulations with one shelf arrangement were performed using increasingly larger sampling times (Figure 15). The results confirm that small sampling times (<4 s) produce positively skewed frequency distributions and larger sampling times produce distributions more symmetrical in shape. It was decided to sample bubble release every 1 s in the following analysis to observe bubble release at a fine temporal resolution.

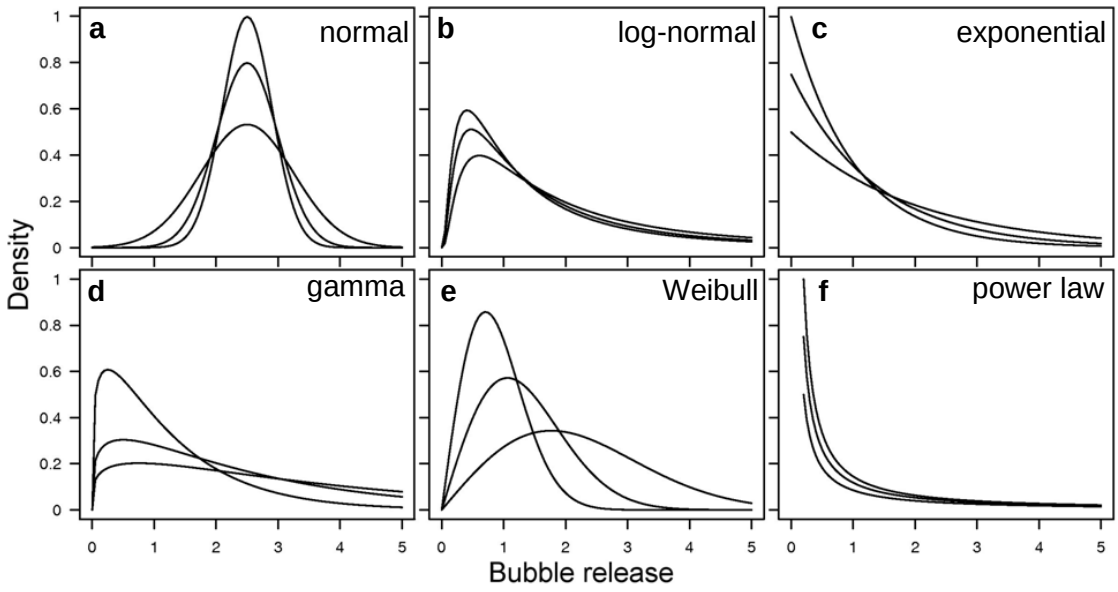

Figure 16. Candidate distributions fitted to bubble release.

Examples of (a) normal, (b) log-normal, (c) exponential, (d) gamma, (e) Weibull and (f) power law distributions.

For each bubble release time series histograms were produced by binning the release data into 10 classes of equal interval, and normalizing the frequency, as per the bubble size data. What resulted was a mix of symmetrical and positively-skewed histograms, and a review of distributions with similar shape were identified for further distribution fitting (Figure 16). Here, the objective was to summarize general patterns in the bubble release with distributions and not to demonstrate that bubble release can be represented by a particular statistical distribution. For this reason, the best fitting distribution amongst possible candidate distributions was selected using the Akaike Information Criterion (AIC) [*Akaike*, 1974]. AIC is a measure of relative goodness of fit that is commonly used to select amongst possible distributions, and it is not an absolute test for goodness of fit.

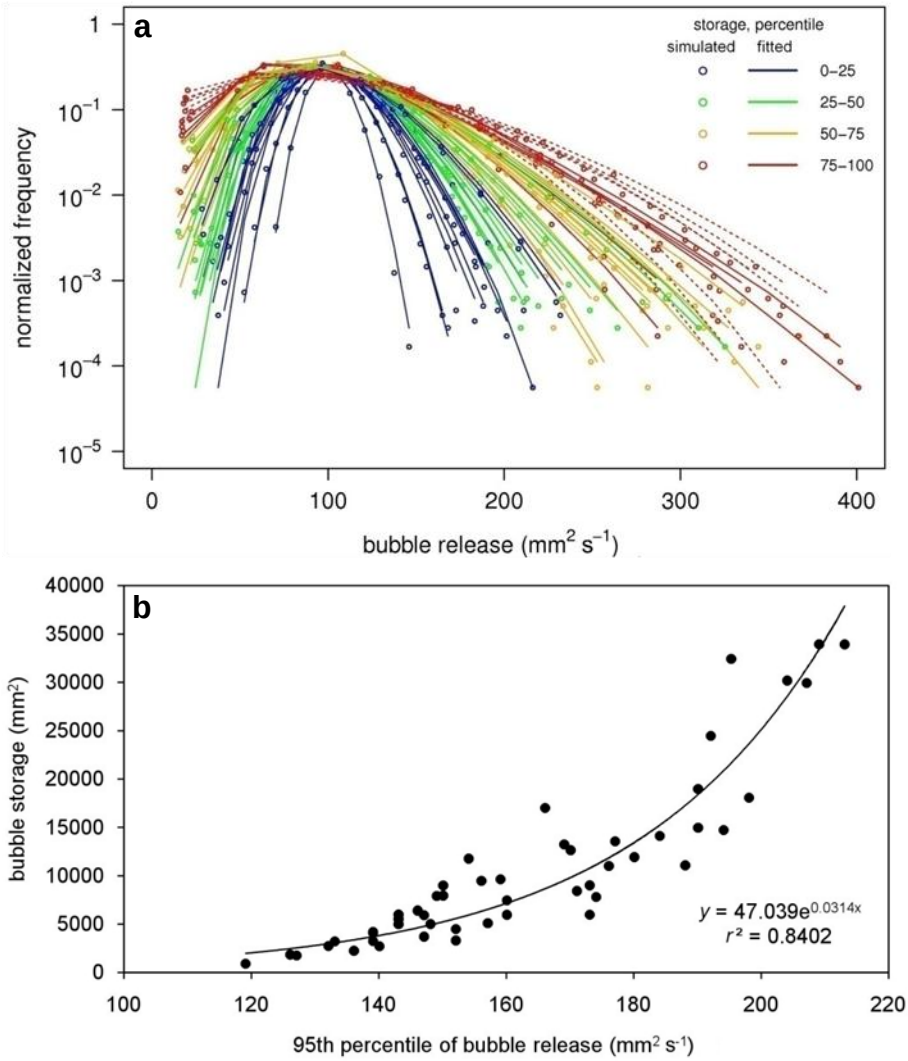

Figure 17. Patterns in bubble release from numerical model.

(a) Simulated bubble release magnitude and frequency with fitted gamma (solid line) or Weibull (dashed line) distributions shaded according to percentile of bubble storage (note log scale on y-axis). (b) Exponential correlation between 95th percentile of bubble release, and bubble storage.

The resulting fitted distributions to bubble release from MEGA were similar to the positively skewed, non-normal distribution patterns found in observed CH_4 ebullition from peat (Figure 17a). Of the 51 simulations of shelf length and quantity, 44 were fitted to gamma distributions, and 7 to Weibull distributions. The shape of these distributions provides evidence that small bubble releases occur frequently, and larger events are rare. The most frequent magnitude bubble

release occurs at about 100 bubbles; this is the approximate mean of all the distributions, and is equivalent to the number of bubbles entering the simulation (100 bubbles s^{-1}). A noticeable difference between the fitted distributions is that some distributions are almost symmetrical, whilst others are asymmetrical. This asymmetry is mostly pronounced in the tails of all the distributions that extend from 150-422 bubbles s^{-1}.

An explanation for the variability in bubble release can be found in the amount of bubble storage per peat profile. This relationship between bubble release and storage becomes apparent when the bubble release distributions are coloured according to the bubble storage percentiles (Figure 17a). As demonstrated earlier, bubble storage regulates bubble size, and this is also reflected in bubble releases, which is bubble size summed over a time interval. The emergence of this secondary pattern indicates that shelf arrangements with high storage capacity produce larger bubble release than low storage capacity shelf arrangements. Further evidence for this pattern is supplied by extracting the bubble release 95^{th} percentile, as a metric of near maximal dispersion, from each simulation and comparing it against bubble storage to derive an exponential relationship (Figure 17b).

2.5. Physical models of gas transport and ebullition

Hardware models of bubbles in saturated porous media have been constructed to collect laboratory observations of gas flow patterns [Kong et al., 2010], the sizes of bubbles emerging from granulated media [Meier et al., 2011], and bubble velocities [Roosevelt and Corapcioglu, 1998]. These physical models are often simplified

porous media, consisting of glass beads or sand, and are packed to form homogenous structures. Under these simplified conditions, physical models have proved useful for testing numerical models of bubble movement. For example, *McCray and Falta* [1997] validated a numerical model of multiphase flow with observations of gas plume shape and size measured in a physical model consisting of a water filled tank of glass beads with less permeable layers [*Ji et al.*, 1993]. Likewise, *Corapcioglu et al.* [2004] parameterized and validated their mathematical model of bubble velocity with observations of terminal bubble velocity measured within a physical model of water saturated glass beads [*Roosevelt and Corapcioglu*, 1998]. This thesis also adopts the approach of comparing patterns from physical and numerical models. Here, physical models are used to generate observations of bubble storage, size, and release that are analysed for patterns. These patterns are compared directly to patterns extracted from bubble storage, size, and release output from MEGA.

The first physical model, the shelved bubble machine (SBM), is a water tight, thin (10 mm) enclosure that can be fitted with various shelf arrangements (Figure 18a). The SBM was designed to closely resemble MEGA which represents a 2D space, and lacks depth. The frame of the SBM is constructed out of opaque plastic, the remaining parts are clear Perspex (acrylic), and the shelves are made from high density foam. Operation of the machine begins by arranging the shelves, sealing the enclosure, and filling it with water. Next, precise amounts of air are delivered automatically from syringes to needles inserted in seven openings fitted with rubber septa at the base of the SBM. The needles produce bubbles that move up the enclosure and become trapped underneath the shelves. Here a video camera

is positioned to record bubble storage under shelves. Eventually bubbles of various sizes are released from the shelves and enter a shelf free part of the enclosure (dashed area Figure 18a). At this location bubbles are video recorded using a second video camera to later extract bubble sizes. Next the bubbles make their way to an air tight cylindrical gas trap located at the top of the SBM. When the air enters the gas trap it lowers the water level by displacing a quantity of water that exits the machine via a tube. A third video camera is positioned to record the gas trap and estimate the volumetric rate of bubble release. The water exiting the SBM enters a completely water filled small beaker and the water is allowed to overflow into a larger beaker. When the water level within the larger beaker approaches the level of the smaller beaker, the experiment is stopped, and the larger beaker is emptied. By maintaining the water level of the smaller beaker constant, the water pressure within the physical model remains the same throughout all experimental runs.

A second physical model, the cylindrical bubble machine (CBM), was designed and constructed to hold a sample of peat (Figure 18b). The operation of this machine is similar to the shelved bubble machine, but the major difference is the insertion of a peat sample into a cylindrical enclosure. The peat lies at the base of the machine and 16 needles are inserted into the base of the peat at the same depth. Video cameras are used to record the size of bubbles exiting the peat surface (dashed area Figure 18b) and total gas release collected in the gas trap. The succeeding chapters will provide details of how both machines were used to generate data on bubble storage, release and size.

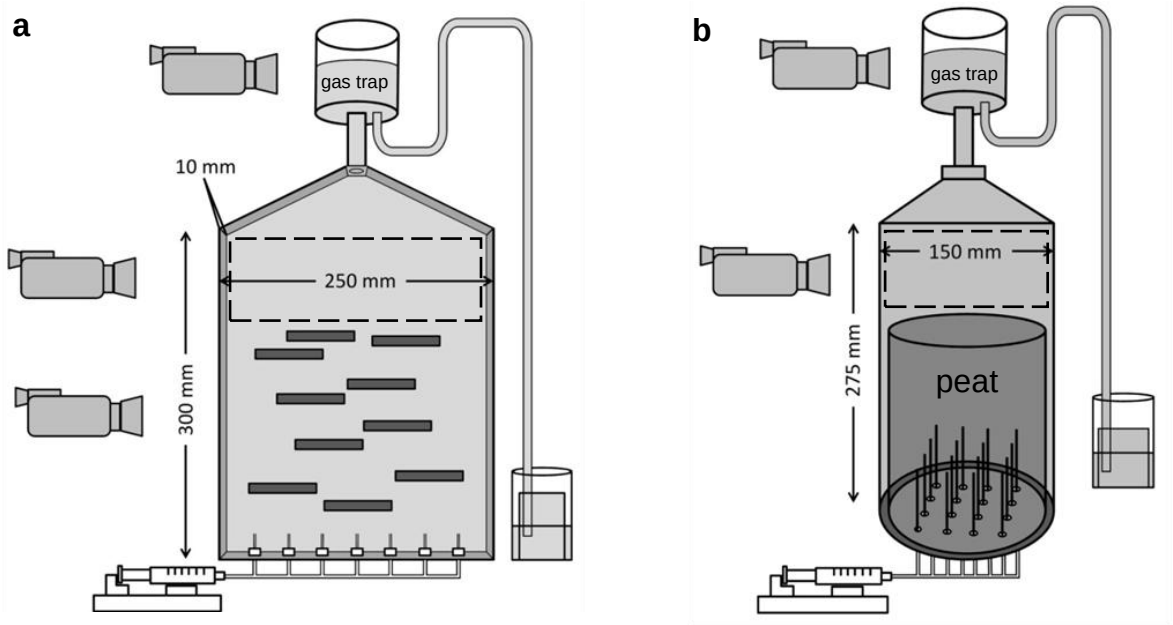

Figure 18. Schematic of (a) shelved bubble machine and (b) cylindrical bubble machine.

Chapter 3 Testing of MEGA

3.1. Introduction

In the previous chapter, a Pattern Oriented Modelling (POM) approach was used to highlight similarities between patterns found in gas storage and ebullition in peatlands and MEGA. Below is a summary of the patterns identified and the model processes/properties included within MEGA to reproduce these patterns (Table 1). These patterns will be the metrics used in the subsequent chapters to test MEGA. Specifically in this chapter, the intention is to test MEGA by generating patterns of bubble storage, size and release using a physical analogue of MEGA, the Shelf Bubble Machine (SBM). The laboratory experiments are replicated in MEGA, and the resulting patterns are directly compared to those produced by the SBM.

Table 1. Summary of patterns and processes.

Patterns from peatlands and MEGA. Processes and properties included in MEGA to produce identified patterns in ebullition from peat.

	Pattern in peat	Pattern in MEGA	Model process/property
Bubble storage	Increasing gas storage with low peat porosity or permeability.	Shelf arrangements with many large shelves store more gas than arrangements with fewer small shelves.	Spatial representation of pore structure Bubble coalescence Surface tension holds bubble in pore
Bubble size	Not available	Small bubbles occur frequently, and larger bubbles occur less frequently. Shelf arrangements with high storage capacity produce larger bubbles than low storage capacity shelf arrangements.	Bubble coalescence
Bubble release	Small ebullition events often occur, and extreme bubbling events are rarer.	Small bubble release occurs frequently, and larger events are rarer. Shelf arrangements with high storage capacity produce larger bubble release than low storage capacity shelf arrangements.	Buoyancy overcomes surface tension

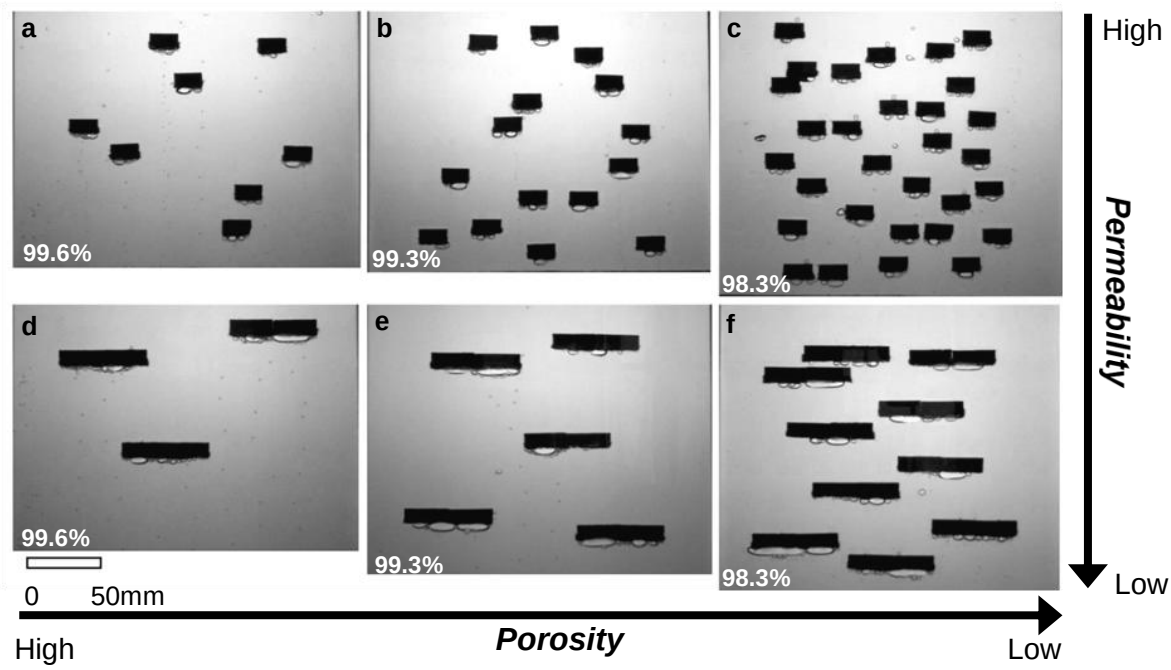

Figure 19. SBM shelf arrangements.

Arrangements with shelf lengths of (a, b, c) 20 mm and (d, e, f) 60 mm. Porosity of shelf arrangements indicated.

3.2. Methods

As described in Chapter 2, the SBM was designed as a 1:1 scale representation of MEGA. Before conducting the experiments within the SBM, several prototype physical models were constructed and trialled to develop the methods presented in this section (Appendix, Section 2). Two sets of experiments were performed with the SBM using different sizes and quantities of shelves. The first set of experiments utilized smaller shelves 20 mm x 1 mm, and three shelf arrangements were produced with eight, 15, and 30 shelves (Figure 19 a,b,c). A second set of experiments used larger 60 mm x 1 mm shelves in quantities of three, five, and 10 shelves (Figure 19 d,e,f). These shelf arrangements were chosen to investigate the effect of porosity and permeability on bubble storage, size, and release. Three levels of shelf arrangement porosity (99.6%, 99.3%, 98.3%) and two levels of

permeability were constructed (Figure 19). With relation to actual peat structure, the smaller shelf arrangements represent peat that is highly permeable, and arrangements with larger shelves are peats that are less permeable. The porosity of shelf arrangements is controlled by increasing the quantity of shelves. Arrangements with few shelves represent higher porosity peat (Figure 19 a,d), and arrangements with more shelves are lower porosity peat (Figure 19 c,f).

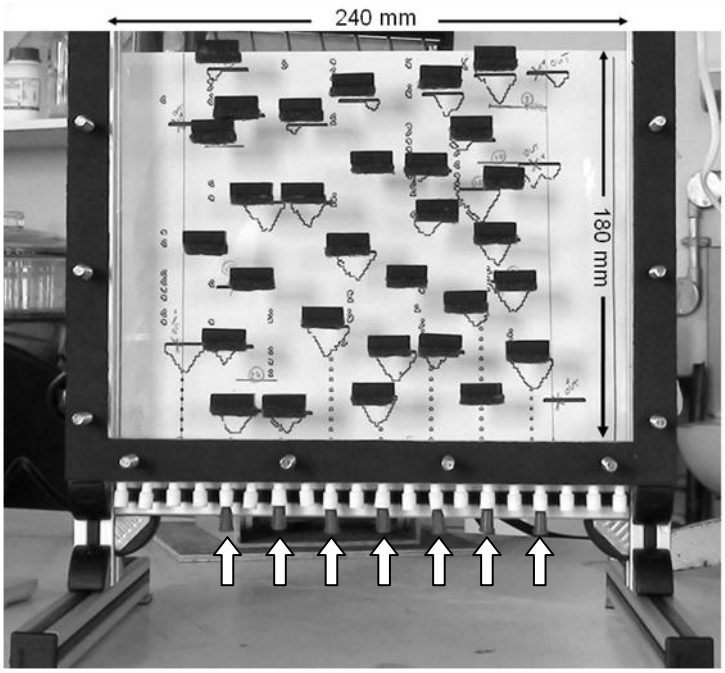

Figure 20. SBM model shelf set-up.

Blueprint of 30 randomly placed 20-mm shelves produced using MEGA, and used to arrange shelves in the SBM. Some shelves do not correspond to blueprint because shelves were rearranged to ensure that every shelf could potentially intercept bubbles injected into the SBM from below (white arrows).

Prior to running the experiments with the SBM, preliminary numerical simulations were performed with MEGA to determine the placement of the shelves within the SBM. MEGA was set up with dimensions similar to those in the SBM (240 mm x 180 mm), and shelves were placed within the area using a random number generator to select a location. The resulting shelf arrangement was drawn as an

image and printed to produce a 1:1 scale blueprint to guide placement of shelves within the SBM (Figure 20). Further adjustment of shelf location was made to ensure that every shelf could potentially intercept bubbles added to the SBM from below. Shelves were prepared by gluing sections of scouring pad to each shelf underside. The scouring pad increases the shelf roughness and promotes bubble accumulation underneath shelves. Double-sided tape was used to fix the shelves to the bubble machine walls.

Seven 30-gauge blunt dispensing needles were inserted into the base of the shelved machine and connected via tubing to 10 mL syringes. Syringes were filled with air and loaded onto a syringe pump that was programmed to deliver 0.03 mL s^{-1}. The resulting steady bubble production from each needle was 9 bubbles sec^{-1}, with bubbles averaging 1 mm in diameter. Emptying of the seven syringes took 273 s, and 60 mL of air was injected at a rate across all syringes of 0.22 mL s^{-1}. Five complete injections were performed for each shelf arrangement. Data from all five injections were aggregated into one dataset for analysis of each shelf arrangement.

To highlight bubble edges, the SBM was fitted with a uniform background consisting of a frosted plastic sheet, with backlighting for the shelves provided by a 500-W halogen lamp and a separate halogen light for the gas trap. Furthermore, to help differentiate between air and water, the water within the SBM was dyed blue. Data on bubble storage, size and release were collected simultaneously at three locations using high-definition cameras (Sony HDR-SR10E, Sony HDR-XR105E, Kodak Zi8) recording at 50 frames per second (fps) (Figure 21a).

Throughout the experiment bubble storage was defined as the total area of air underneath a shelf (Figure 21b). Bubble size is the area enclosed by the edge of a bubble and was recorded within the SBM in an area above the shelf arrangement that contained no shelves (Figure 21c). The volumetric rate of bubble release was recorded at the top of the bubble machine within a cylindrical gas trap. Bubbles enter the trap and displace water that flows out of the trap via a tube fitted to its base. Bubble release is the change in the area occupied by water within the cylinder when the cylinder is viewed from the side (Figure 21d).

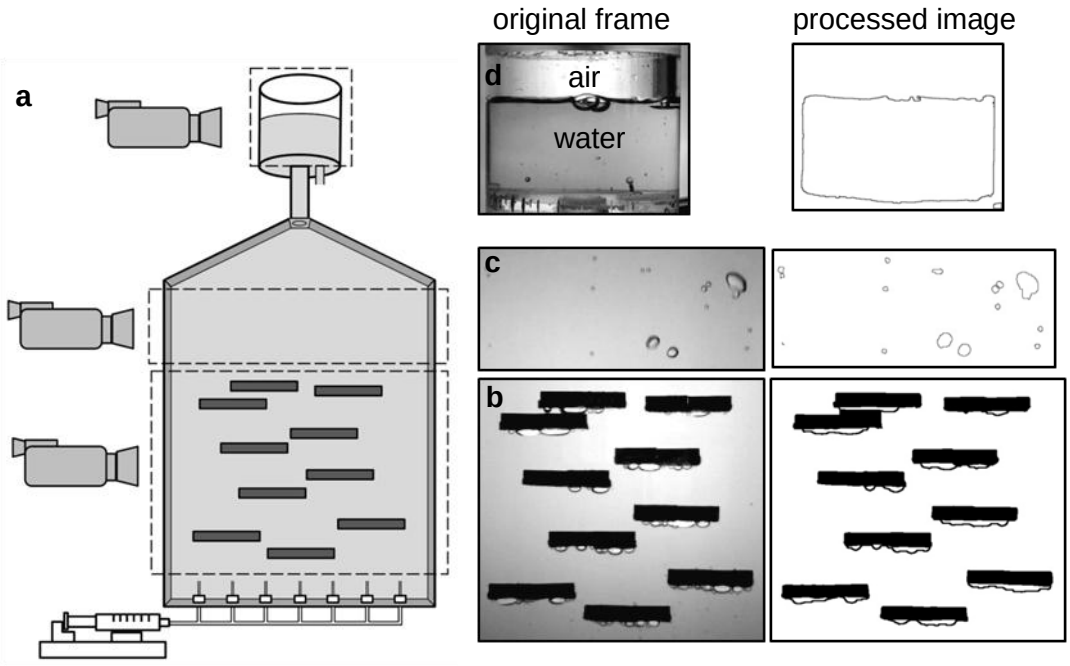

Figure 21. Camera positions and analysis of bubble storage, size, and release.

(a) Field of view of three video cameras recording bubble storage, size, and release (dashed polygons). Original frames and processed images of (b) bubble storage, (c) size and (d) release.

All video footage was converted into images to extract measurements of bubble storage every 1 s, bubble sizes every 0.5 s, and bubble release every 1 s. Sampling bubble sizes every 0.5 s meant that all bubbles exited the camera's field of view before the next measurement; therefore, bubbles were not double counted.

This method did not allow every bubble to be measured, but a sufficient number of bubbles could be measured to construct a reliable bubble size distribution. Images were automatically processed within an image processing program (ImageJ, [*Schneider et al.*, 2012]) using customized image-processing scripts (examples provided in Appendix, Section 4). A Sobel edge-finding technique [*Gonzalez and Woods*, 1992] was used to delineate and extract the area representing the bubble storage underneath each shelf (Figure 21b) and the size of bubbles exiting the model (Figure 21c). A colour-thresholding technique based on image hue saturation and brightness was used to measure the area of water within the cylinder used to collect released bubbles (Figure 21d). The performance of the image processing scripts was estimated by manually digitizing a subset of frames of bubble storage, size, and release and comparing them to values extracted automatically (Figure 22). Overall, there was sufficient amount of agreement between observed and extracted measurements to have confidence in the image-processing scripts. Further quality control of post-processed images found that bubbles with size <1 mm^2 were micro bubbles that formed on the interior surface of the SBM, presumably by dissolved gas coming out of solution, and were not included in the analysis.

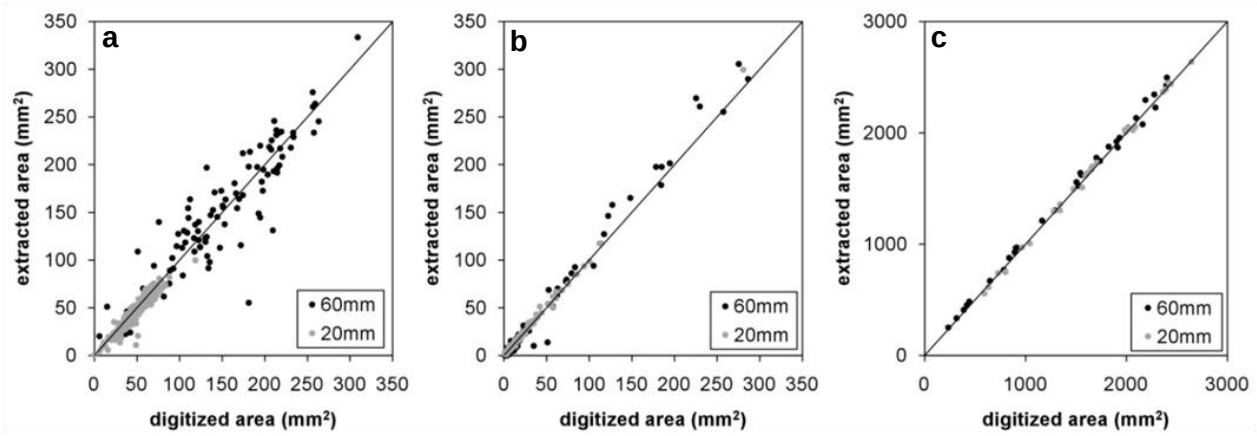

Figure 22. Validation of image processing.

Comparison between manually digitized and automatically extracted area of (a) bubble storage, (b) size and (c) release for shelf experiments with smaller shelves (20 mm) and larger shelves (60 mm).

For the measurements of volumetric rate of bubble release it was found that the minimum discernible amount of change in area of the gas trap containing water was approximately 17 mm^2 (equivalent to a 0.28-mm change in water level), and changes in area less than this amount were not analyzed. Furthermore, it was estimated that an area of 1 mm^2 within the gas trap is equivalent to an area of 4.7 mm^2 within the main tank of the SBM where bubble sizes are recorded. To convert bubble release and bubble sizes into a common unit of measure, all bubble release records were multiplied by 4.7.

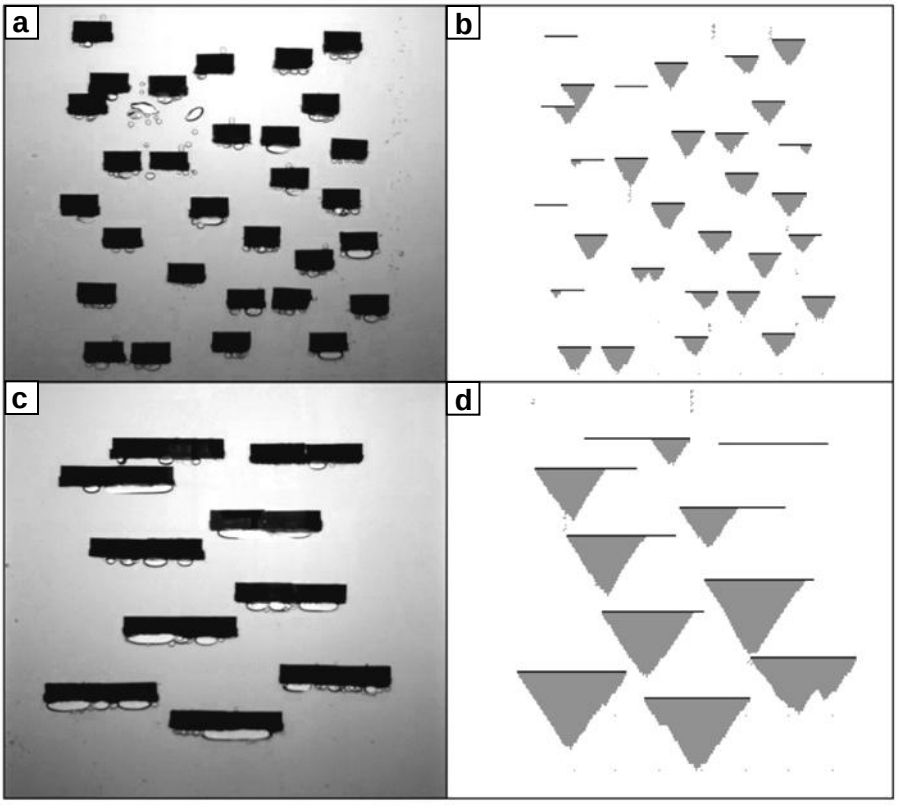

Figure 23. Examples of bubble storage in the CBM and MEGA.

Shelf arrangement and bubble accumulation within the CBM and MEGA using (a, b) smaller 20-mm shelves and (c, d) larger 60-mm shelves.

MEGA was set up to replicate as closely as possible the situation pertaining in a run of the SBM (Figure 23). The computational cells in MEGA were set to the same size as the bubbles released from the syringes in the SBM (1 mm). Bubbles within MEGA cannot accelerate, and bubble velocity is not dependent on bubble size. Therefore, all bubbles in MEGA, regardless of size, have a fixed terminal velocity. In Chapter 2 rise velocity in MEGA was set to 282 mm s^{-1} after measuring the terminal velocity of a rising 1-mm diameter bubble in clean water. This may have been an overestimation of bubble velocity because bubble velocity changes as bubbles are held up and released from shelves. To account for the interaction of bubbles with shelves, the rise velocity of bubbles in MEGA was set to

the maximum observed terminal velocity (185 mm s^{-1}) of a bubble in water saturated porous medium [*Corapcioglu et al.*, 2004; *Roosevelt and Corapcioglu*, 1998]. As in the SBM, bubbles were added at the base of MEGA at seven locations at a rate of nine bubbles s^{-1}, and a size of 1 mm^2. Each simulation was run for 1000 s, which is comparable to the duration of video processed from all five injections for each shelf arrangement.

Prior to collecting data on bubble storage, size and release, shelf arrangements within MEGA were saturated with bubbles to allow 'sand' piles to develop fully. Every 1 s a screenshot of the bubbles accumulating under the shelves within MEGA were saved and image processing scripts were developed to calculate the area of bubbles beneath each shelf. As described in Chapter 2, individual bubbles consisted of vertical chains of pixels that were proximate to each other, and bubbles separated by ≥1 cm were considered separate bubbles. The separation threshold of 1 cm was set after running preliminary runs of MEGA, and noting that lower thresholds limited MEGA output to small bubbles, but a threshold greater than 1 cm would represent a separation distance between bubbles that is unrealistic. Bubble sizes exiting the model were measured continuously, and bubble release was calculated by summing the size of the bubbles exiting the top of the model every 1 second.

The performance of MEGA was measured by its ability to match patterns in bubble storage, size and release produced by the SBM. In both models, mean storage was calculated for each shelf arrangement, and histograms of bubble size and

release were fitted with the distributions from the candidate distributions presented in Chapter 2.

3.3. Results

A trend of increasing values was found in bubble storage in the SBM and MEGA, and this storage pattern is related to the interaction between shelf porosity and permeability (Figure 24). Higher porosity shelf arrangements represented by fewer shelves consistently stored less gas than lower porosity arrangements consisting of more shelves. This relationship between gas storage and porosity is found in both the SBM (Figure 24a, c) and MEGA (Figure 24b, d). Furthermore, in both models, the increase in average bubble storage was positively related to the number of shelves and this was true for both small and large shelf arrangements (20-mm shelves: mixed factor ANOVA, with model type SBM and MEGA as random factor: F=5852.805; p<0.0001) and (60-mm shelves: mixed factor ANOVA, with model type, SBM and MEGA as random factor: F=4675.915; p<0.0001).

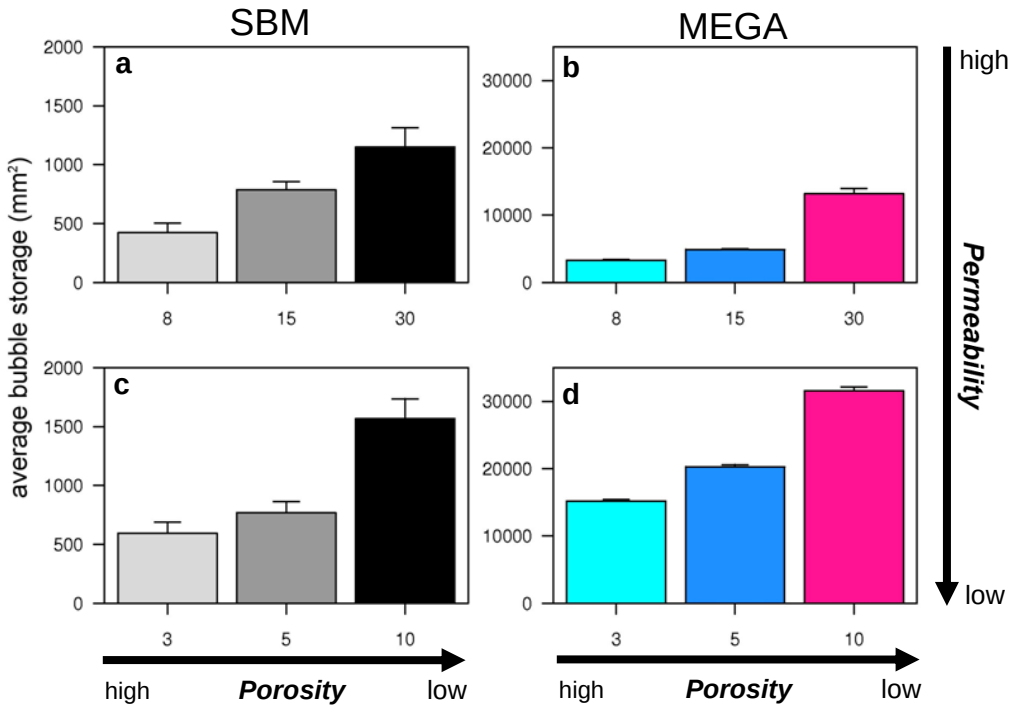

Figure 24. Comparison of bubble storage patterns.

Average and standard deviation of total bubble storage of SBM runs (grayscale) and MEGA simulations (colour) for shelf sizes of (a, b) 20 mm and (c, d) 60 mm.

The effect of shelf arrangement permeability is to amplify the positive trend in average bubble storage. This amplification is most apparent in MEGA where the combined average bubble storage from low permeability shelf arrangements (Figure 24d) was 103% greater than the combined average bubble storage from all high permeability arrangements (Figure 24b). The difference between SBM bubble storage within high and low permeability shelf arrangements is more subtle (Figure 24 a,c), with the greatest increase in average storage occurring between arrangements of low porosity.

The relationship between bubble size and frequency produced in the SBM and MEGA reflects a power-law pattern, where small bubbles occur frequently and larger bubbles occur less frequently (Figure 25). Bubble-size predictions from

MEGA were consistently smaller than the observed sizes recorded in the SBM. The effect of porosity on bubble size is seen in Figure 25 a,b where, regardless of shelf size, increasing the shelf quantity in the SBM and MEGA (i.e., decrease shelf arrangement porosity) produces larger bubbles. It was also observed in both the SBM and MEGA that shelf arrangements with larger shelves (low permeability, Figure 25b) generated larger bubbles than arrangements with smaller shelves (high permeability, Figure 25a).

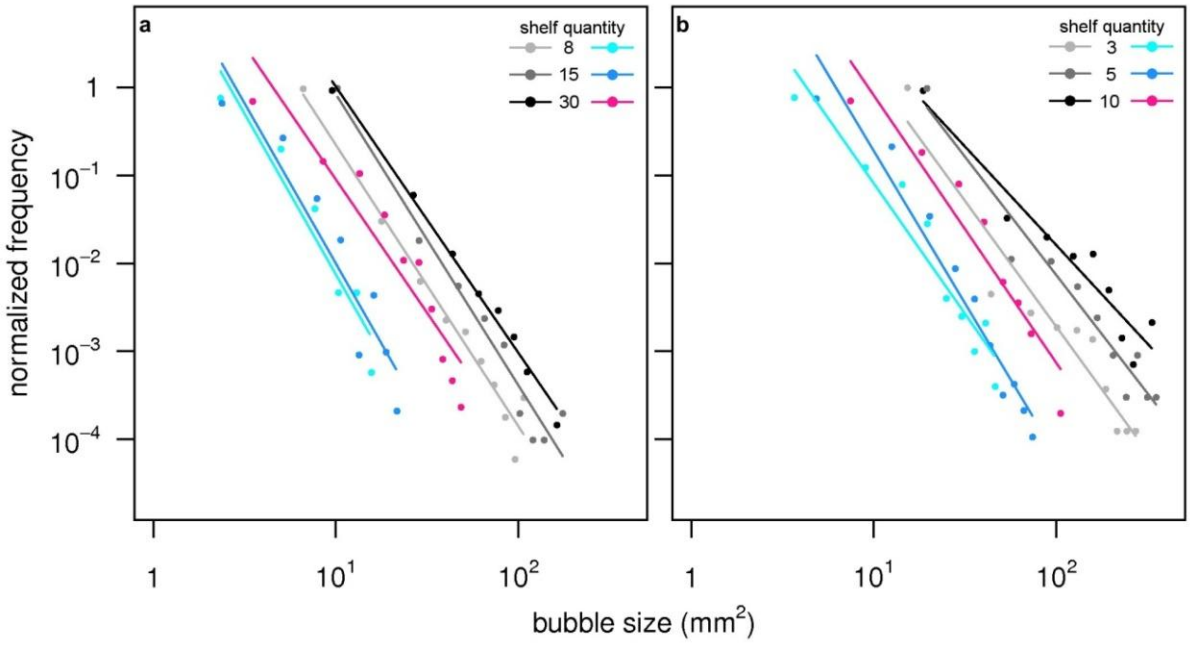

Figure 25. Comparison of bubble size patterns.

Bubble size probability density functions from SBM runs (greyscale), and MEGA simulations (colour) for (a) smaller 20-mm shelves and (b) larger 60-mm shelves. All fitted power law distributions have $p<0.05$ and $r^2>0.86$.

Bubble releases in MEGA and the SBM both exhibit power-law patterns (Figure 26), where small bubbling events occur frequently, and larger, extreme bubbling events are rarer. Even though this pattern exists in both models, MEGA considerably under predicts bubble release magnitude and frequency, and produces steeper power-law functions than the SBM. Furthermore, bubble

releases in the SBM and MEGA are contingent on the quantity and size of shelves. Generally, shelf arrangements with greater quantities of shelves (low porosity) or larger shelves (low permeability) produce larger bubble releases than structures with fewer shelves (high porosity) or smaller shelves (high permeability).

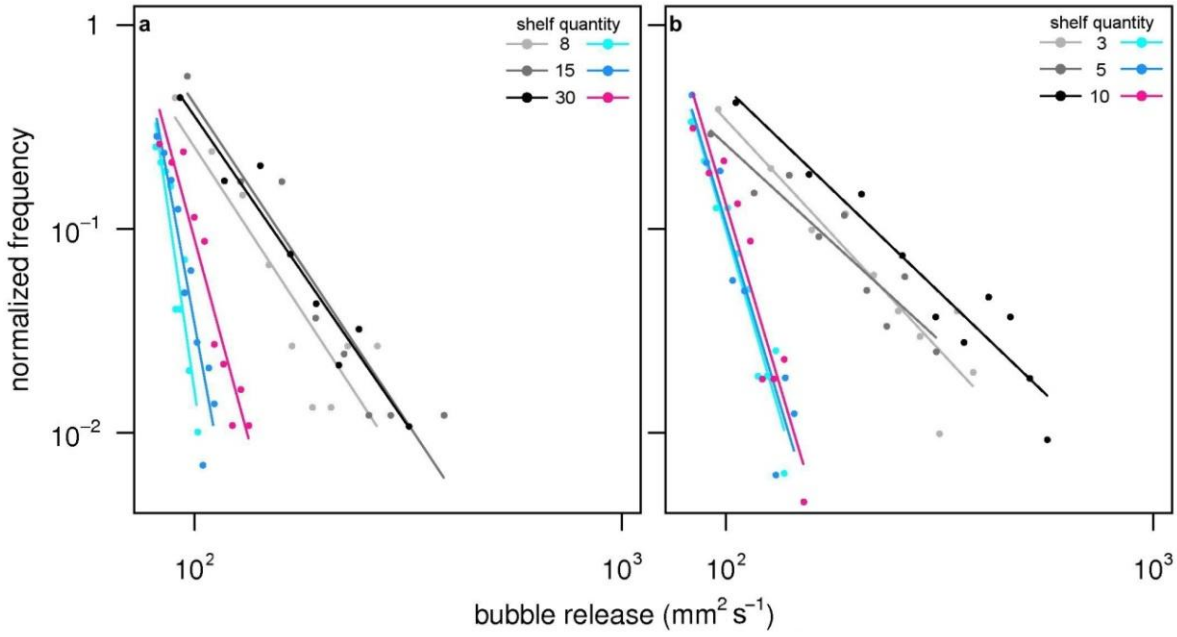

Figure 26. Comparison of bubble release patterns.

Bubble release histograms from the SBM runs (grayscale), and MEGA simulations (colour) for (a) smaller 20-mm shelves, and (b) larger 60-mm shelves. All fitted power law distribution have $p<0.05$ and $r^2>0.76$.

3.4. Discussion and Conclusions

This experiment demonstrates that a simple computer model is able to reproduce general patterns found in ebullition. Similarities between SBM and MEGA include:

1. Increasing gas storage with decreasing shelf permeability and porosity.
2. Positively skewed, non-normal (power law) patterns in bubble sizes and bubble release.
3. Larger bubbles and release with decreasing shelf permeability and porosity.

This provides evidence that the MEGA does contain the key processes and properties needed to model ebullition from the SBM. Furthermore, aside from changes in gas production, these findings indicate that the spatial structure of a porous medium is an important factor affecting ebullition magnitude and frequency. Specifically, the interaction between porosity and permeability determines how much gas is trapped within the porous medium and available for ebullition events. In this study, porosity of the porous medium was controlled by increasing shelf quantity and the permeability through shelf size. It was found that the combination of low porosity and low permeability shelf arrangements were most effective at intercepting and storing gas. These denser shelf arrangements exclusively produced extremely large bubbles and large release events when gas moved from shelf to shelf coalescing and destabilizing large amounts of stored gas. These rapid large bubbling events, in both the SBM and MEGA, are similar to large but rare ebullition occurring at field locations with low porosity/permeability peat layers possibly trapping and releasing gas [*Glaser et al.*, 2004; *Rosenberry et al.*, 2003]. A contrasting situation occurs in our study when shelf arrangements are highly permeable and porous. These shelf arrangements store less gas because they have a small surface area, and a lower probability of intercepting bubbles. As a result, less gas builds up in these arrangements and many bubbles never interact with shelves and may bypass storage altogether. The resulting ebullition consists of small bubbles and small release events, and is similar to ebullition measured at peatlands with loosely-packed (i.e., high porosity), and highly-permeable peat [*Goodrich et al.*, 2011].

To further bolster the patterns obtained from the SBM experiments it would have been necessary to have replicates for each shelf arrangement. For each arrangement this would require keeping the number of shelves the same, but repositioning the shelves, and performing the experiment again. This was not carried out due to the amount of time required to analyze the video of bubble storage, size and release. Although it is unlikely that different patterns would emerge from repositioning shelves, without replicates the conclusions reported remain less reliable.

There are several differences between the patterns from the SBM and MEGA. First, bubble storage in MEGA is 7-25 times larger than the storage in the SBM. This difference can be explained by gas storage in the SBM occupying a three dimensional space underneath a shelf. As a result, stored gas within the SBM assumes an ellipsoidal shape that imaged in profile has a small surface area. In MEGA, space is represented in two dimensions and stored gas is forced to accumulate as tall sand piles with large surface areas. As no physical model can be truly two dimensional, reducing the difference between observed and simulated storage would require the development of a three dimensional version of MEGA. By adding a third dimension gas could accumulate across all shelf dimensions by 'avalanching' in eight directions (i.e., Moore neighbourhood), as opposed to two directions in the current 2D version of MEGA.

Bubble sizes in MEGA are smaller than the SBM, and this may be caused by bubble deformations occurring in the SBM. The shape of a bubble is determined by the interaction of surface tension, viscous, and hydrodynamic forces [*Yang et*

al., 2007]. Bubbles less than 1 mm in diameter maintain a spherical shape due to surface tension forces minimizing the surface area of the bubble. As bubbles become larger, viscous, and hydrodynamic forces opposing vertical bubble movement will result in flattened or elongated bubbles [*Haberman and Morton*, 1953]. These larger bubbles, when measured in profile, will have surface areas that are greater than a spherical bubble of equivalent volume. Visually inspecting video frames of the bubbles generated from SBM indicated that a degree of elongation did occur in larger bubbles. This change in bubble geometry does not occur in MEGA, but this effect could be accounted for by applying a post-simulation correction factor to the bubble sizes. Accounting for bubble deformation in MEGA would also reduce the difference between observed and simulated bubble release. Bubble release within MEGA is directly calculated from bubble sizes. Thus, the under prediction of bubble sizes has produced smaller bubble releases.

Another reason for the differences in bubble size and release between the physical model and MEGA could be due to the manner in which bubbles are added to MEGA. Bubbles added to shelf arrangements in MEGA enter from below at a single location and move vertically without horizontal movement. After observing video from the SBM it was noticed that input bubbles move vertically and horizontally. Horizontal bubble movement, in the SBM, allows bubbles to access more of the shelf arrangement, which results in greater storage and larger bubble sizes and release. In MEGA horizontal bubble movement, except for avalanching, has not been developed, but adding this process to the computer model would lead to greater use of the shelf arrangement and may generate larger sandpiles that produce larger bubble sizes and releases. Thus adding horizontal bubble

movement to MEGA may reduce the differences between the physical and computer models.

Chapter 4 Ebullition patterns from peat

4.1. Introduction

In Chapter 3 experiments using the SBM were performed to test MEGA by comparing observed and simulated patterns of bubble storage, bubble size, and volumetric rate of bubble release. It was found that the structure of a porous medium, made of shelves, determines the amount of bubble storage and that this in turn affects the magnitude and frequency of bubble sizes and releases. The purpose of the work reported in this chapter was to supplement the existing data on bubble release from peat reported in the literature [*Goodrich et al.*, 2011; *Kellner et al.*, 2006; *Stamp et al.*, 2013], and in particular to generate data on bubble sizes because such data have not been collected previously. This information will be used to determine if the patterns that MEGA is capable of producing are similar to the patterns in peats. In this way, it will be possible to determine if MEGA is suitable for modelling ebullition from peat.

The experiments on ebullition from peat were performed using the Cylindrical Bubble Machine (CBM) introduced in Chapter 2. The CBM is operated in a similar way to the SBM, but (i) shelves are replaced with peat samples, (ii) different shelf arrangements are represented by structurally-different peats, and (iii) the injection of air into the peat samples represents the production of CH_4. In this way, the CBM becomes a physical model of ebullition in peat, but with the advantage of being able to record bubble sizes and rates of bubble loss, whereas most field [*Comas and Wright*, 2012; *Goodrich et al.*, 2011; *Stamp et al.*, 2013] and laboratory [*Green and Baird*, 2011; *Kellner et al.*, 2006] investigations of ebullition have only

recorded rates of bubble loss. Use of the CBM also makes it possible to control external variables that can affect ebullition including temperature [*Waddington et al.*, 2009], sunlight [*Panikov et al.*, 2007], and atmospheric pressure [*Tokida et al.*, 2005a]. Controlling these external variables is important because the CBM experiments was performed with different peat samples and, for the most part, differences in ebullition patterns between samples will not be caused by changes in external variables. Instead, the structural differences between the peat samples were used to explain the differences in ebullition patterns.

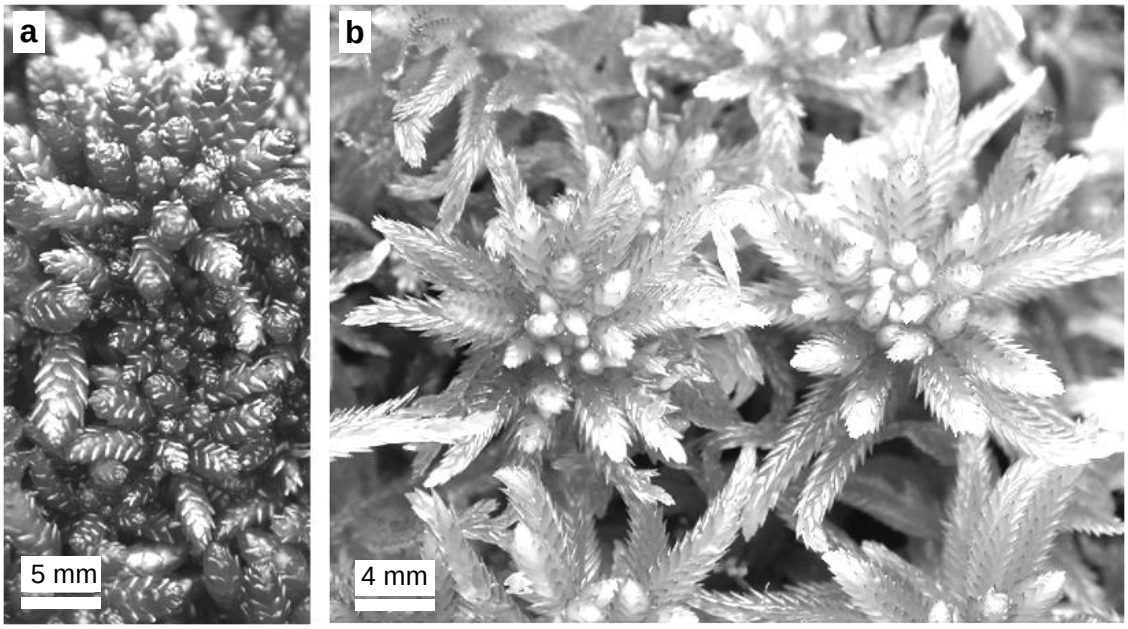

Source: www.bbsfieldguide.org.uk

Figure 27. (a) *Sphagnum magellanicum*, and (b) *Sphagnum pulchrum*.

4.2. Methods

4.2.1. Cylindrical bubble machine experiments

A sample of near-surface *Sphagnum magellanicum* Brid. (Figure 27a) and one of *Sphagnum pulchrum* (Lindb. ex Braithw.) Warnst. (Figure 27b) were collected from Cors Fochno, a raised bog in west Wales (4°1W’ 52°30’N). The samples collected

were in the early stages of decomposition, and these two species were selected because studies have shown that they can be structurally different [*Kettridge and Binley*, 2011]. Structurally *Sphagnum magellanicum* tends to decompose in such a way that the plant retains its shape during growth until fairly advanced decomposition. In contrast, the leaves of *Sphagnum pulchrum* become detached from the branches during the early stages of decomposition and the stems collapse, forming a relatively dense ‘mush’ of stems and loose leaves.

In the field, each peat sample, approximately 160 mm height and 160 mm diameter, was cut out using the 'scissor method' reported by *Green and Baird* [2013]. Each sample was placed within a plastic container and transported to the laboratory where it was kept in cold storage. Prior to the experiment, each sample was removed from cold storage, excess water within the container was drained, and the upper growing surface (1-2 cm) was trimmed using scissors. To make further trimming easier, the sample was frozen overnight. After 24 hours the frozen sample was removed from the container and allowed to slowly thaw at ambient temperature within the laboratory. Once the outer layers of the peat sample were thawed, the sample was trimmed to the dimensions of a transparent acrylic tube (130 mm height, 130 mm diameter) with dimensions smaller than the bottom cylinder of the CBM (275 mm height, 150 mm diameter) (Figure 28a). The sample was carefully inserted into the acrylic tube and allowed to thaw completely in cold storage. The acrylic tube containing peat serves as a self-contained module, and allows peat samples to be easily inserted and removed from the CBM without causing further damage to the peat structure. Further details of how the modules were constructed can be found in the Appendix, Section 3. This module was

marked to record the orientation of the peat sample inside the CBM. The module was inserted into the CBM and a foam collar attached to the base of the module held the module in place.

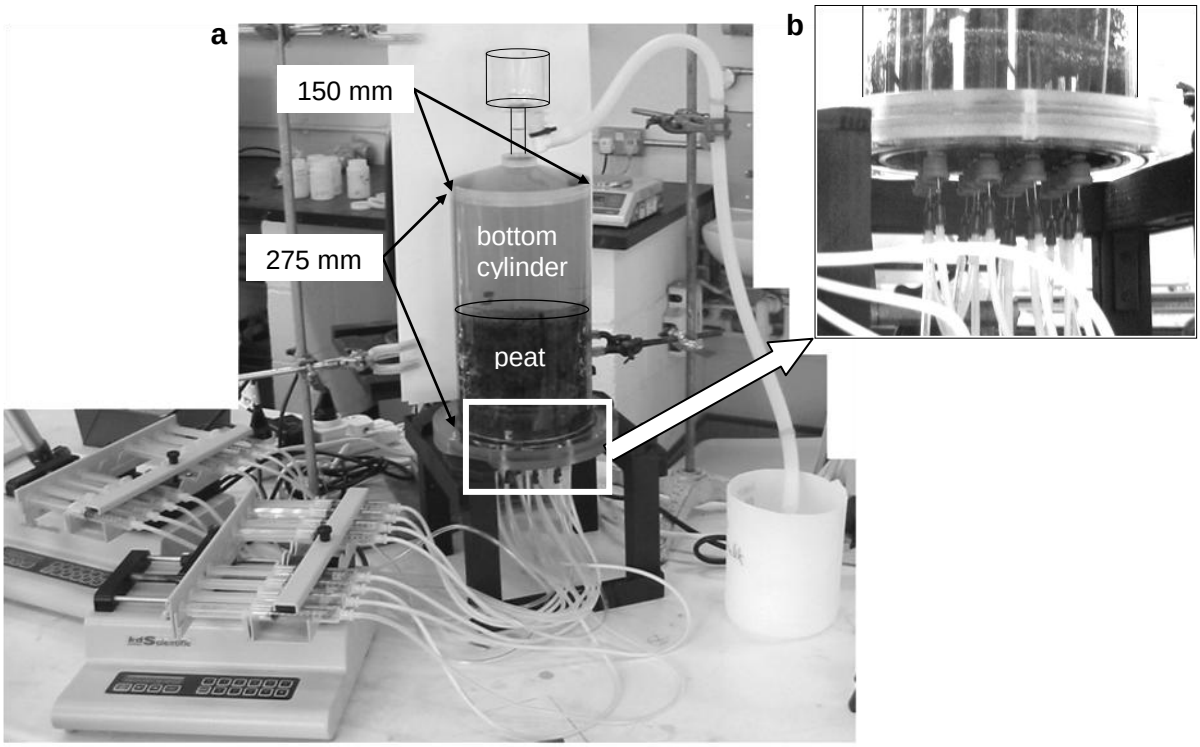

Figure 28. Experimental setup.

(a) Cylindrical bubble machine and (b) close-up of syringes inserted into peat sample.

The CBM was filled with de-aired water that was prepared by boiling de-ionized water for 10 minutes which was then cooled in an airtight container. The use of de-aired water minimizes the amount of bubbles coming out solution during the experiment. The de-aired water was dyed blue to improve the contrast between air and water. To ensure a high level of saturation, filling the CBM, was performed slowly from the base by raising the water level within the CBM by 2 cm hr^{-1}. Sixteen 22-gauge, 7.5 cm-long, blunt-nose needles were inserted 4 cm into the base of the peat through openings sealed with septa (Figure 28b). Each needle

was connected to a 10 mL syringe that was placed onto a syringe pump pre-programmed to deliver from an individual syringe a quantity of 8 mL of air at a rate of 1 mL min^{-1}. A complete injection of air consisted of simultaneously injecting 16 syringes into the peat sample, and 10 injections were performed per peat type (*S. magellanicum* and *S. pulchrum)*.

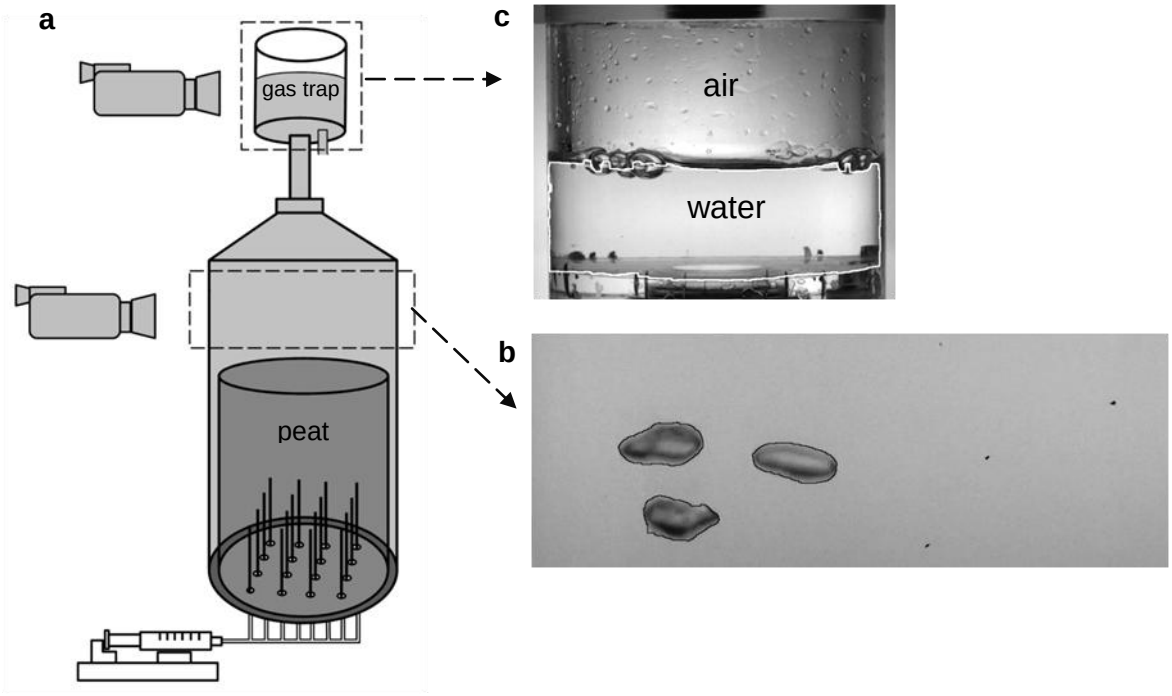

Figure 29. Filming CBM.

(a) Field of view of video cameras filming the CBM and example video frame of (b) bubbles and (c) water within the gas trap.

A high definition video camera (Sony HDR-XR105E) recording at 50 frames per second (fps) filmed the bubbles exiting the surface of the peat sample to measure bubble sizes (Figure 29a). Bubble size in this experiment was defined as the area encompassed by the edge of a bubble (Figure 29b). To highlight bubble edges, the bubble machine was fitted with a uniform background consisting of a frosted sheet, and backlighting was provided by a 500-W halogen lamp. To measure the

volumetric rate of bubble release from the peat, a second high definition video camera (Sony HDRSR10E) was positioned to record the change in water level within a cylindrical gas trap (Figure 29c). To improve contrast between air and water within the gas trap backlighting was provided by a second halogen light.

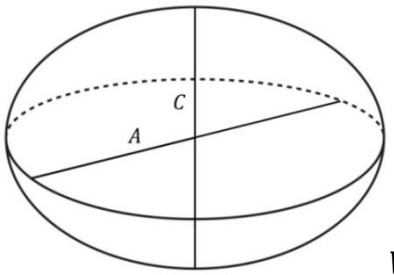

$$V = \frac{1}{6}\pi A^2 C$$

Figure 30. Oblate spheroid

Geometry of oblate spheroid described with major (A) and minor (C) axis, and equation to calculate volume of oblate spheroid.

The video footage was converted into images at the rate of 1 fps for bubble sizes. Images were automatically processed using a Sobel edge detector [*Gonzalez and Woods*, 2011] within an image processing program (ImageJ [*Schneider et al.*, 2012]) to identify individual bubbles emitted from the peat and extract each bubble's major-axis (A) and minor-axis (C) (Figure 30). From the images it was not possible to determine the depth of the bubble and it was assumed that the unknown third axis of the bubble was equal to the major-axis (A). Using these dimensions, all bubbles became oblate spheroids and the volume of each bubble could be estimated (Figure 30). For reference, a bubble with a volume of 0.0005 mL could have a major-axis of 1 mm and minor-axis of 1 mm. Bubbles <0.0005 mL were excluded from analysis because they were not bubbles emerging from the peat but bubbles that formed on the interior surface of the CBM, presumably by dissolved gas coming out of solution. Due to the main tank (Figure 29a) of the

CBM being cylindrical, a considerable amount of distortion occurred if bubbles were recorded near the tank's left and right edge, and bubbles near these tank edges were not analysed.

The video footage of the volumetric rate of bubble release was sampled every 5 s. Image processing of bubble release was performed using a colour-thresholding technique based on image hue saturation and brightness [*Schneider et al.*, 2012]. This technique was used to select the image pixels within the gas trap consisting of water, and measure their total area. By measuring the change in water area, the area occupied by air could be calculated and converted into a volume using the dimensions of the gas trap. It was found that the minimum discernible amount of change in area was approximately 17 mm^2 (equivalent to a volume of 0.79 mL), and changes in area less than this amount were not analyzed.

An additional control experiment was carried out where the CBM contained no peat sample, but was operated as the experimental runs with peat. Data from the control run was video of the volumetric rate of bubble release measured within the gas trap and was sampled every 5 s. This video footage was processed with the same image processing techniques used for the peat sample runs of the CBM. Ideally a steady input of gas injected into the empty CBM would produce a near constant volumetric rate of bubble release. If the volumetric rate of bubble release is variable, these deviations may be caused by error (experimental or image-processing) and this error may also exist in the bubble release from the CBM peat runs. Removing this error from the volumetric rate of bubble release from the CBM peat runs may be possible, but was not performed. Instead the mean of the

volumetric rate of bubble release from the empty CBM run was chosen as an uncertainty threshold. Volumetric rate of bubble release values collected in the CBM peat runs below this threshold may be a product of error and caution was made when drawing conclusion about these release events. Volumetric rate of bubble release values above the threshold are more likely valid releases of gas from the peat.

Patterns in bubble size and volumetric rate of release were extracted by producing frequency magnitude plots with bin sizes $1/10^{th}$ of the data range. Using the candidate distributions presented in Chapter 2, the best fitting distributions were fitted to the observations. The absolute goodness of fit of the distribution was computed using the F-test for bubble sizes and chi-squared statistic for volumetric rate of release.

4.2.2. Estimating pore structure of peat

To determine if structural differences in the peat affect ebullition, various methods were considered to describe the pore structure of the peat samples quantitatively. Bulk density and porosity [*Boelter*, 1969] can provide information on the peat sample as a whole, but do not provide information about the location and size of pores. These metrics were discounted because they do not help distinguish between peats that have similar overall porosities, but different pore size distributions and pore connectivity. To obtain this additional information studies have adopted methods including slicing and imaging peat sections [*Quinton et al.*, 2008], or imaging entire peat samples using x-ray computed tomography [*Kettridge and Binley*, 2011; *Quinton et al.*, 2009; *Rezanezhad et al.*, 2009]. Of the methods available, x-ray computed tomography is the least intrusive, and provides fine

spatial resolution images of peat structure in two or three dimensions. However, for this study easy access to an x-ray computed tomography scanner was not possible to image the CBM peat samples.

Slicing the peat into thin sections was adopted as the method for imaging the CBM peat. Traditionally peat samples are prepared for slicing by removing the moisture from the peat with acetone, and impregnating the peat with resin [*Quinton et al.*, 2008]. This preparation can lead to complications that can cause shrinkage of the pore network or the peat sample can secrete wax and make it difficult to image the pore structure [*Quinton et al.*, 2009]. Therefore, this method was not used, and another slicing method was developed (Appendix, Section 5) that is explained herein.

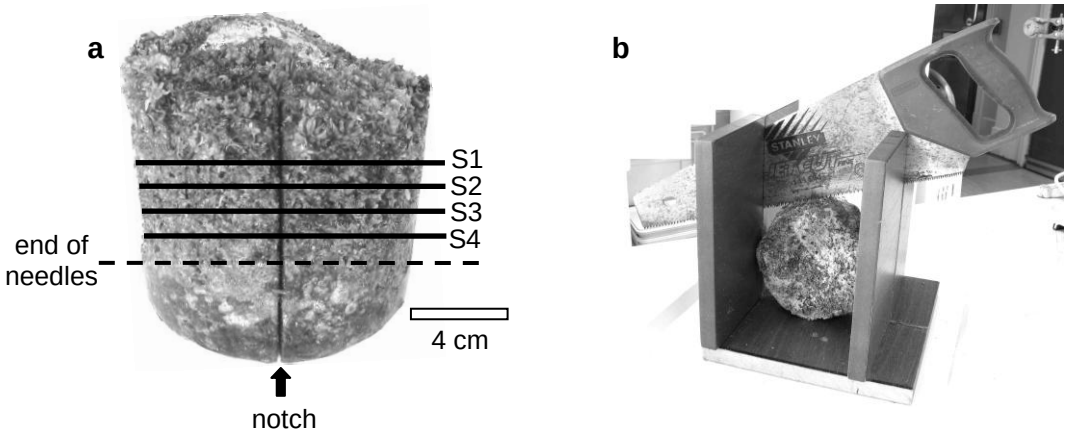

Figure 31. Slicing peat sample.

(a) Four slices at 1 cm intervals obtained from a peat sample. Dashed line marks approximate ends of the bubble-injection needles. (b) Setup used to cut slices.

After the CBM experiments, each peat sample within its module, was drained and placed in the freezer. To obtain slices from a sample, the sample was removed from the freezer and a 2 cm notch was made vertically along the full length of the

sample at the location where the sample was facing forward in the CBM experiments (Figure 31a). Next, the sample was placed horizontally in a custom built mitre box (Figure 31b) and a medium-cut hand saw (8 teeth per 25 mm) was used to saw four latitudinal sections of peat spaced 1 cm apart (Figure 31a). More slices were not obtained from the base of the sample because this portion of the sample was not injected with air during the CBM experiments due to the length of the inserted needles (Figure 31a). All peat slices were placed in the freezer until photographing took place.

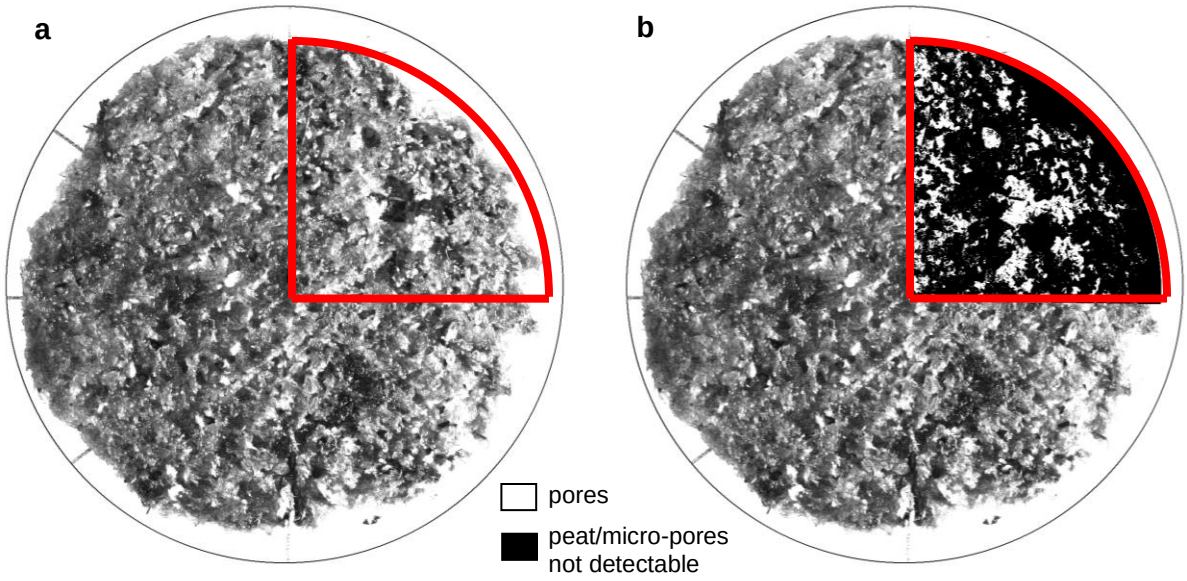

Figure 32. Peat quadrant analysis.

(a) Peat slice of *S. magellanicum* with illumination from the east and upper right quadrant highlighted. (b) Classified image of pore locations.

To photograph the peat, a slice was removed from the freezer and placed on a plastic board with clearly marked ground control points, cardinal directions, and rulers for scale. The peat slice was thawed at ambient temperature and positioned underneath a digital camera (Canon PowerShot A650 IS, 12.1 mega pixels) that was perpendicularly mounted at a height of 29 cm. The slice was lit from above

with ambient fluorescent lighting and obliquely using a 500-W halogen lamp to produce shadows caused by topographic depressions in the peat. All photographs were taken at night to keep lighting constant over the entire photo session (i.e., to remove light-bleeding effects from daylight windows in the laboratory). Each slice was photographed a total of four times, with each photo recording the slice illuminated from a single cardinal direction (N, E, S, W). This was done to obtain shadows of the slice from more than one direction.

Inspection of the photos revealed that shadows coinciding with pores could only be extracted from the NE quadrant of each peat slice (Figure 32a). This was possibly due to the positioning of the halogen lamp. Therefore, for each slice it was decided to analyze only the upper right quadrant from each of the four photos illuminated from each cardinal direction. Each photo was cropped to the extent of the upper right quadrant and was imported into a geographic information system (GIS, ESRI ArcMap 9.3). Here the images were classified into 10 classes using a minimum Euclidean distance classification method (ISODATA) that is commonly used to perform unsupervised classification of remotely-sensed images [*Ball and Hall*, 1965] (another method of classification tried is discussed in the Appendix, Section 5). This classification method assigns each image pixel (consisting of red, green, and blue values) to a cluster of pixels with similar RGB values. Each of these clusters represents a class, and the darkest pixels in the peat images formed a single cluster/class that represented shadows/pores. The resulting classified raster images of the slice quadrants were re-classified from ten classes into two classes. The new classification scheme contained one class with all the classified pixels that corresponded to pores and a second class containing the remaining pixels that

represented peat or micro-pores that were not detectable (Figure 32b). These classified images were converted into vector GIS format and the size of each pore was calculated as an area (mm^2).

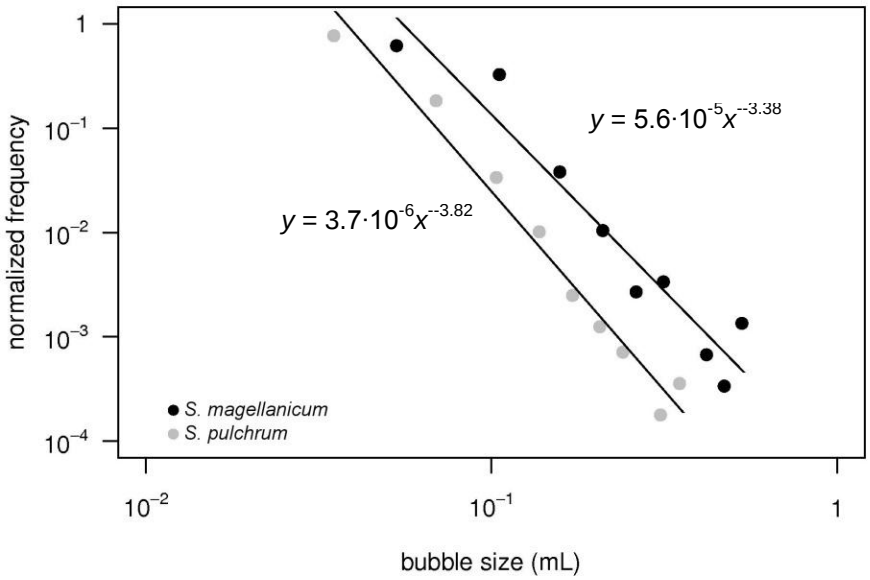

Figure 33. Bubble sizes from CBM experiment

Bubble size magnitude and frequency from *S. magellanicum* and *S. pulchrum* with fitted power law distributions having $p<0.05$ and $r^2>0.92$.

4.3. Results

Bubble size distributions from *S. magellanicum* and *S. pulchrum* both displayed power law patterns with similar slopes (Figure 33). Where the two peat samples differ is in the magnitude and frequency of bubble sizes. On average, the *S.* Pulchrum (avg. bubble size=0.025 mL) sample produced smaller bubbles than the S. magellanicum sample (avg. bubble size=0.052 mL). This is a 70% difference in average bubble size. The size range, maximum to minimum, of the *S. pulchrum* sample's bubbles is smaller than (0.0008-0.3429 mL) that from the *S. magellanicum* sample (0.0008-0.5233 mL). The largest bubbles from the *S. magellanicum* sample were 1.5 times larger than the largest bubble produced by the *S. pulchrum* sample. Overall, for each bubble size bin in Figure 33, the *S.*

magellanicum sample had a higher probability of producing a larger bubble than the *S. pulchrum* sample.

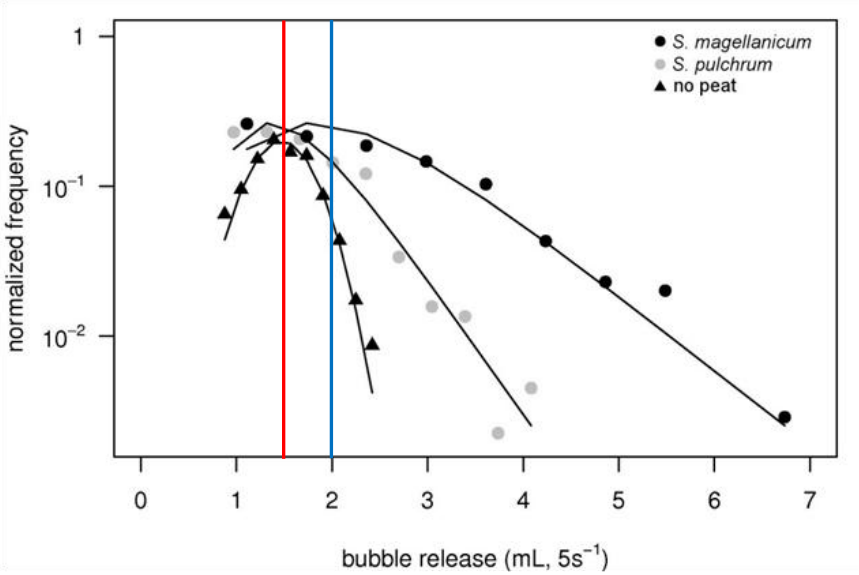

Figure 34. Volumetric rate of bubble release from CBM experiment

Volumetric bubble release from *S. magellanicum*, *S. pulchrum*, and the CBM with no peat. The mean volumetric bubble release of the CBM run with no peat (1.5 mL $5s^{-1}$) represents the uncertainty threshold (red line). The blue line marks the divergence in *S. Magellanicum* and *S. Pulchrum* release.

The volumetric bubble-release data from both peat samples were fitted with positively-skewed distributions, with smaller bubble release events occurring frequently and larger events rarely (Figure 34). The best fitting distribution to *S. magellanicum* release was a gamma distribution (χ^2=6.4, p=0.6) and to *S. pulchrum* it was a log-normal distribution (χ^2=15.1, p=0.06). The bubble release from the CBM run without peat was normally distributed (χ^2=9.0, p=0.3), with a mean bubble release of 1.5 mL $5s^{-1}$, and this value was set as the uncertainty threshold (red line in Figure 34). Overall release from *S. magellanicum* ($\bar{x}$=2.30 mL $5s^{-1}$, σ=1.14 mL $5s^{-1}$) is greater and more frequent than events from *S. pulchrum* ($\bar{x}$=1.65 mL $5s^{-1}$, σ=0.60 mL $5s^{-1}$). In Figure 34 it can be seen that both peat types

have a similar probability of producing smaller release events (<2 mL $5s^{-1}$), but a different probability of producing relatively larger release events (>=2 mL $5s^{-1}$) occurring at the tail end of the distributions.

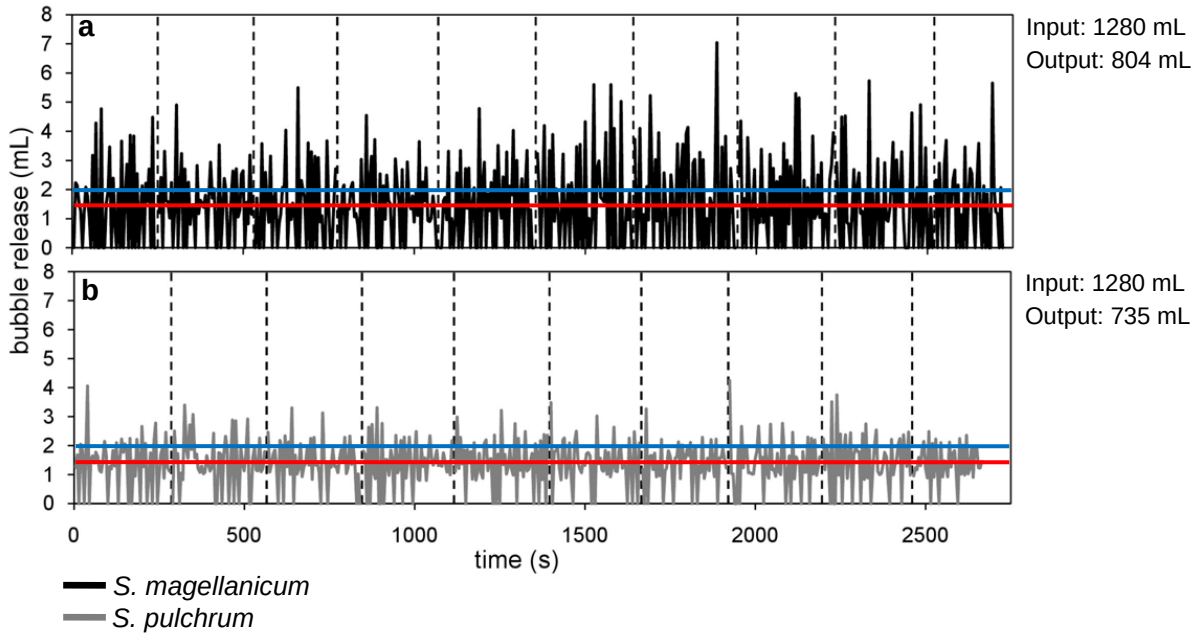

Figure 35. Time series of rate of volumetric bubble release.

Time series of bubble release for (a) *S. magellanicum* and (b) *S. pulchrum*. Time series from 10 separate injections are plotted end-to-end for visualization purposes, and vertical dashed lines mark the end of each time series. The blue line marks the divergence in *S. Magellanicum* and *S. Pulchrum* release distributions. The red line is the uncertainty threshold.

This difference in release is also visible when the release data are plotted as time series and a horizontal line at 2 mL is drawn to demarcate where the two bubble release distributions begin to differ (blue lines in Figure 35). Clearly *S. magellanicum* peat (Figure 35a) produces larger release events more frequently than *S. pulchrum* peat (Figure 35b). Of the 349 release events recorded for *S. magellanicum*, 53% were greater than 2 mL, and only 25% of the 446 releases from *S. pulchrum* were greater than 2 mL. These larger, more frequent release events contribute to *S. magellanicum* peat (coefficient of variation (CV) = 49%)

producing ebullition that is characteristically erratic when compared to the regularly occurring ebullition produced by *S. pulchrum* (CV = 36%). Furthermore, 72% of the bubble releases from *S. magellanicum* and 54% of the bubble releases from *S. pulchrum* were above the uncertainty threshold (red lines in Figure 35).

In Figure 36a the size and location of pores for each slice are visualized to determine if structural differences exist between the peat types and between the peat slices. Both peat types have pore sizes that are dominated by smaller pores (<10 mm^2) with relatively fewer large pores (>50 mm^2) (Figure 36b). The porosity of the peat types were calculated from the slices, but this porosity is an underestimate of true porosity because micro-pores (<0.004 mm^2) could not be detected. For this reason porosities are reported as detectable porosity. As a whole, the two peat types do not differ in detectable porosity, with average detectable porosity of *S. magellanicum* and *S. pulchrum* being 23% and 22.25% respectively. Where the two peat types differ is the location of large and moderately sized pores at different peat depths. For example, the *S. magellanicum* peat slices S2, S3, S4 have similar porosities, with small to moderate pores occurring throughout (Figure 36a). This contrasts with the shallowest slice of *S. magellanicum* (Figure 36a, S1) peat which has a 9-10% increase in porosity and greater occurrence of large pores (Figure 36b, S1). Structural changes between peat slices of *S. pulchrum* are different than *S. magellanicum*. In *S. pulchrum* two layers of different detectable porosity can be distinguished between the combination of slices S3/S4 and S1/S2 (Figure 36a). The deeper peat layer (S3 and S4) has an open pore structure with large pores

and the shallower peat layer (S1 and S2) has a closed structure dominated by smaller pores (Figure 36b).

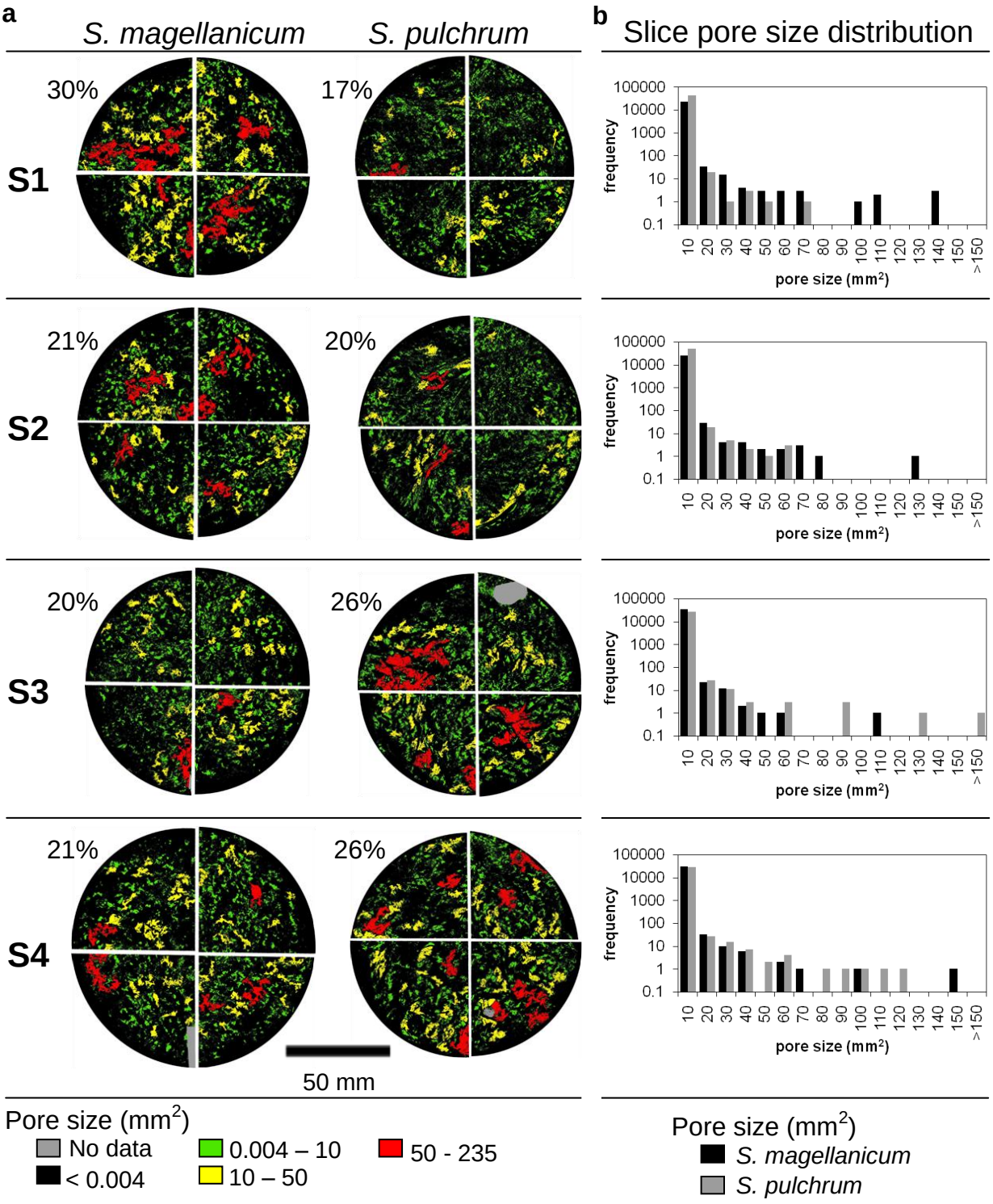

Figure 36. Mosaic and distribution of pore sizes.

(a) Analysed quadrant mosaiced to reconstruct slice pore size and location for *S. magellanicum* and *S. pulchrum*. Detectable porosity per slice is indicated. (b) Pore size distributions of each slice for each peat species.

4.4. Discussion and Conclusion

This study has provided the first record on bubble sizes from peat injected with air. The bubble sizes from both peat types exhibit a power law pattern, and this information can now be used to guide the development of models of ebullition from peat like MEGA. Although MEGA was not used to simulate the CBM experiments, simulations in the previous two chapters produced power law distributions for bubble sizes, and this suggests that MEGA does capture the processes necessary to replicate bubble sizes from peat. The second pattern produced by both peat types were positively skewed distributions for volumetric bubble release. These bubble-release patterns are similar to patterns found in published studies [*Goodrich et al.*, 2011; *Kellner et al.*, 2006; *Stamp et al.*, 2013], and patterns produced by MEGA in Chapter 2. The similarity in bubble release patterns from the CBM and the natural system perhaps also indicates that the CBM is capable of representing the natural system. This provides some assurance that direct gas injection into peat is similar to natural methane production within a peat profile.

It is possible to explain the differences in bubble release between the two peat types from the structural information obtained by slicing the peat. The pore sizes of the shallowest slices of peat (S1 and S2) may explain why *S. magellanicum* produces larger individual releases than *S. pulchrum*. From the pore-size information provided by Figure 36 the shallow slices of *S. magellanicum* contain large pores that can easily release gas stored in deeper slices. Overall, the pore

structure of the shallow peat slice in *S. magellanicum* form a less tortuous pore network that allows stored gas to reach the peat surface and produce larger, more erratic bubble releases. In contrast, shallow slices of *S. pulchrum* contain a tortuous pore network consisting of small pores. Although *S. pulchrum* is able to store relatively large amounts of gas in its deeper slices (S3 and S4), the movement of gas through the shallower slices (S1 and S2) is difficult because passage through smaller pores requires greater amounts of buoyancy. Perhaps these shallow slices of peat found in *S. pulchrum* effectively produce a 'seal' that prevents the deeper gas from easily reaching the peat surface. In this experiment we do not have evidence that a less permeable peat layer or 'seal' will trap gas and rupture to produce extremely large bubble releases [*Glaser et al.*, 2004]. Instead bubble release from *S. pulchrum* suggests that less permeable layers of peat can trap gas, but these layers act like a 'valve' and regulate the release of gas. This 'valve' effect results in smaller, more regularly occurring bubble releases from *S. pulchrum* in comparison to *S. magellanicm*.

It remains difficult to explain the differences in bubble size between the two peat species. As bubbles move through the peat they change shape and size as they deform and conform to the geometry of the pores [*Corapcioglu et al.*, 2004]. When the bubbles emerge from the peat, it is possible that bubble size is related to the last pore a bubble has occupied. If we assume that this is occurring, the moderate to large pores existing in the shallow slice of *S. magellanicum* peat would produce more moderate to large bubbles (Figure 33). This contrasts with the shallow slice from *S. pulchrum* which contains small pores, and would produce small bubbles emerging from the peat.

The method presented here of imaging slices does not produce porosities that compare well with porosities reported using finer resolution methods like x-ray tomography. Studies using x-ray tomography have reported porosities from peat that range from 43-61% [*Quinton et al.*, 2009; *Rezanezhad et al.*, 2010], whilst the slicing method presented here found porosities between 17-30%. The difference in porosity between the two methods is most likely due to x-ray tomography producing images that are two times finer in spatial resolution than the digital images of the peat slices. This means that the peat slicing method is not suitable for imaging micro pores (<0.004 mm^2), but performs well when imaging larger pores.

Until now we have not known whether signals of ebullition were simply a product of variations in gas production [*Coulthard et al.*, 2009], atmospheric pressure [*Comas et al.*, 2011; *Glaser et al.*, 2004; *Tokida et al.*, 2007; *Tokida et al.*, 2009] or whether the structure of the peat was also important. The results from this investigation confirm that peat structure does appear to have an important role in regulating bubble size and release from peat. The patterns also show that peat structure alone can cause probability distributions of bubble sizes to be power law in form and volumetric rate of bubble release to be positively skewed. Moreover, changes in peat structure at different depths of peat can apparently determine if ebullition occurs erratically, or more regularly. Overall, these findings suggest that it is flawed to assume that two peat types with the same porosity must have the same bubble-release behaviour. Similarly it cannot be assumed that large-pore porosities are a guarantee of similar ebullition behaviour.

One of the limitations of this experiment was the lack of replication as only one peat sample was obtained per peat type. Variability in pore structure between and within a peat type can be different. As demonstrated here, these differences in pore structure would affect the magnitude and frequency of bubble sizes and release from peats. For this reason it is possible that repeating this experiment with additional peat samples, of the same peat types, would likely produce the same patterns that were observed in bubble size (power law distribution) and release (non-normal, positively skewed distribution), but different magnitudes and frequencies for these patterns. For example, another sample of *S. pulchrum* may have a pore structure that results in significantly larger bubble sizes and release than observed from the sample used in this experiment. For this reason, throughout this investigation we refrain from making any conclusions that are specific to a peat type and focus on differences in bubbles size and release related to evidence obtained on pore structure.

The recommendation for models of ebullition from peat is that peat structure must be accounted for to accurately predict ebullition from different peat types. Models that treat the peat profile as a single entity, may not always be capable of representing ebullition (bubble release) properly [*Kellner et al.*, 2006]. MEGA provides a viable approach that could be used to model ebullition from peat, but more evidence is needed to test the model. This would require patterns of bubble size and release from a greater range of peat types with different pore structures. The method used in this study to obtain the peat pore size information would have to be modified. Presently the slices from the peat provide a planform view of the pore size and location, whilst MEGA requires a profile view of the peat. Thus, to

model the peat samples in MEGA it would require slicing the peat sample longitudinally. A method would also have to be developed to convert peat pore data into shelf arrangements. This method would have to consider the spatial variability of the porosities within the peat. Future work may also allow methane to build up in peat samples naturally and record the natural ebullition patterns through, for example, cameras that are triggered by ebullition events or time lapse cameras [*Comas and Wright*, 2012]. These natural ebullition patterns would be compared against MEGA simulations, and provide greater confidence in the model.

Chapter 5 Ebullition of methane from peatlands: does peat act as a signal shredder?

5.1. Introduction

The last two chapters have demonstrated that MEGA can reproduce the patterns of bubble storage, size and release from physical models of gas flow in simple porous media and peat. These studies provided validation for MEGA, and we now have some confidence that the model includes the primary processes required to model ebullition in peat. Having achieved this, it is now possible to use MEGA to construct scenarios and investigate the response of ebullition to various drivers. In this next chapter, synthetic peatlands are created within MEGA, and different forms of ebullition are produced to understand how peat structure affects ebullition.

Recent developments in field methods [*Burrows et al.*, 2005] have made it possible to record CH_4 ebullition at high temporal resolution and to investigate how ebullition is linked to a range of environmental factors that affect CH_4 production, consumption and transport. For example, *Goodrich et al.* [2011] found cyclical – diurnal and seasonal – variations in ebullition. They were unable to isolate the environmental variable(s) responsible for diurnal cycles, although seasonal cycles were probably related to overall CH_4 production as mediated by peat temperature and the production of labile substrates. Ebullition may also be characterized by non-cyclical 'spikes' in flux – so-called episodic ebullition – that has been linked to processes that increase bubble mobility and volume such as short-term (hourly) changes in atmospheric pressure [*Comas et al.*, 2011; *Glaser et al.*, 2004; *Tokida*

et al., 2007; *Tokida et al.*, 2009], or longer-term (days to weeks) variations in water-table elevation [*Glaser et al.*, 2004; *Shurpali et al.*, 1993].

However, studies have also shown that ebullition can occur in the apparent absence of environmental forcing, and that relationships between ebullition and physical environmental factors are not always clear cut. For example, *Waddington et al.* [2009] monitored the ebullition flux of CH_4 from laboratory-incubated samples of peat for 178 days. They recorded 339 pressure periods (periods during which atmospheric pressure was consistently increasing or decreasing), but only in 28% of these periods did episodes of ebullition occur. It seems too that both increases and decreases in pressure can cause ebullition [*Waddington et al.*, 2009] and that ebullition can also be stimulated during periods of high atmospheric pressure [*Comas and Wright*, 2012], contrary to the study of *Tokida et al.* [2007] who found that falling atmospheric pressure was a trigger. Findings that ebullition data are often 'noisy' and that different environmental forcings seem to apply across different studies suggests that some other control on the system needs to be considered, with an obvious candidate being the structure of the peat. The structure of the peat and its down-profile variation will affect bubble storage and movement and will mediate how production and consumption affect fluxes from the peatland surface. Structural effects are clear at large scales (e.g. 10s of meters across peatlands and through the whole peat profile) where layers of woody peat may act as barriers to upwards bubble migration. Bubbles appear to accumulate below these barriers until their buoyancy causes the barrier to rupture, the bubbles are then released after which the barrier re-seals [*Glaser et al.*, 2004; *Rosenberry et al.*, 2003]. At smaller scales (e.g. the upper ~30 cm of peat profile) and in peat

in which woody layers are absent, *Panikov et al.*, [2007] observed irregular ebullition from peat cores in which there were clear diurnal oscillations in CH_4 production at depths down to 20 cm. Although no mechanism was provided to explain the difficulty in linking the ebullition in a simple way to the environmental forcing, the data from *Panikov et al.,* [2007] suggests that the capacity of peat to store gas and release it at a later time provides a possible explanation. *Jerolmack and Paola* [2010] observed similar behaviour occurring in sedimentary systems that are subject to environmental forcings. In their study, the systems did not respond to forcings in a linear manner, and a one-to-one correlation could not be made between forcing and a system response. Moreover, it was suggested that intermittent autogenic processes were responsible for producing noise that 'shreds' any discernable pattern in the environmental forcing and can de-couple forcing from system response.

The evidence from these studies suggests that autogenic processes like bubble storage and release within near-surface peat could 'shred' a CH_4 production signal. In other words, it suggests that the peat profile cannot be considered as a simple entity that responds uniformly to production, consumption and physical factors that affect bubble size and stability. It is very difficult to examine this role of peat structure experimentally because of problems imaging bubbles in the peat profile over regular time intervals [*Kettridge et al.*, 2011] and problems controlling the production signal within the peat profile. We therefore carried out numerical experiments with MEGA. Although not a substitute for investigating real peats, our model results suggest that peat structure does, indeed, determine the degree to which CH_4 production signals affect ebullition flux at the peat surface.

5.2. Method

The computer model of ebullition in peat described in *Coulthard et al.* [2009] was utilized within this study and is called Model of Ebullition and Gas storAge (MEGA). In summary, MEGA conceptualizes peat as a two dimensional cellular grid where a location within the model consists of peat solids or particles, with the spaces in between occupied by gas or water. In MEGA, the peat solids, and therefore the pore structure, are represented by a series of shelves, and the number and size of these can be set according to the physical characteristics of the peat, with fewer shelves representing highly-porous peat, and more shelves denser peat (Figure 37 a,b). The movement of gas bubbles within the peat is governed by a simple rule set adopted from an avalanche model [*Bak et al.*, 1987]. In MEGA, gas accumulates under shelves in a manner akin to an inverted pile of idealized sand grains, and the steepness of the pile determines if gas will 'avalanche' upwards to shallower shelves or whether it remains stationary and accumulates. The avalanching process encapsulates the opposing forces of buoyancy and surface tension that act upon the gas [*Birovljev et al.*, 1995; *Corapcioglu et al.*, 2004; *Mumford et al.*, 2010]. An avalanche (gas movement) occurs when the accumulation of gas beneath a shelf is sufficiently large for its 'buoyancy' to overcome the surface tension forces (described by the steepness of the pile) keeping it in place.

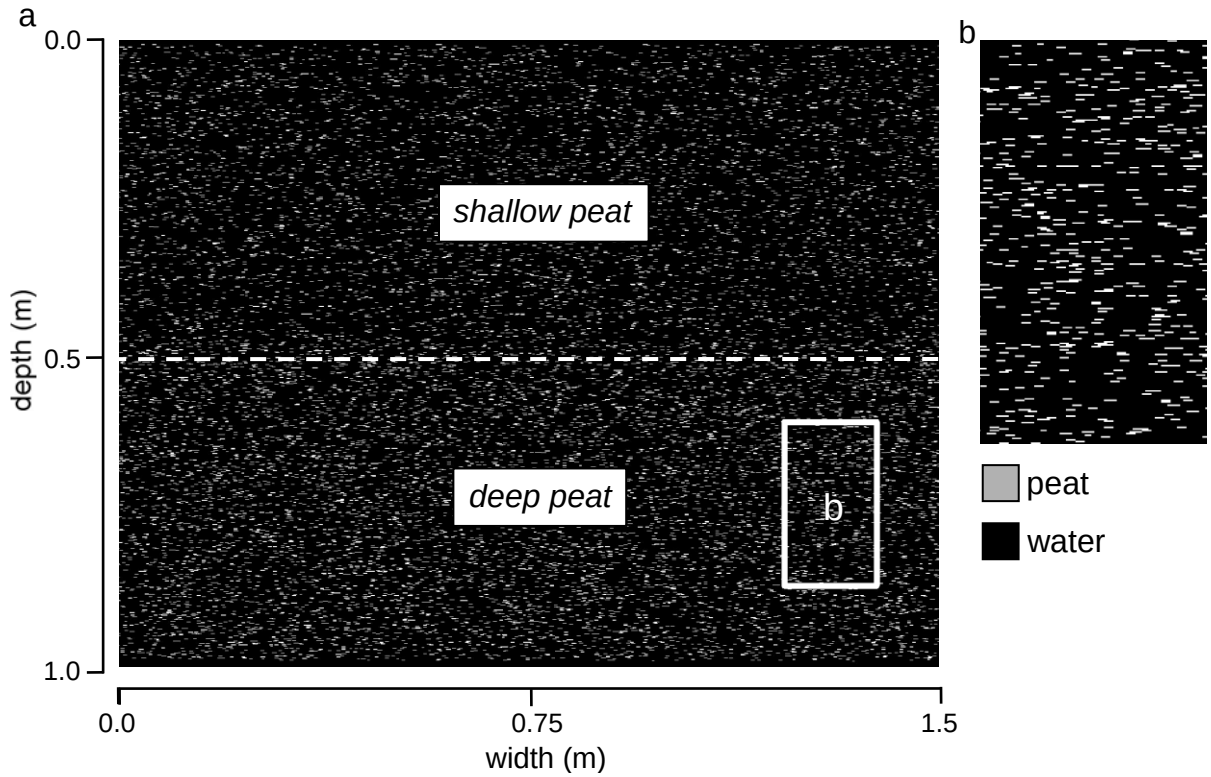

Figure 37. Two layered peat profile.

(a) Shelves randomly arranged to represent peat profile (1.5 m wide, 1 m deep) with higher porosity at shallower depths (0.0-0.5 m), and lower porosity at deeper depths (0.5-1.0 m). (b) Inset of peat with shelves (in gray) saturated with water (in black).

To test the idea that peat structure can 'shred' environmental signals in ebullition we used a series of model scenarios to represent peats of varying pore structure and introduced gas production signals into the peat profiles at different depths. These production signals have regular patterns that we will use to represent possible environmental forcings for ebullition. If evidence of the production signal pattern is not present in the ebullition at the peat surface, our simulated peat has shredded the production signal, thus severing any link between cause and effect of ebullition events. Conversely, if the production signal pattern is mirrored in the ebullition, the production signal is preserved, and ebullition patterns are caused by the environmental forcing.

Our modelled peat profiles were 1.5 m wide and 1 m deep (thick), and the grid cell size was set to 1 mm x 1 mm (Figure 37a). Published measurements of *Sphagnum* branches [*Kettridge and Binley*, 2008] were used to guide the setting up of the model, and shelf lengths were randomly selected from a normal distribution (average shelf length=5.7 mm , st. dev=0.8 mm). The peat profile was partitioned into two layers of equal depth/thickness to reflect the spatial variation in decomposition often found in peats [*Clymo*, 1984]. The shallower layer comprised less decomposed peat of greater porosity, whilst the deeper layer was less porous to represent peat undergoing compression and more advanced decomposition [*Boelter*, 1965; *Quinton et al.*, 2000; *Quinton et al.*, 2008]. Measured values of porosity in shallow peats (91-98%) [*Kettridge and Binley*, 2008; *Kettridge and Binley*, 2011; *Parsekian et al.*, 2012] were used in the model. In total three peat profiles were created by placing shelves randomly within each peat layer to obtain a shallow layer porosity of 95% and deeper layer porosities of 95%, 93%, and 92%.

To drive MEGA we set a bubble production rate based on data from *Stamp et al.* [2013], who reported maximum, seasonally-averaged, bubble fluxes of 709 mL m^{-2} d^{-1} from *Sphagnum* lawns in a Welsh raised bog. Converting the field measurements into model CH_4 production rates took into account that the modelled peat represents a cross-section. The smallest bubble within MEGA is 1 mm^2 and the downscaled flux resulted in 709 mm^2 bubbles d^{-1} available to construct hourly CH_4 production signals (bubbles hr^{-1}). Four production signals were produced based on the patterns observed by *Panikov et al.* [2007] and are shown in Figure 38. Each production signal was further deconstructed into three sub-signals added

to the modelled peat profile at three depth zones to reflect the spatial variability in CH_4 production at different depths [*Frenzel and Karofeld*, 2000; *Strack and Waddington*, 2008; *Sundh et al.*, 1994]. The first production signal was strongly diurnal (SD) and a 24 hr oscillation used all of the available daily CH_4 production (709 bubbles) (Figure 38a). A second production signal was created to represent time periods of lower production and this weakly diurnal signal (WD) was created with 50% of the total daily CH_4 production (Figure 38b). Two more signals were produced to represent sharp increases in bubble volume that are related to falling atmospheric pressure [*Tokida et al.*, 2007]. These signals are SD signals with bubble spikes occurring every 10 hours. One of these signals contains large spikes (LS) (Figure 38c) and the other small spikes (SS) (Figure 38d).

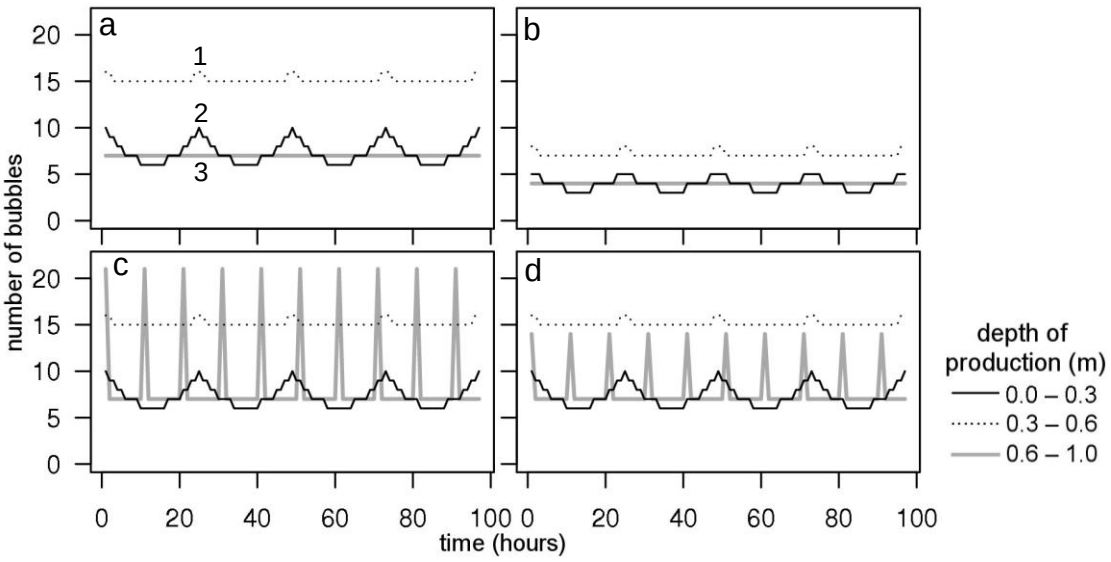

Figure 38. Methane production signals.

Production sub-signals that are weakly diurnal (1), strongly diurnal (2), and steady (3). (a) Strong diurnal (SD) CH_4 production signal decomposed into sub-signal 1, 2, 3 consisted of 50%, 25%, 25% of the daily CH_4 production accordingly. (b) Weak diurnal (WD) CH_4 production consisting of 50% of SD sub-signals. (c) Large spike (LS) signal consisting of SD plus 200% increases in steady production occurring every 10 hours. (d) Small spike signal (SS) with 100% increase in steady production.

A simulation was run for every peat profile and production signal combination. With three peat profiles (low, medium high porosity) and four production signals (SD, WD, LS, SS). This resulted in a total of 12 simulations. For every model hour a quantity of bubbles corresponding to the production sub signals was added to the peat profile as 1 mm^2 gas bubbles within the specified depth zone at random locations. To avoid edge effects, bubbles were not added within 0.25 m of the left and right hand edges of the profile. Using theoretical relationships between bubble size and rise velocity within a porous medium [*Corapcioglu et al.*, 2004], it was estimated from median bubble size calculated from a preliminary simulation, that bubble velocity would be a constant 6 mm s^{-1}. Ebullition flux was 'measured' at the top of the peat profile, which was also the position of the model water table, at hourly intervals. On average the flux from each profile is equivalent to the total production over a time period. Given this, each peat profile was driven by their production signal until the average 10 day ebullition flux stabilized and data collected after this time period was analyzed.

For each simulation 15,000 hrs of flux measurements were analyzed for evidence of periodicity by estimating power spectra using a multitaper method [*Thomson*, 1982]. This method was chosen because it performs a harmonic *F* variance-ratio test (*F*-test) for each frequency, and can be used to distinguish between noise and significant peaks in spectra. Due to the large number of flux records analyzed it is possible that random fluctuations in flux can periodically occur and produce inflated *F* values. To account for this *Thomson* [1990] suggests that significance levels for non-randomness are set at $1 - 1/N$, where N is the number of flux samples. Using this recommendation, peaks in spectra were significant at the 99.99% level.

Dominant peaks in spectra were located at frequencies corresponding to the production cycles every 24 hrs and spikes occurring every 10 hrs, and peaks in spectra ±1hr from those locations were also inspected to account for any lag effects in flux.

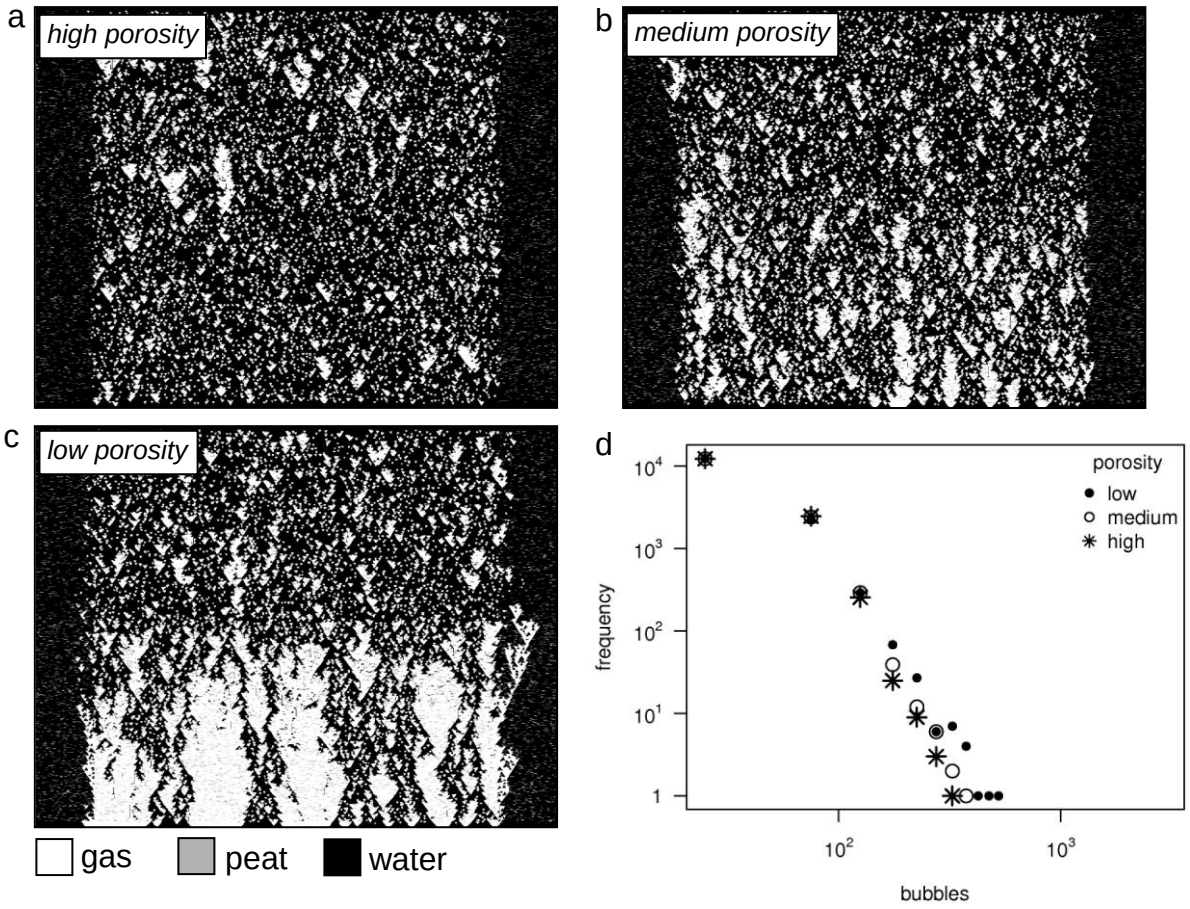

Figure 39. Gas storage and ebullition flux.

Gas accumulation after simulating strong diurnal (SD) CH_4 production in peat with a deep peat layer of (a) high, (b) medium, and (c) low porosity. (d) Frequency plots of corresponding hourly ebullition flux. Bin sizes are 50 bubbles.

5.3. Results

Gas storage measured at the conclusion of three SD simulations clearly shows that decreasing peat porosity increases gas storage (Figure 39 a,b,c) with the percentage of gas stored within the peat of high, medium and low porosity being

19%, 25% and 35% respectively. The effect of the additional gas storage is evident in the magnitude and frequency of hourly ebullition flux (Figure 39d). Although the difference in total and mean flux between the three simulations is minimal (<1%), which is to be expected, the lower-porosity peat is able to store more gas and release extreme gas flux events that rarely, or never occur in peat of medium, and low porosity.

Four out of the six diurnal simulations did not shred the diurnal production signal. This can be seen in Figure 40 where the highlighted spectrum peaks signify the occurrence of diurnal ebullition. Figure 40 a,b,c clearly show that SD production signals are always measurable in gas flux at the peat surface (frequency~0.04, which is nearly a 24 hr cycle). For WD production, a signal was detectable in high porosity peat (Figure 40d), but no significant peaks in spectra were found for peat of medium and low porosity (Figure 40 e,f).

Only two of the simulations with spiked signals produced ebullition with spiked fluctuations occurring every 10 hrs. (frequency~0.1). This signal was noticeable from high porosity peats (Figure 41 a,d), but no evidence of spikiness was noticeable in flux from medium, and low porosity peat (Figure 41 b,c,e,f). Moreover, diurnal signals were detected in all simulation except for the lowest porosity peat with the weaker spiked signal (Figure 41f).

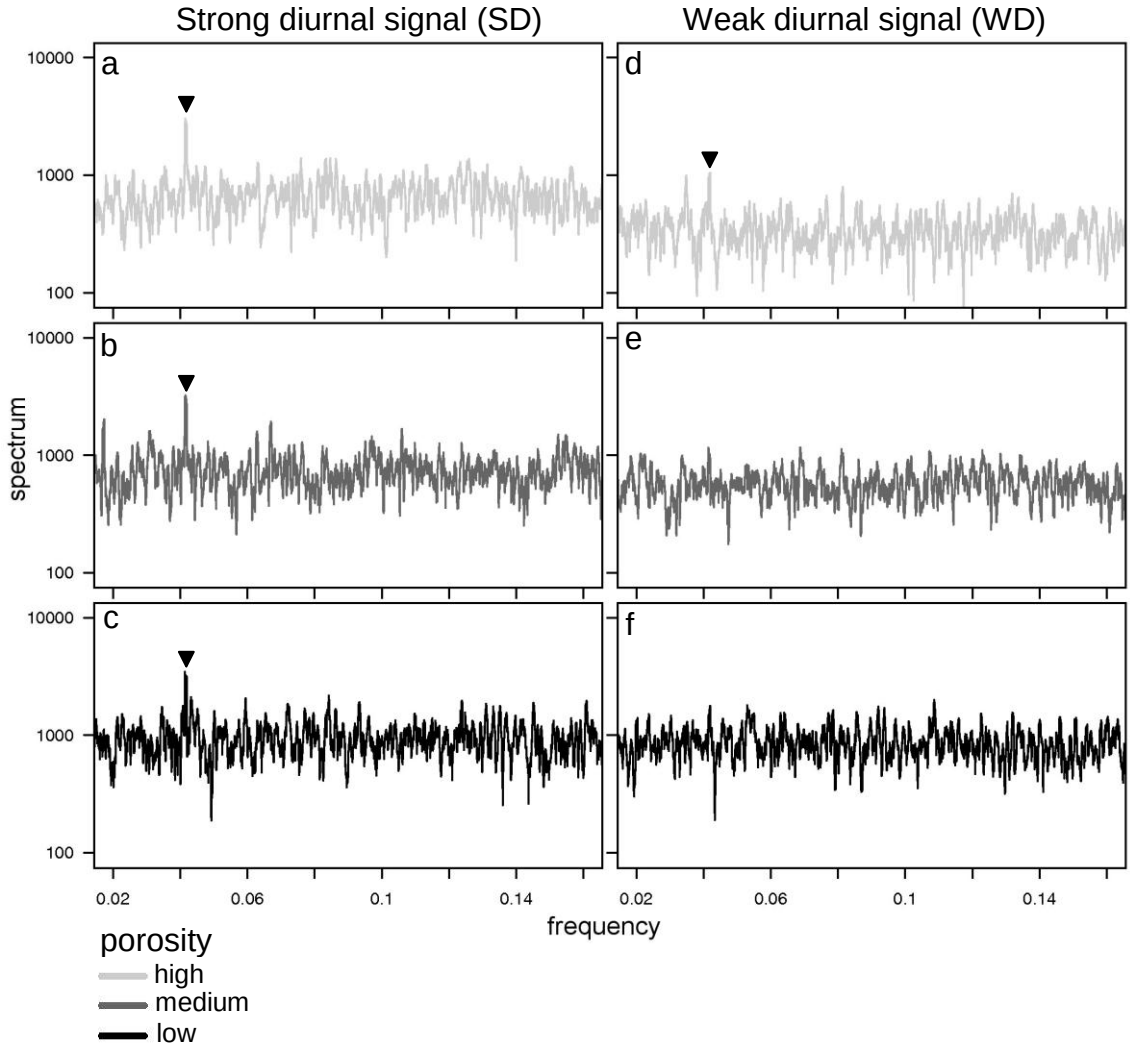

Figure 40. Spectral analysis of diurnal ebullition.

Spectrum of CH_4 flux resulting from a (a,b,c) strong (SD) and (d,e,f) weak (WD) diurnal production signal for peat with high, medium, and low porosity. Triangle indicate significant spectrum peaks (frequency~0.04) that represent periodic flux response to diurnal input signal.

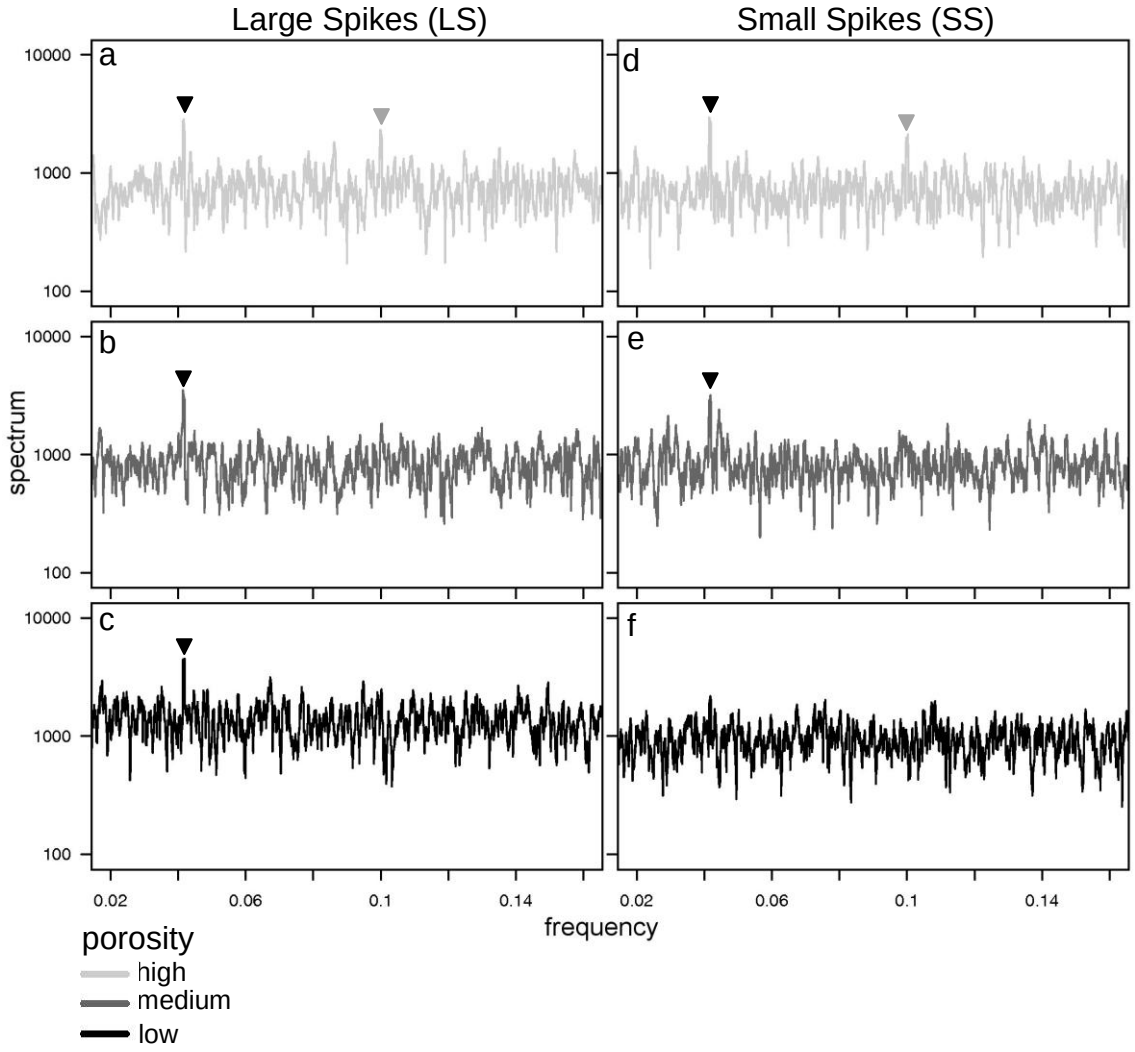

Figure 41. Spectral analysis of spiked ebullition.

Spectrum of CH_4 flux resulting from a strong diurnal production with (a,b,c) large spikes (LS) and (d,e,f) small spikes (SS) for peat with high, medium, and low porosity. Gray triangle indicate significant spectrum peaks (frequency~0.1) that represent flux response to spikes in input signal occurring every 10 hrs. Black triangles indicate significant spectrum peaks that represent diurnal flux response.

5.4. Discussion and Conclusion

This study demonstrates that a near one-to-one link between environmental forcing and CH_4 flux is dependent on peat pore-scale structure. If there was a strong relationship the bubble flux at the surface would mirror the integrated production signals (Figure 42a). Peat with high porosity has less gas storage, and fluctuations in gas production or bubble mobility at depth translate into losses at the peat

surface with minimal time delay. Thus, the openness of the peat structure imparts minimal interference on the original bubble production signal, and traces of this signal exist in the flux (Figure 42b). In stark contrast, lower porosity peat can entirely de-couple environmental forcing and flux response (Figure 42c). The mechanism responsible for this decoupling is pore-scale gas accumulation, storage, and release. In lower porosity peat large amounts of gas are stored within the peat matrix, and released at a time that is distant from the original production fluctuation. This appears to be the case in simulations with weaker signals and medium to low porosity peats. A secondary effect of lower porosity and greater bubble storage is the possibility of producing unsteady bubble flux containing more moderate to large bubbling events (Figure 39d). The overall effect of these events is to produce background noise within the bubble flux, and further masks the presence of the bubble production signals within the bubble flux.

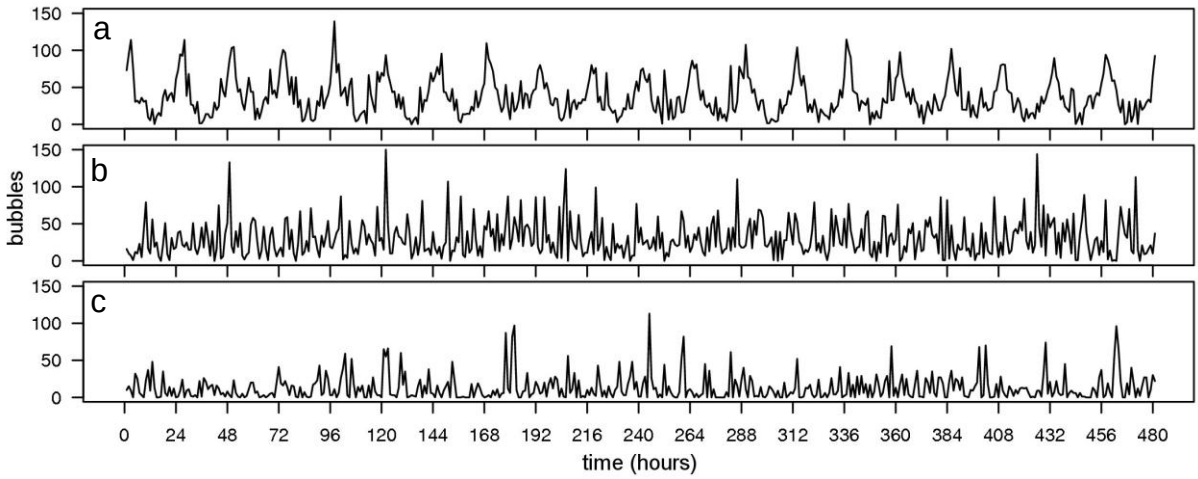

Figure 42. Diurnal ebullition.

Ebullition from peats driven by diurnal production where ebullition (a) mirrors diurnal production, (b) lower porosity peat begins to shred the diurnal signal and (c) the lowest porosity peat completely shreds the signal.

Importantly, the porosity of the deep peat layers does not change dramatically (92-95%), but the resulting signal shredding is very different. For example, a 2% difference in porosity can affect whether a diurnal (Figure 40 d,e) or spiky (Figure 41 a,b) production signal is no longer present in the bubble flux. In the model, this difference in peat porosity contributes to greater amounts of gas storage, and more signal shredding. Although no study to date has investigated if signal shredding occurs in peats, it has been observed that small differences between measured peats (1-4%) can double the amount of gas stored [*Strack and Mierau*, 2010], and affect ebullition [*Strack et al.*, 2006]. With increased gas storage occurring in peats with small structural differences, it is likely that signal shredding will vary greatly over a peatland, and this explains the difficulty in correlating ebullition to environmental forcings.

Lastly, we find that regardless of peat porosity bubble flux from strong bubble signals, occurring diurnally or as spikes, can be correlated to the environmental forcing causing the change in bubble production. Given that peat structure imparts a strong influence on the timing and size of ebullition events, we recommend that peat structure should always be quantified, and locations where peat porosity is low, caution is taken when linking cause and effect between the occurrence of ebullition and explanatory environmental forcings.

Chapter 6 The effect of sampling size and duration on measurements of ebullition from peat

6.1. Introduction

Planning a field investigation of CH_4 ebullition from peat requires consideration of spatial and temporal variability within a peatland. Spatially, a peatland can vary in vegetation cover [*Bubier et al.*, 1995; *Pelletier et al.*, 2007], rates of decomposition [*Belyea*, 1996; *Moore et al.*, 2007], position of water table [*Bubier et al.*, 1993a; *Laine et al.*, 2007], near-surface peat temperature [*Bubier et al.*, 1995] and microforms [*Belyea and Clymo*, 2001]. These characteristics can be spatially irregular across a peatland, and may have an effect on where and when ebullition occurs. Workers have also suggested that variability in peat structure imparts a strong influence on ebullition. For example, differences in peatland permeability have provided explanations for ebullition hotspots and locations where ebullition rarely or does not occur. In a study measuring changes in bog elevation, *Glaser et al.* [2004] recorded rapid decreases in bog elevation caused apparently by the release of gas (ebullition) stored underneath woody impermeable layers. In a separate study, *Strack et al.* [2006] measured ebullition at two sites located within a fen, and suggested that structural differences between the two sites explained differences in ebullition occurrence. At one site with highly permeable peat ebullition occurred regularly, whilst the second site contained less permeable peat that prevented bubbles from reaching the water table.

The magnitude and frequency of ebullition is also dependent on temporal variability in environmental forcings that partly drive the process. These forcings include

short-term (hourly) changes in atmospheric pressure [*Comas et al.*, 2011; *Glaser et al.*, 2004; *Tokida et al.*, 2007; *Tokida et al.*, 2009], or longer-term (days to weeks) variations in water-table elevation [*Glaser et al.*, 2004; *Shurpali et al.*, 1993]. As discussed in Chapter 5, forcings like drops and rises in atmospheric pressure can trigger large episodic ebullition events that can span short time periods (hours). For example, *Tokida et al.* [2007] measured ebullition at 30 min intervals for four days and found that eight ebullition events coinciding with drops in atmospheric pressure comprised 50% of the total CH_4 flux from a peatland.

Thus, the sampling design for a field investigation of peat ebullition should take into account the effect of (i) peatland spatial variability and (ii) temporal variability in environmental forcings that drive ebullition. These two factors are especially important because they can determine where ebullition occurs in a study area and whether the ebullition at a particular site is characteristically erratic, or occurs regularly. If ebullition is spatially variable, many measurement locations are needed to 'capture' the range in flux and the site-wide average across a peatland. A study by *Stamp et al.* [2013] highlighted this point by demonstrating the amount of error in ebullition estimates when few measurement locations ($n \leq 5$) are used. In their study, ebullition from a bog was measured over two microform types (mixed sedge and *Sphagnum* lawns, and mud-bottomed hollows) using 14 inverted funnels per microform type. Overall flux varied spatially, with nine funnels from the total of 28 accounting for ~76% of the summed seasonal flux, and two funnels accounted for ~30% of the total (Figure 43). By calculating the mean flux (per microform type) for every combination of five funnels, it was possible to estimate that there was a ~20% probability of obtaining a mean flux that was 50% less than

the mean calculated with 14 funnels. This suggested that greater sampling effort (n>5) would be necessary to obtain an accurate estimate of ebullition from a peatland with this amount of spatial variability in the process.

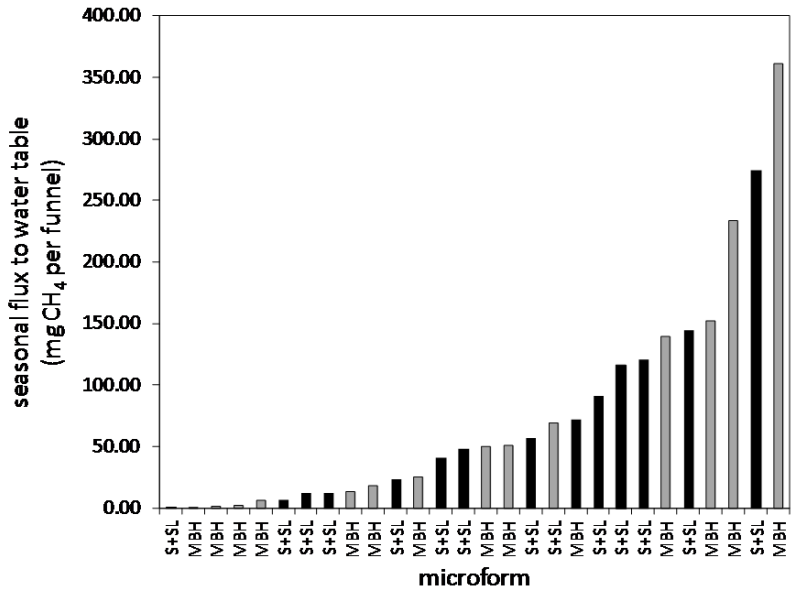

Figure 43. Spatial variability of CH_4 ebullition flux.

Ebullition at the water table measured using 28 inverted funnel gas traps on mixed sedge and *Sphagnum* lawns (S+SL, black bars) and mud-bottomed hollows (MBH, grey bars). Plot taken from *Stamp et al.* [2013].

The frequency of sampling at an individual site where ebullition occurs should consider the temporal variability of the ebullition. If the ebullition occurs erratically over time, a greater number of measurements should be made at that site to record the variability in flux, whilst flux that occurs regularly requires fewer measurements. To illustrate this point, Figure 44 presents examples of characteristically erratic (Figure 44a) and steady (Figure 44b) CH_4 flux (steady ebullition and diffusive flux through peat and plants) obtained from incubated peat samples [*Christensen et al.*, 2003]. Here the erratic ebullition contains infrequent large ebullition events that are short-lived, and may not be recorded if

measurements of ebullition are infrequent. Whereas regularly-occurring or steady ebullition does not contain these large ebullition events and would not require frequent measurements to correctly estimate flux. This difference in the amount of temporal sampling effort required to measure ebullition was noted by *Coulthard et al.* [2009]. In their example of hypothetical ebullition, ebullition events were random in time and occurred on average once a day. From these ebullition data they calculated that measuring ebullition at a site for 30 minutes per week, which is typical for CH_4 flux studies using manual chamber methods, would result in a probability of 1.3% of recording an ebullition event. This suggests that a greater number of measurements are needed to record erratic ebullition events.

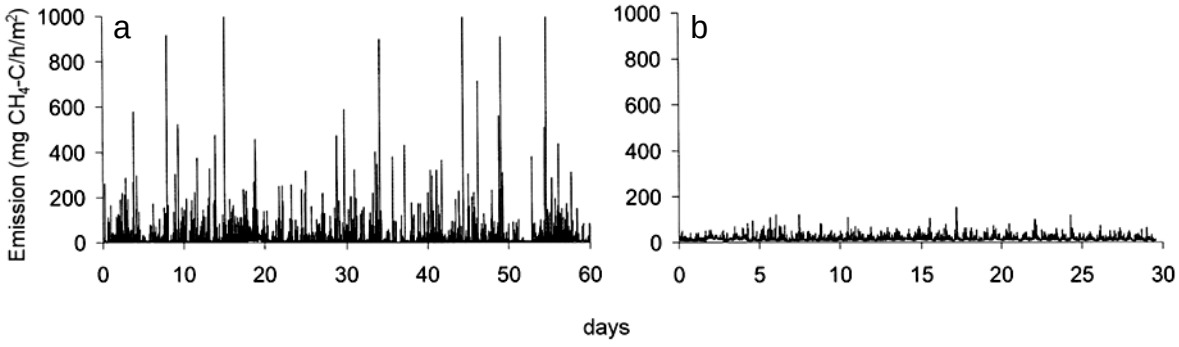

Figure 44. CH_4 flux from incubated peat samples.

CH_4 flux from peat where ebullition comprised (a) 52% and (b) 17% of the total flux (plots taken from Christensen et al. [2003]). These time series may represent (b) regularly-occurring or (a) erratic ebullition. Regularly-occurring ebullition would occur as a steady stream of bubbles, and when measured at the water table may be difficult to separate from gas flux transported via other methods (e.g. molecular diffusion, plant-mediated transport). Erratic ebullition would consist of short-lived bursts of bubbles that are more variable than background steady fluxes, and easier to detect in flux measurements [Green and Baird, 2011].

Resampling methods like bootstrapping offer the possibility to gauge the precision of observations using different amounts of sampling effort. This was the method adopted by *Stamp et al.* [2013] to estimate the number of funnels needed to have acceptable levels of uncertainty in ebullition estimates. In summary, bootstrapping

begins by randomly selecting (with replacement) a sample of *n* records from the available observations (e.g. ebullition fluxes), and calculating a sample statistic (e.g. average hourly ebullition) [*Efron*, 1979; *Sokal and Rohlf*, 1995]. This process of randomly selecting records, and calculating a sample statistic is repeated many times (100s-1000s of replicates) to obtain a distribution of sample statistics. Afterwards, the precision of the sample statistics, provided a certain amount of sampling effort (*n*), can be gauged by calculating the sample statistic's standard deviation or confidence intervals. Here the width of the confidence interval can be interpreted as the amount of precision in the sample statistic. Larger confidence intervals would represent less precise and more uncertain sample statistics, whilst small confidence intervals are sample statistics that are more precise and less uncertain.

Various questions remain unresolved as to the amount of spatial and temporal sampling effort needed to accurately estimate ebullition from peatlands. In this chapter a bootstrapping method was applied to ebullition generated by a computer model. Furthermore, the bootstrapping was performed on ebullition from a modelled peatland that was spatially variable in structure. In doing this it was possible to understand the amount of sampling needed to estimate ebullition from structurally-different peats. It would have been preferable to bootstrap field observations of ebullition from structurally different peats, but this was unfeasible given the number of sampling sites (n=20) and frequency of measurements (hourly) required. Thus bootstrapping the ebullition from the computer model provided a general indication of the errors involved in field sampling peatlands, and this method could show if workers are falling short of the sampling effort needed for

reliable estimates of site-wide ebullition. Specifically, the aim here is to answer the following research questions: (i) How many sites are required to estimate with certainty ebullition flux from a variably structured peatland? (ii) What is the effect of ebullition flux measurement duration on the certainty of ebullition estimates?

6.2. Methods

Using the Model of Ebullition and Gas storAge (MEGA), ebullition from a field-scale 2D profile of spatially-heterogeneous peat was simulated. The profile used in the model was 10 m wide and 1 m deep (thick), and the grid cell size was set to 1 mm x 1 mm (Figure 45a). This resulted in a profile partitioned into 10,000,000 cells, with 1,000 rows and 10,000 columns. The length of shelves representing peat in MEGA were set according to the empirical measurements of *Sphagnum* branches [*Kettridge and Binley*, 2008]. Shelf placement throughout the profile was determined using two right trapezoidal distributions. One distribution was used to randomly select a row within the profile, and the second distribution to randomly select a column. By using right trapezoidal distributions it was possible to produce a variable peat structure that changed in porosity along a vertical and horizontal gradient (Figure 45a). In general, the peat profile had higher porosity shelf arrangements near the peat surface and towards the left side of the profile (Figure 45a). These higher porosity shelf arrangements represented less decomposed peat, whilst shelves located in deeper parts of the profile represented peat undergoing compression and more advanced decomposition [*Boelter*, 1965; *Quinton et al.*, 2000; *Quinton et al.*, 2008]. The resulting profile had porosities (Figure 45b) that were similar to measured values of porosity in shallow peats

(91%-98%) [*Kettridge and Binley*, 2008; *Kettridge and Binley*, 2011; *Parsekian et al.*, 2012].

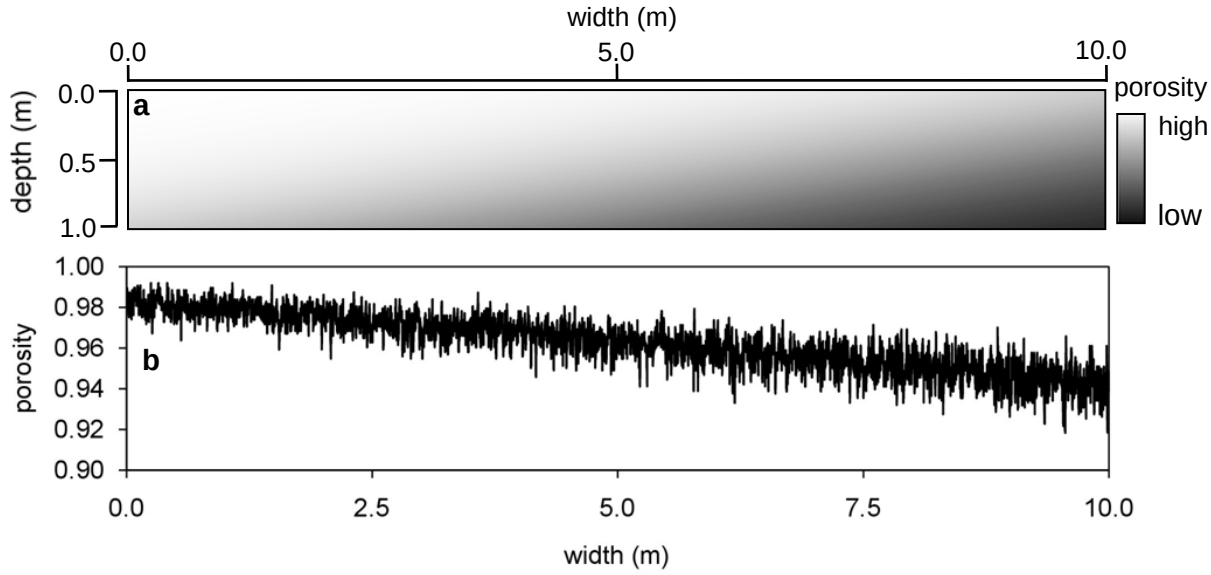

Figure 45. Spatially variable peat profile.

(a) Representation of porosity in spatially variable peat profile (10 m wide, 1 m deep). (b) Profile gradually becomes less porous from left to right.

As in the preceding chapter, bubble production rate was based on data from *Stamp et al.* [2013], who reported maximum, seasonally-averaged, bubble fluxes of 709 mL m^{-2} d^{-1} from mixed sedge and *Sphagnum* lawns in a Welsh raised bog. The smallest bubble within MEGA was 1 mm^2 in area and the up scaled flux for a 10m profile resulted in 7090 mm^2 bubbles d^{-1} available to construct an hourly CH_4 production signal (bubbles hr^{-1}) based on the diurnal patterns observed by *Panikov et al.* [2007]. As in Chapter 5, to reflect the spatial variability in CH_4 production at different depths [*Frenzel and Karofeld*, 2000; *Strack and Waddington*, 2008; *Sundh et al.*, 1994] this production signal was composed of three sub-signals added randomly to the modelled peat profile at three depth zones (0.0-0.3m, 0.3-0.6m, 0.6-1.0m) (Figure 46). Median bubble sizes from a preliminary simulation and theoretical relationships between bubble size and rise velocity within a porous

medium [*Corapcioglu et al.*, 2004] were used to set bubble velocity at a constant 1 mm s^{-1}.

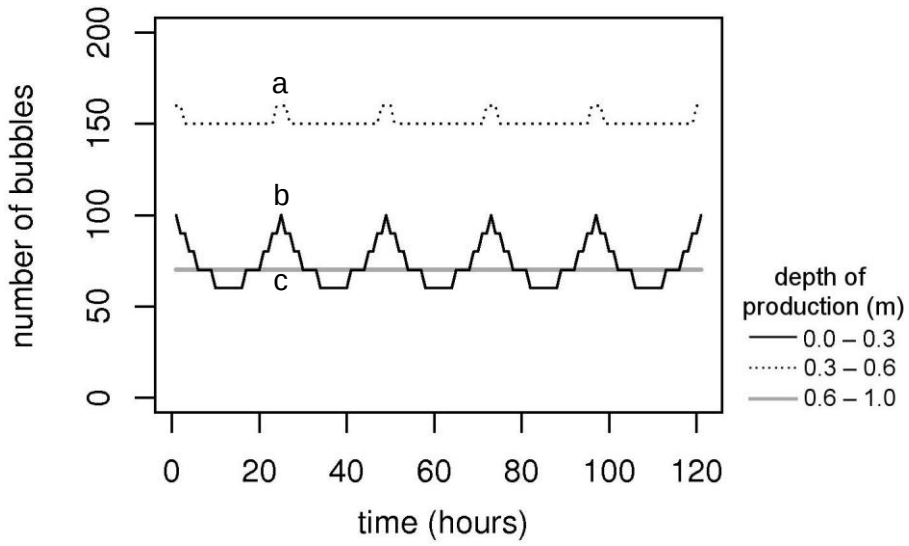

Figure 46. Methane production signals.

CH_4 production decomposed into sub-signals that are (a) weakly diurnal, (b) strongly diurnal, and (c) steady. Sub-signal a, b, c consisted of 50%, 25%, 25% of the daily CH_4 production accordingly and the gas equivalent in bubbles was added at three depth zones across the entire peat profile.

Hourly ebullition totals were 'collected' from every millimetre (1 cell) at the model's peat surface, which was also the height of the water table. The unit of measure for ebullition was the number of 1 mm^2 bubbles per hour. The sizes of the bubbles which comprised the ebullition were recorded. As explained in Chapter 2, bubble size was determined by the length of pixel chains, and reported here as a total area (mm^2). Additionally, the amount of gas stored within the profile at the end of the simulation was recorded. To establish initial conditions and saturate the profile with gas, the profile was driven with the production signal until the ebullition flux, averaged over a 10-day period, stabilized. Model data 'collected' after this time period were analyzed. The duration of the collection period was 6087 hrs (~254

days), and was similar in duration to a field survey measuring ebullition from peat by Goodrich *et al*. [2011]. The model simulation took 222 hrs to complete on a single computer with a six core processor operating in parallel.

Bootstrapping the modelled ebullition made it possible to gauge the amount of spatial and temporal sampling effort required to estimate ebullition flux from the structurally-varying peat profile. Here it was assumed that the ebullition would be sampled using chambers that were attached to the peat surface. This method, in the field, involves visiting a site at a time interval (e.g. weekly), placing an air-tight enclosure over an area of peat and measuring the concentration of CH_4 over a short period of time (30 mins) [*Tokida et al.*, 2007]. Workers then plot the concentration of CH_4 samples against time and search for nonlinearities in the plot (e.g. steps) that indicate erratic ebullition. Rates of ebullition in the computer model of ebullition were calclutated as total ebullition (bubbles), per hour, per chamber. This was accomplished by subdividing the peat profile vertically into 40 model chambers, with each chamber having a width of 250 mm. These chambers were placed end to end on the peat surface and from these 40 chambers unique random combinations of chambers were created for bootstrapping.

Temporal sampling effort was determined by the time interval (e.g. hourly, daily, weekly) upon which a chamber was placed on the peat surface and one hour of ebullition was recorded. A total of 580 combinations of chambers and sampling time intervals were performed (Figure 47). This included between 1 and 20 chambers with increments of one chamber, and sampling time intervals between 1 and 168 hr, incrementing by six hours. Temporal sampling effort at long time

intervals (e.g. 168 hr) were chosen to represent traditional chamber methods that sample sites infrequently (weekly) [*Coulthard et al.*, 2009], and shorter time intervals (e.g. 1 hr) represented frequent sampling using automated chambers [*Goodrich et al.*, 2011].

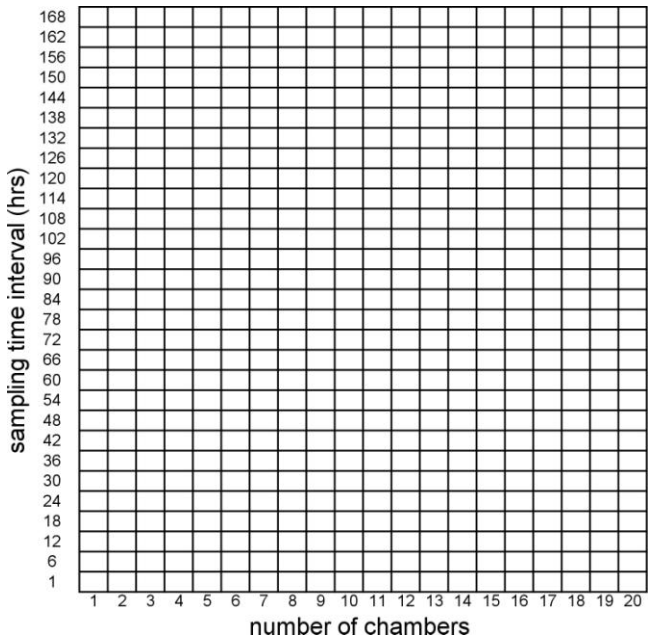

Figure 47. Sampling effort.

Matrix of bootstrapping combinations performed with different number of chambers and chamber revisit times.

Determine the number of chambers available (e.g. 10 chambers).

Determine the sampling time interval for chamber placement and ebullition measurement (e.g. 168 hrs).

Repeat until 1000 replicates of average ebullition obtained.

Repeat for number of randomly selected chambers.

Select the ebullition records that correspond to the sampling time interval.

Calculate the **average** ebullition (bubbles chamber^{-1} hr^{-1}) of the sampled events from all chambers.

Calculate 95% confidence interval of the 1000 **average** ebullition values.

Figure 48. Bootstrap algorithm.

Figure 48 presents the algorithm used in the bootstrap method for one combination of chambers and sampling time interval. This method was applied to each of the

580 combinations of chambers and sampling time intervals to produce distributions of average ebullition (*n*=1000 per distribution). To gauge the uncertainty of the average ebullition the 95% confidence interval of each distribution was calculated. Here, as an example of bootstrapping outputs, three distributions of average ebullition are provided with temporal sampling effort kept constant, but increasing amounts of spatial sampling effort (Figure 49). From these distributions it can be seen that the peat profile sampled with few chambers (Figure 49a) produced wider 95% confidence intervals for average ebullition than sampling performed with more chambers (Figure 49 b,c). Moreover, the width of the confidence intervals suggests that increasing the number of chambers decreases the uncertainty in average ebullition.

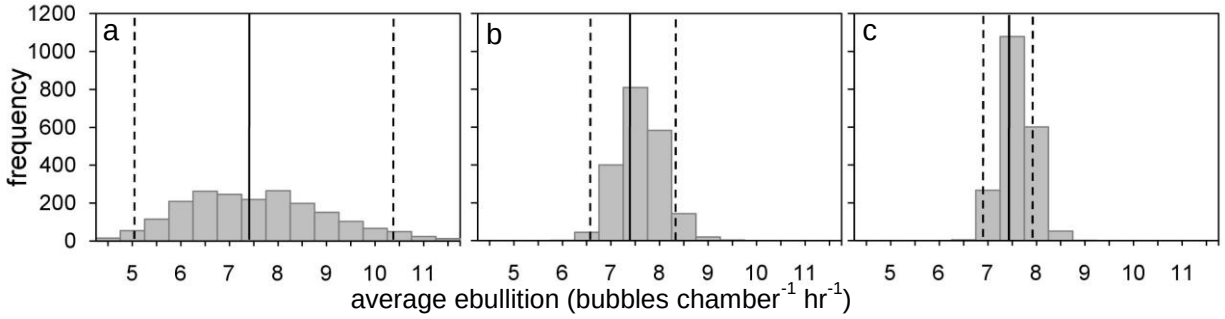

Figure 49. Distributions of average ebullition.

Distributions of average ebullition from the profile sampled every 168 hrs with (a) one, (b) 10 and (c) 20 chambers. Lines indicate 95% confidence interval (dashed) and bootstrapped average of distributions (solid).

The true average ebullition from the modelled peat profile was 7.5 bubbles chamber^{-1} hr^{-1}. To quantify the effect of different amounts of sampling effort (spatial and temporal), the relative error between the average of the ebullition distributions and the true average ebullition were calculated. Furthermore, the error between the 95% confidence interval (lower and upper) of the ebullition

distributions and the true average ebullition were calculated. All relative errors are presented as percentages.

6.3. Results

A total of 469,953 bubbles exited the peat profile over the 254 model days. The mean bubble size was 4 mm^2, with a minimum and maximum size of 1 mm^2 and 115 mm^2 respectively. Overall bubble sizes from the peat profile display a power law pattern (Figure 50a), with many occurrences of small bubbles and fewer large bubbles. For every hour of the 6087 hr simulation at least one ebullition event occurred consisting of multiple bubbles. The smallest hourly ebullition event was 79 bubbles and the largest 609 bubbles. The mean hourly ebullition was 299 bubbles. Plotting the magnitude and frequency of ebullition events (Figure 50b) produced a histogram that was non-normal and positively skewed (skewness = 0.5, this value was interpreted as moderate skewness).

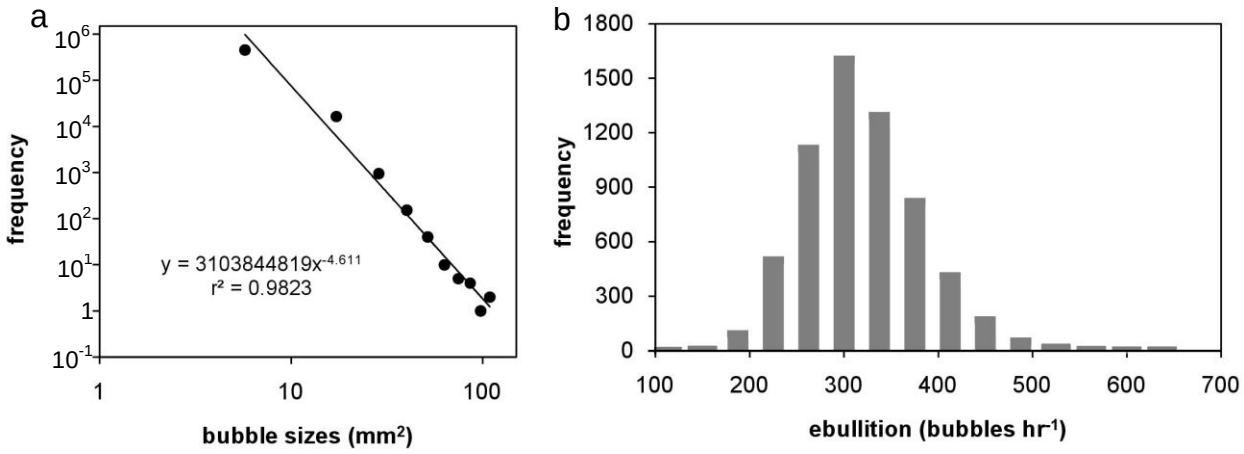

Figure 50. Bubble size and hourly ebullition from peat profile.

(a) Magnitude and frequency of bubble size with fitted power law distribution having $p<0.05$. (b) Magnitude and frequency of hourly ebullition.

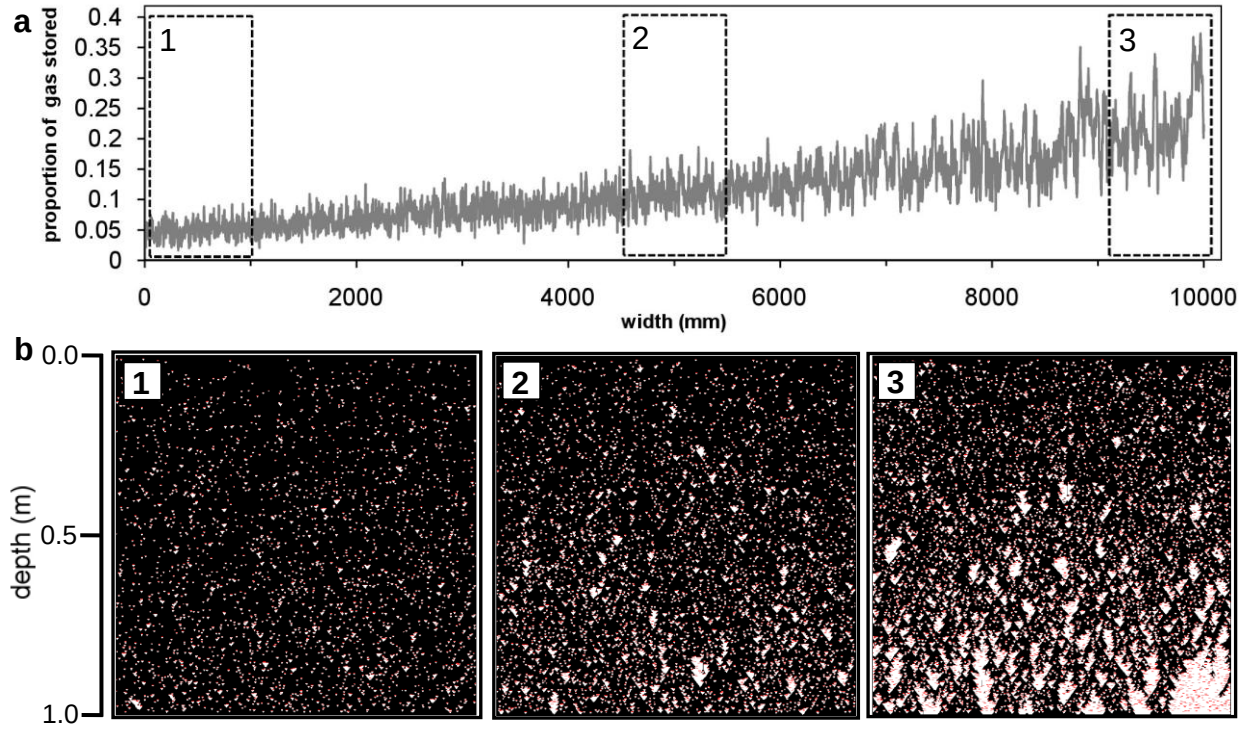

Figure 51. Gas storage.

(a) Proportion of vertical gas storage per millimetre of peat profile. Dashed boxes correspond to shelf arrangements below. (b) Examples of gas storage from MEGA for (1) high, (2) moderate and (3) low porosity shelf arrangements (peat in red, gas in white, and water in black).

Gas storage throughout the entire profile was 11%, and was within the range of measured gas storage in peat (0-19%) [*Rosenberry et al.*, 2006]. The structural difference within the peat profile led to variability in gas storage. This variability in gas storage was a result of the two gradients (horizontal and vertical) that were used to position the shelves within the profile. Across the profile, from left to right, the porosity of the shelf arrangements, when measured vertically per millimetre, decreased from 98% to 93% and gas storage, measured in the same manner, increased linearly from 3% to 37% (Figure 51a). This positive trend in gas storage can also be visualized in three subsets of the profile taken at the end of the simulation (Figure 51b). By calculating the shelf porosity and bubble storage of each subset it was possible to ascertain that the left side of the profile (Figure 51b,

inset 1) had a shelf porosity that is high (98%) and a low amount of gas storage (5%). In contrast the subset from the right side of the profile (Figure 51b, inset 3) had lower shelf porosity (95%), and higher gas storage (23%).

The effect of the vertical gradient used to place more shelves at greater depths contributed to more bubble storage at the base of the peat profile. Thirty-two percent of the bubbles stored in the entire profile were located at shallower depths ≤0.5 m) and 68% of the stored bubbles were found at deeper locations in the profile >0.5 m). This difference in bubble storage was most evident on the right side of the profile (Figure 51b, inset 3) where gas storage was greatest at a depth near 1 m.

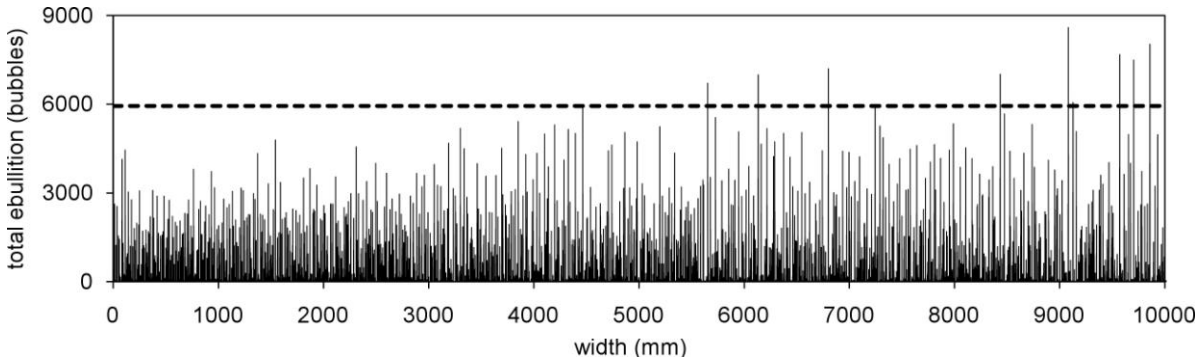

Figure 52. Spatial variability in ebullition.

Total ebullition from peat profile. Dashed line is 99.9th percentile of total ebullition.

The spatial variability of total ebullition differed across the peat profile (Figure 52). Of the 10 m of peat simulated, only 47% of the peat produced ebullition, and 50% of the ebullition came from 3% of the profile. In general the ebullition from the profile became more variable in space with lower shelf porosities. The effect of shelf porosity on the location of ebullition can be seen by comparing the higher porosity, left side of the profile (LSP, distance across the profile <5000 mm) with the lower porosity, right side of the profile (RSP, distance across the profile >5000

mm). Although both sides of the profile produced similar amounts of total ebullition after spin up (~900,000 bubbles), the RSP had greater spatial variability with highly irregular ebullition (st. dev=699 bubbles per mm of profile), and the LSP produces ebullition occurring more uniformly in space (st. dev=614 bubbles per mm of profile) (Figure 52). Locations of extreme ebullition were identified using the 99.9th percentile of the total ebullition across the profile. Using this cut-off, locations of greater ebullition only occurred on the RSP (Figure 52, dashed line=99.9th percentile). Furthermore, these extreme amounts of ebullition were proximate to locations of low ebullition and this disparity in ebullition contributed to greater spatial variability in ebullition from the RSP.

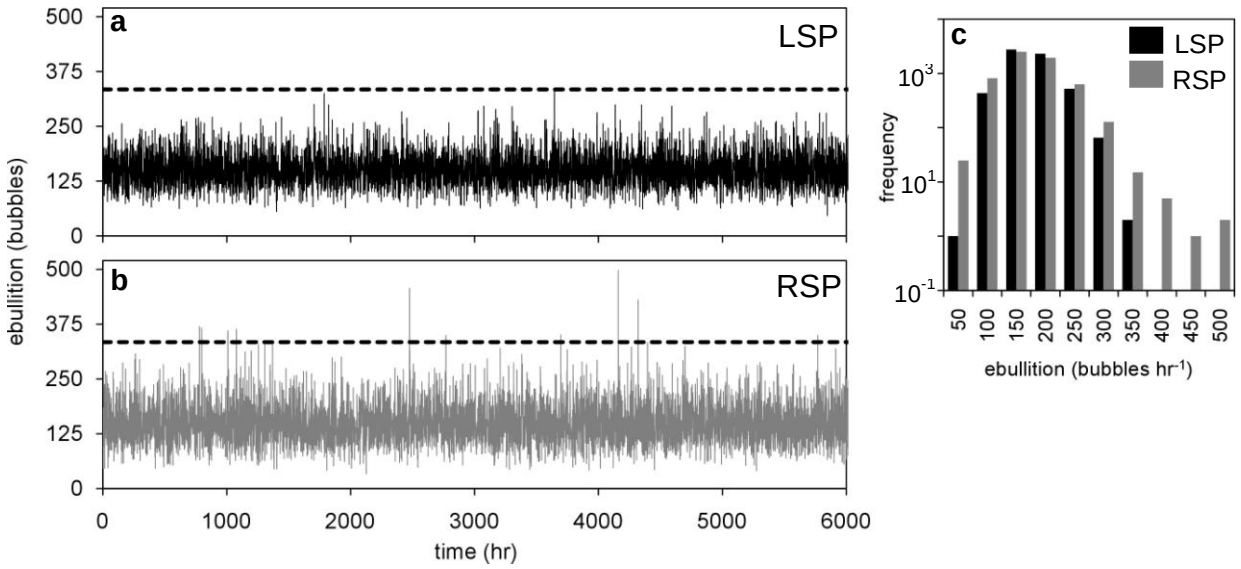

Figure 53. Temporal variability in ebullition.

Hourly ebullition events from the (a) LSP and (b) RSP. Dashed line is 99.9th percentile of hourly ebullition events from the entire profile. (c) Histograms of the hourly ebullition events from the LSP and RSP.

The temporal variability of hourly ebullition was also dependent on the porosity of the underlying shelf arrangements. Over the course of the 254 simulated days the high porosity LSP and low porosity RSP had noticeably different amounts of

temporal variability in ebullition (Figure 53 a,b). Here both sides of the profile had similar mean hourly ebullition (~150 bubbles hr^{-1}), but the RSP generated hourly ebullition that was more erratic (min=15 bubbles hr^{-1}, max=498 bubbles hr^{-1}, st. dev=46 bubbles hr^{-1}) than ebullition from LSP (min=46 bubbles hr^{-1}, max=337 bubbles hr^{-1}, st. dev=37 bubbles hr^{-1}). Moreover, the extremely large hourly ebullition events (>99.9th percentile) only occured on the RSP (Figure 53 a,b, dashed line=99.9th percentile). The erratic nature of ebullition from the RSP can also be identified in side-by-side histograms of hourly ebullition from the LSP and RSP (Figure 53c). The RSP produced considerably more small (<100 bubbles) and large (>350 bubbles) ebullition events than the LSP.

Error in average ebullition estimates decreases with greater spatial and temporal sampling effort. This trend is visible in the decreasing amount of error in the averages and 95% confidence intervals of ebullition distributions produced by performing the bootstrapping resampling with 1-20 chambers, and visiting the profile once every hour, day, or week (Figure 54a). Comparable amounts of error can be obtained with different amounts of sampling effort. For example, to obtain a maximum of ±10% error in average ebullition the profile could be sampled with 14 chambers every week, four chambers every day, or one chamber every hour (Figure 54a, dashed lines). These error plots (Figure 54a) also show that the upper and lower confidence intervals are nearly symmetrical, indicating an equal probability of over or under estimating average ebullition for these sampling combinations.

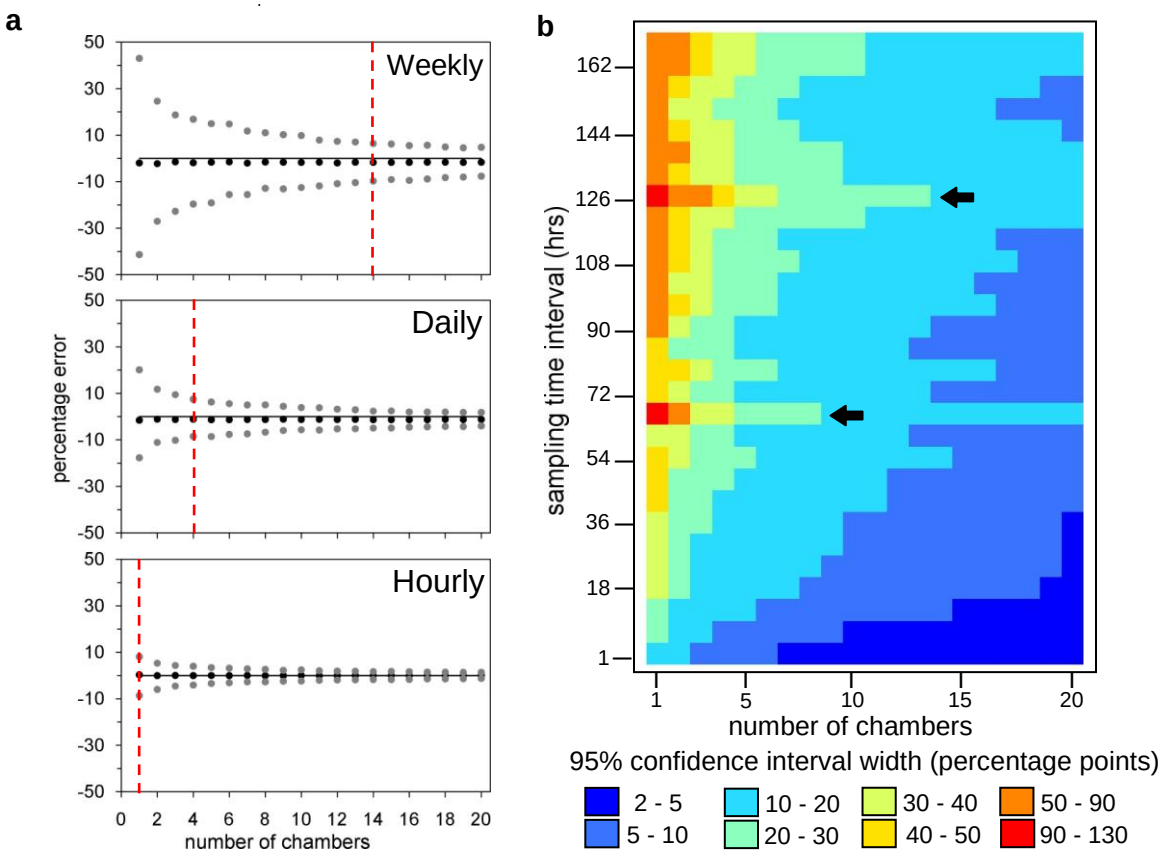

Figure 54. Error in average ebullition.

(a) Percentage error between the true average ebullition and the average (black points) and 95% confidence interval (grey points) of the average ebullition distributions from 1-20 chambers sampled weekly, daily and hourly. Dashed red line indicates locations of ±10% error. (b) Error map representing the width of the 95% confidence interval of the average ebullition distributions. Black arrows indicate peaks in error.

Another approach to visualize the error in the average ebullition is to calculate the width of the 95% confidence interval (i.e., the area between the upper and lower confidence intervals) (Figure 54b). As before, the amount of possible error in predicting the true average ebullition is provided as a relative error. Figure 54b summarizes the possible error for each combination of chamber and sampling time interval as an error map. From the error map it is possible to distinguish regions with similar amounts of error, but different amounts of sampling effort. For example, the lower right corner of the map indicates sampling schemes that

produce the lowest amount of error. This includes schemes with high temporal and low spatial sampling effort (e.g. seven chambers sampled hourly) or moderate temporal and high spatial sampling effort (e.g. 20 chambers sampled every 36 hrs). Unexpectedly the greatest amount of error does not correspond to sampling with the fewest chambers, and sampling infrequently (1 chamber, every 168 hrs). Instead error is greatest with one chamber visited every 126 hrs and the second largest amount of error occurs with one chamber visited every 66 hrs.

6.4. Discussion and Conclusions

In this investigation a field-scale (10 m) simulation of ebullition from peat was performed using MEGA. This simulation demonstrated the computational efficiency of the reduced complexity approach implemented within MEGA. In less than 10 days of computer time, MEGA routed 100,000s of micro gas bubbles (1 mm^2) through a model peat profile consisting of shelves that were represented by a gridded structure of 10,000,000 cells. This simulation was a major advancement in modelling field scale gas movement, storage and ebullition in peat.

Ebullition from the simulated peat profile resulted in a positively-skewed distribution of ebullition events and was similar in shape to results reported by workers measuring ebullition in the field [*Goodrich et al.*, 2011; *Kellner et al.*, 2006; *Stamp et al.*, 2013] and laboratory experiments (Chapter 4). The simulated ebullition was comprised of bubble sizes that displayed power law patterns, and were consistent with patterns found from laboratory experiments on peat (Chapter 4). Gas storage within the peat profile was 11% and within range of gas storage in northern peatlands (0–19%) (see *Rosenberry et al.* [2006] for review). Furthermore, the

spatial distribution of storage in the simulation was dependent on the porosity of the shelf arrangements. At the base of the profile the shelf arrangement porosity were lower and large amounts of gas accumulated underneath shelves. These gas trapping properties have also been observed in peats with lower porosity [*Glaser et al.*, 2004; *Strack and Mierau*, 2010].

The structure of the peat profile in this simulation had contributed directly to the variability of ebullition in space and time. Here, the variability in ebullition was directly caused by the porosity of the shelf arrangements and the resulting amounts of bubble storage; as no environmental controls, such as changes in atmospheric pressure and peat temperature, were simulated. Locations in the profile with high shelf porosity and low bubble storage had few bubbles available for ebullition. These conditions were found in the LSP and resulted in ebullition that occurred uniformly in space, and regularly in time. In contrast, low shelf porosity and high bubble storage resulted in large quantities of bubbles stored. These isolated bubble storage 'hotspots' were found in the RSP, and resulted in ebullition that was spatially irregular and temporally erratic.

The near vertical banding in the error map (Figure 54b) indicated that error in ebullition was more dependent on the number of chambers deployed than the frequency of measurements performed. Where the vertical banding was irregular, temporal variability in ebullition contributed to uncertainty in ebullition estimates. This uncertainty was greatest when sampling the profile at time intervals of 66 and 126 hours (Figure 54b, black arrows). At these sampling intervals the error propagated through the error map as horizontal peaks. This pattern suggested

that increasing the spatial sampling effort at these sampling intervals (66 and 126 hrs) had a reduced effect on minimizing error. To understand these unexpected horizontal peaks in the error map the variability in the ebullition was examined at these sampling intervals. The temporal variability of ebullition across the entire profile at the time intervals of 66 hours (Figure 55a) and 126 hours (Figure 55b) reveals that a spike in ebullition was recorded in both time series at the time of 4,158 hours. Furthermore, the spatial distribution of this ebullition spike was distributed across the peat profile in a highly clustered manner (Figure 55c). This resulted in an ebullition 'hotspot' that occured within one chamber (chamber 38) and accounted for 58% of the ebullition spike.

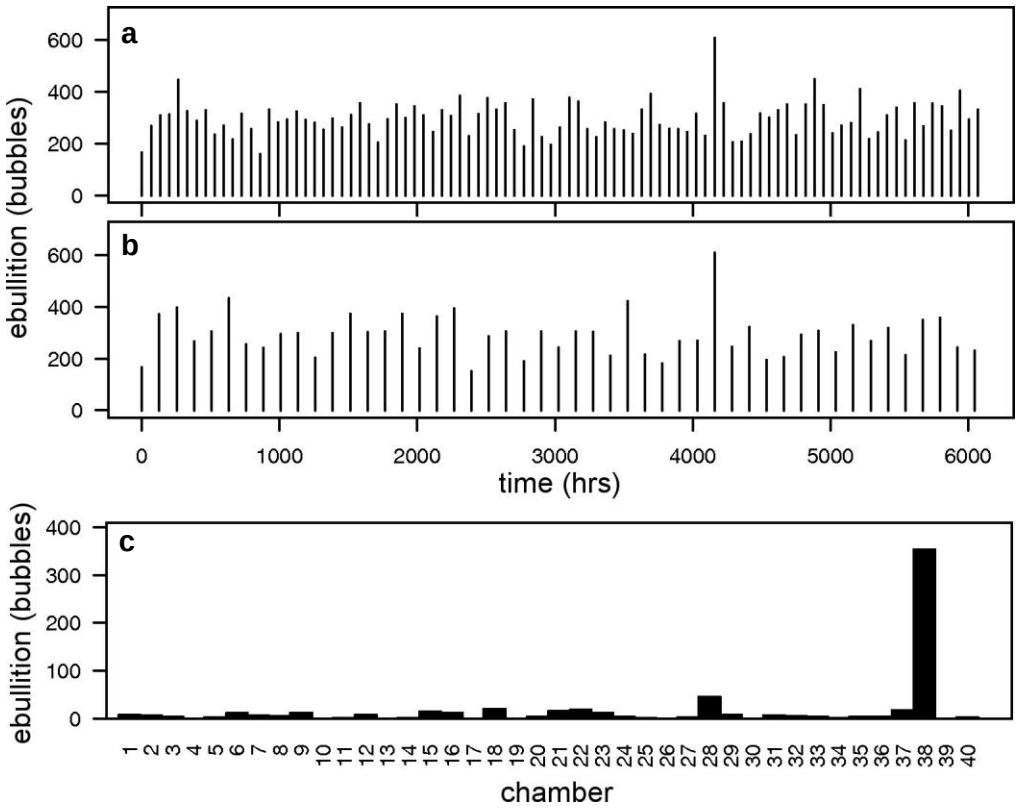

Figure 55. Ebullition spike in time and space.

Total ebullition sampling the peat profile at time intervals of (a) 66 hours and (b) 126 hours. (c) Spatial distribution of one hour of ebullition occurring at hour 4,158 of the simulation.

The overall effect of this ebullition spike concentrated over a small area of the profile was the tendency to overestimate average ebullition. From the perspective of temporal sampling effort, the low number of records obtained when sampling the peat every 66 and 126 hours, *n*=93 and *n*=49 respectively, allowed the spike in ebullition to skew the average ebullition. When combining these low sample sizes, with a low number of deployed chambers, the probability of overestimating or underestimating the average was compounded. For example, sampling with one chamber visited every 126 hours, the error in average ebullition may be overestimated by 88% or underestimated by 42%. The effect of the ebullition spike was reduced when the peat profile was sampled with more chambers, and increasing the number of chambers to five produced symmetrical amounts of error of ±20%.

The variability in ebullition produced uncertainty in ebullition estimates, especially when low amounts of sampling effort were used. With traditional chamber methods that measure ebullition once a week, with few chambers (*n*=4), the results suggested up to 20% error in ebullition estimates. Furthermore, this amount of error may be conservative because the variability in ebullition is solely produced by the storage and release of gas from the shelf arrangements. Greater variability and uncertainty in ebullition would be expected from a model that includes variable gas production and external triggers that produce large bubble releases. Another interesting result was that low sampling effort can ‘capture’ large bubble events that likely result in ebullition overestimates. A study that bootstrapped weekly field measurements of ebullition recommended a sample size (e.g. number of chambers) >14 [*Stamp et al.*, 2013]. Here the bootstrapping of simulated ebullition

supports this conclusion, but additionally recommends that chambers should be visited more frequently (hourly to daily).

Chapter 7 Conclusions and future work

7.1. Conclusions

The statistician George E. P. Box wrote “Remember that all models are wrong; the practical question is how wrong do they have to be to not be useful.” [*Box and Draper*, 1987]. This quote essentially summarizes the work performed within this thesis. In Chapter 2 the upside down sand pile model (MEGA) was introduced as a model of gas movement, storage, and release (ebullition) from peat. This unorthodox model was presented as an alternative to modelling approaches that are physically rigorous, but limited by computational expense or numerical instability (e.g. CFD and lattice-Boltzmann models). At the core of MEGA are the explicit representation of peat structure and the process of bubble storage. Although these two model components are ‘key’ to simulate ebullition, they have been underappreciated or neglected by modellers of ebullition from peat. To this end, the bulk of the work reported in this thesis set out to determine the answers to three questions: (i) How ‘wrong’ is MEGA? (ii) How ‘useful’ is MEGA? and (ii) What is the effect of peat structure on ebullition?

In Chapter 2 preliminary simulations from MEGA indicated that the model contained the key processes needed to predict ebullition from porous media like peat. Patterns from peat bubble storage and ebullition from published literature were mirrored in MEGA outputs. These included (i) increases in gas storage with decreases in shelf/peat porosity or permeability, and (ii) small ebullition events occurring often, and large bubbling events occurring rarely. To further test MEGA, in Chapter 3 empirical observations were obtained through laboratory experiments

using the shelved bubble machine (SBM). The SBM was a physical analogue of MEGA that was designed to measure gas storage, bubble size, and volumetric rate of bubble release from a porous medium represented by shelves. Patterns from these experiments were compared directly to MEGA output, allowing us to conclude that both models:

- Produced bubble storage that increases with decreasing shelf porosity and permeability.
- Produced bubble sizes distributed according to a power-law distribution.
- Produced volumetric bubble release distributed according to a power-law distribution.

This initial evidence indicated that MEGA was not entirely 'wrong'. Although there were differences between the two models that were likely caused by scaling issues and bubble distortion, the overall patterns for bubble storage, size, and release were similar. Furthermore, the exceptional performance of MEGA suggested that pore structure and bubble storage are important model components for a model of ebullition.

Chapter 4 used a physical model of ebullition from peat, the cylindrical bubble machine (CBM), to generate patterns of bubble size and release from two peat types that were structurally different. Although MEGA was not used to directly simulate these physical experiments, the patterns obtained from the CBM provided indirect evidence that supports MEGA. These patterns included:

- Bubble sizes that were distributed according to a power-law distribution.
- Volumetric bubble release that were non-normal and positively-skewed.

These patterns were similar to those produced by MEGA in the model sensitivity analysis in Chapter 2. Additionally, analysis of the pore spaces in the two peats used in the CBM suggested that differences in pore structure alone can produce characteristically different ebullition. Although it was not possible to measure gas storage within the peat samples, the data on pore sizes suggested that 'erratic' ebullition occurred when large amounts of gas stored at depth could easily move through shallower layers of open peat. In contrast, regularly occurring ebullition occurred when dense shallower layers of peat formed a 'seal' that regulated the flow of gas emitted from the peat. This conclusion differed from our initial expectation where less permeable peat layers trap gas and rupture to produce extremely large bubble releases. Another important finding from the CBM experiments was the similarity in ebullition patterns between published observations of ebullition from the field and the CBM bubble release. This indicated that injecting air into peat could be a valid proxy for naturally occurring ebullition, and this was reassuring because bubble release patterns from the CBM provided indirect support for MEGA.

At this stage of the thesis (Chapter 5 and 6) it was assumed that MEGA was not 'wrong' and may be 'useful' as a model of ebullition from peat. The remaining two chapters of the thesis were numerical exercises that investigated the effect of peat structure on ebullition. Chapter 5 looked at the 'shredding' of environmental signals that may be present in ebullition. Results from MEGA simulations suggested that a simple correlation between ebullition and environmental forcing factors (e.g. atmospheric pressure or solar radiation receipt) may not always occur. In these simulations, the explanation for decoupling between cause and effect of

ebullition was the structure of the peat. It was found that low porosity peat can store gas for lengthy periods of time, and act as a buffer that releases bubbles at a time completely disconnected from the forcing. When this occurs, the resulting ebullition at the peat surface, bears no resemblance to the underlying forcing (represented, e.g., by diurnal or 'spiked' production signals). It was also found that buffering of the forcing was reduced when peat porosity is high, and a clearer link was maintained between forcing and ebullition. The results from this exercise suggested that peat structure may be an important variable that needs to be taken into account when trying to understand and model ebullition.

Chapter 6 investigated the effect of sample size and sampling duration on ebullition estimates from peat. A field scale (10 m), seasonal scale (>90 days) simulation of ebullition from a structurally-varying peat profile was modelled using MEGA. The spatial and temporal scale of this simulation was possible because of the computational efficiency of the reduced complexity approach implemented in MEGA. The patterns of ebullition from this large scale simulation were consistent with the patterns obtained from the SBM and previous MEGA simulations (Chapter 2 and 3). These patterns included:

- Bubble storage increased with decreasing shelf porosity and permeability.
- Bubble sizes were distributed according to a power-law distribution.
- Volumetric bubble releases were non-normal and positively-skewed.

The simulated ebullition from the peat profile suggested that decreases in peat porosity produce ebullition that becomes increasingly patchy in space and erratic in time. Furthermore, it was possible to determine the uncertainty in ebullition

estimates by applying different amounts of spatial and temporal sampling effort to measure the process. The resulting ebullition estimates suggested that the combination of high sampling effort (spatial and temporal) produced low uncertainty in ebullition estimates, but, unexpectedly, the lowest sampling effort (spatial and temporal) did not produce estimates with the highest uncertainty. Instead the highest uncertainty in ebullition estimates occurred when spatial sampling effort was low, and temporal sampling was moderate. At this level of sampling effort, the combination of few observations of ebullition and the possibility of measuring large ebullition events can result in overestimations of ebullition.

7.2. Future work

The testing of MEGA in this thesis has provided some encouraging results, and more research on ebullition could be carried out using the model. The work in this thesis found that peat structure strongly influenced ebullition, and this suggests that more MEGA simulations should be performed using different shelf arrangements. Of particular interest would be the inclusion of macroscale (cm-m) structures found within peat profiles. At present, shelf arrangements in MEGA were constructed to obtain shelf arrangements of certain porosity, but the spatial distribution of shelves was neglected. Most likely this does not replicate the natural system well; especially when peat may contain folds, voids and fractures [*Comas et al.*, 2008; *Parsekian et al.*, 2011; *Strack and Mierau*, 2010]. This level of complexity can be added to MEGA and could be used to investigate the effect of shelf arrangement spatial structure (i.e., macro peat structure) on ebullition. Work could begin with synthetic shelf arrangements produced with varying degrees of shelf clustering (Figure 56a) or shelf patterning (Figure 56b). For example, some

peatlands can display striped patterning when alternating ridge-hollow microforms occur [*Belyea and Clymo*, 2001]. Ridges typically contain peat types that are densely packed, with woody roots, whilst peat types located in hollows are loosely packed [*Strack and Mierau*, 2010]. This patterning could be implemented in MEGA by designating different porosities to zones representing ridges and hollows within the shelf arrangement (Figure 56b). Another more realistic approach to spatially distribute shelves would be to use existing surveys of peat structure (e.g. ground penetrating radar) to allocate shelves in regions where woody layers or low porosity peat exists.

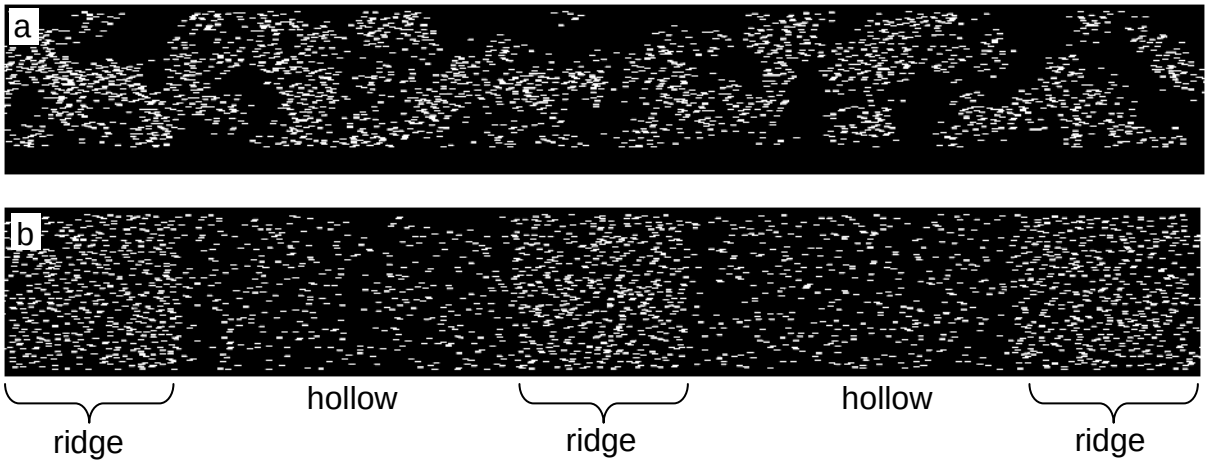

Figure 56. Shelf arrangements with spatial structure.

Shelf arrangement constructed with a (a) clustering and (b) striped patterning algorithms.

Other possibilities to extend the work with MEGA include the representation of additional real-world processes. The simulations performed in Chapter 5 and 6 mainly focus on the spatial and temporal variability of ebullition caused by peat structure. Variability in ebullition may also be caused by variability in gas production, but this process was not fully developed within MEGA. For example, temporal variations in gas production (e.g. diurnal) were represented with production signals (Chapter 5 and 6) that were loaded into MEGA, whilst spatial

variability in gas production occurred within three depth zones at random locations. This approach may be adequate to replicate some of the temporal variability in production, but improvements should be made regarding the location of gas production within peat. Temperature [*Christensen et al.*, 2003] and the availability of labile carbon [*Coulthard et al.*, 2009] are factors that determine the location of gas production and this information could be used to develop model processes that generate spatially distributed gas production.

Other processes that could be developed in MEGA may further increase the variability of ebullition within the model. It is known that fluctuations in atmospheric pressure can trigger large ebullition events by increasing bubble mobility and volume [*Comas et al.*, 2011; *Glaser et al.*, 2004; *Tokida et al.*, 2007; *Tokida et al.*, 2009]. This was replicated in MEGA by superimposing a 'spiked' signal on gas production (Chapter 5). Although this reproduces the effect of changing atmospheric pressure on stored bubbles in peat, it does not directly model the physical process. As MEGA is a cellular automaton, and gas movement in the model is governed by simple rules, new rule sets could be developed to replicate changes in atmospheric pressure on bubbles. Increasing bubble mobility could be accomplished by developing toppling rules that release stored bubbles by reducing the cohesiveness of the inverted sand piles.

Another process that may occur in peatlands is the accumulation of gas underneath less permeable peat layers, and the subsequent rupture of peat that releases large amounts of gas [*Glaser et al.*, 2004]. Rules within MEGA could be developed to identify locations, within a shelf arrangement, where large amounts of

gas are stored and segments of shelves can be removed to reproduce peat rupturing. Figure 57 represents a sequence of MEGA screenshots where a large quantity of stored gas is released after segments of shelves are removed.

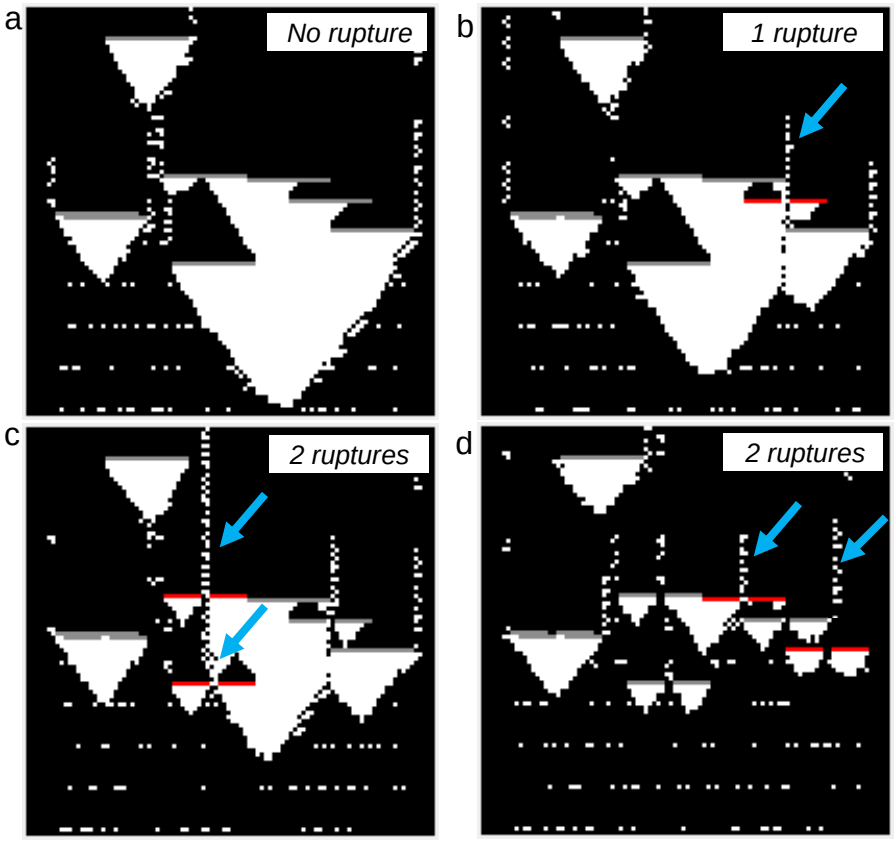

Figure 57. Peat rupture.

MEGA screenshots where a large sand pile is released after segments of shelves are removed to replicate peat rupturing. Ruptured shelves are coloured red, and arrows highlight large releases of gas. Time begins with image 'a' and ends with image 'd'.

A logical next step for MEGA is the development of a three dimensional version of the model (MEGA 3D). MEGA 3D would address the differences in bubble storage between the SBM and MEGA reported in Chapter 3. Furthermore MEGA 3D will allow direct testing of the model against ebullition from peat. Initial work has already begun on MEGA 3D, and this version of the model has adapted the 2D rule set used in MEGA to route and store gas in 3D (Figure 58). In MEGA 3D, peat fibres are represented by shelves with a specified length and width, and shelves

are positioned within a 3D space to replicate the peat structure. As in MEGA, shelf arrangement porosity in MEGA 3D could be used to produce peats that are structurally 'open' (Figure 58a) or nearly 'closed' (Figure 58b). Three-dimensional images of peat collected using x-ray computed tomography [*Kettridge and Binley*, 2011; *Quinton et al.*, 2009; *Rezanezhad et al.*, 2009] could be used to determine the size and position of shelves.

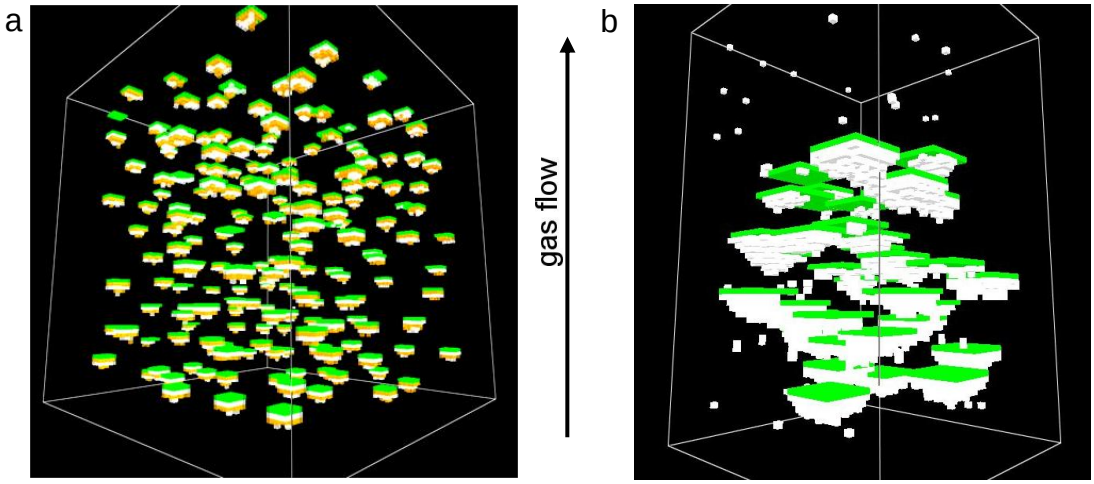

Figure 58. 3D MEGA.

3D shelf arrangements with (a) small and (b) large shelves. Shelves are coloured green with gas coloured white or orange. Gas enters from below and accumulates underneath shelves.

A variety of tests could be developed to test MEGA 3D, but one that is planned should future resources permit is described in some detail below. A laboratory experiment could be performed that measures ebullition from peat. This work could use some of the CBM methods developed in Chapter 4. In such experiments more CBMs could be constructed to collect data on bubble release (ebullition) from a range of peat types. A total of 10 CBMs could be made to hold two replicates of five peat types collected. Peat types could be chosen to represent a wide range of pore structure. The focus of these experiments would be bubble release, meaning

that changes in water level within the gas trap of each CBM would need to be monitored, perhaps with time lapse cameras equipped with flash (for night time measurements) [*Comas and Wright*, 2012]. To 'capture' ebullition at high temporal frequency, the cameras would be set to photograph gas trap water level every 30 min. All CBMs would be exposed to the same environmental conditions by placing them within an environmental cabinet. Within the cabinet temperature and sunlight duration would be controlled to replicate seasonal variations (e.g. summer to autumn). Atmospheric pressure throughout the experiment would be recorded. Maintenance of the CBMs would require occasionally topping up of water levels within the gas trap (via sealed port), replacing camera batteries, and downloading images.

At the conclusion of the experiment the peat samples would be prepared for imaging with a x-ray computed tomography scanner [*Kettridge and Binley*, 2011]. Each peat sample would be imaged in 3D to guide the construction of 3D shelf arrangements for MEGA 3D. A total of 10 MEGA 3D simulations would be performed, one simulation for every peat sample. Baseline gas production in MEGA 3D simulations would be based on CBM average ebullition and may also account for recorded changes in air temperature and daylight. Recorded fluctuations in atmospheric pressure could govern the cohesiveness of the bubbles stored within the shelf arrangements. The total ebullition every 30 min would be collected from each MEGA 3D simulation and these data compared directly to ebullition collected from the CBMs. This experiment may provide supporting evidence for a reduced complexity approach to model ebullition from peat with MEGA 3D.

To date research continues on measuring ebullition in the field. Progress is being made on relatively inexpensive methods of measuring ebullition at high temporal frequency [*Comas and Wright*, 2012; *Stamp et al.*, 2013], and this will make it possible to measure ebullition at more locations within a study site. It is hoped that in the future field-based measurements of ebullition will be accompanied by site information on peat structure. Available methods to obtain peat structural information include ground penetrating radar [*Parsekian et al.*, 2012; *Strack and Mierau*, 2010] or extracting samples of peat and imaging with x-ray computed tomography [*Kettridge and Binley*, 2011; *Quinton et al.*, 2009; *Rezanezhad et al.*, 2009]. With this structural information MEGA (2D or 3D) models could be constructed and tested against field records of ebullition. It is foreseen that coupling field work with MEGA modelling will provide the first steps towards predicting ebullition at the plot scale (peat 1-2 m deep, with a footprint of 10 m^2). Moreover, the combination of affordable high performance computing hardware (e.g. graphic processing units [*Kirk and Hwu*, 2010]) and methods to accelerate computer model computation (e.g. massive parallelization) will have an effect on the scale of MEGA simulations. With faster, greater computation MEGA simulations may continue to increase in area (e.g. peat 1-2 m deep, with a footprint of 100 m^2) whilst preserving the fine scale spatial heterogeneity within the peat.

The expected increase in MEGA's simulation extent will create some opportunities to link MEGA with global scale models of CH_4 emissions. Specifically there is scope to work with global wetland CH_4 models, most of which contain peatlands. At present there is a need to reduce uncertainty in CH_4 estimates from global scale models [*Ito and Inatomi*, 2012]. A major source of error in global scale modelled

CH_4 estimates originates from (i) the lack or inadequate representation of CH_4 production, transport and consumption [*Bridgham et al.*, 2013], and (ii) the limited spatial variability in physical and biogeochemical CH_4 related processes [*Ito and Inatomi*, 2012]. In the future global wetland CH_4 models may address these model deficiencies by developing greater model complexity to represent spatially distributed wetland processes and properties, but information may not exist to parameterize these processes and properties [*Bridgham et al.*, 2013]. It is envisioned that finer spatial scale models that account for spatial heterogeneity in wetlands (e.g. MEGA) could be used to constrain parameters in global wetland CH_4 models. For wetlands types consisting of peat MEGA could be used to provide parameters values including rates of CH_4 ebullition, and amounts of gas storage for different peatland types (e.g. bog, fen).

Appendix

1. Computer model (MEGA) development

Below is the C# code of the version of MEGA, used in batch mode, to perform the sensitivity analysis in Chapter 2 and simulate the shelf arrangements within the shelf bubble machine (Chapter 3). This version of the model (v2.0) contains improvements including a model time step, and bubble velocity. The code is subdivided into the following sections: *libraries*, *variables*, *methods* and *events*. *Libraries* are collections C# commands that were used throughout the model. *Variables* were used to store parameters from the model's graphical user interface (Figure 59). Furthermore, array variables were used to store the location of shelves, stored bubbles and the size of bubbles exiting the shelf arrangement. *Methods* were developed to carry out processes within the model (e.g. topple sand piles, add bubbles to shelf arrangement). *Events* were used to call *methods* that collectively execute the computer program.

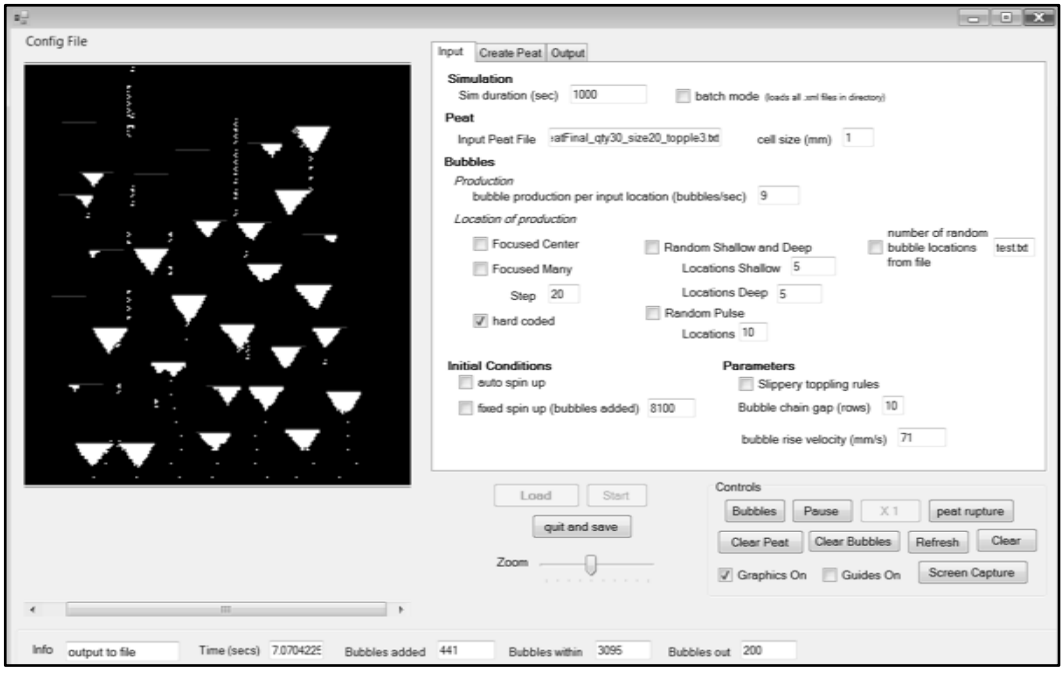

Figure 59. Graphical user interface of MEGA.

MEGA computer code (version 2.0)

1.1 Libraries

```
using System;
using System.Collections.Generic;
using System.ComponentModel;
using System.Data;
using System.Drawing;
using System.Text;
using System.Windows.Forms;
using System.IO;
using System.Threading;
using System.Xml;

namespace WindowsApplication1
{
   public partial class Form1 : Form
   {
```

1.2 Variables

//Global variables

```
      int tCol, tRow;
      int bubbleChainGap;
      int randBubbleInput;
      int simNumb = 0;
      int simCount = 0;
      int topple = 0;
      int bubbleOutContinous = 0; //continuously tallies the amount of release of bubbles
      int rowTopmostShelf, rowBottommostShelf;
      StreamWriter sr2, sr4, sr3, sr20;
      StreamReader sr200;
      double simDuration = 0;
      string cfgname = null;  //Config file name
      string current = Directory.GetCurrentDirectory();
      DirectoryInfo di = new DirectoryInfo(Directory.GetCurrentDirectory());
      double potentialMaxBubblesWithin = 0;
      point[] shelfRuptureCoords;
      int shelfLength, shelfCount = 0;
      int ncolsRandomElev, nrowsRandomElev; //dims of random shelf array
      public static double magnifyValue = 0;
      private Smallwisdom.Windows.Forms.ZoomPanImageBox zoomPanImageBox1;
      private double[] zoomFactor = { .25, .33, .50, .66, .80, 1, 1.25, 1.5, 2.0, 2.5, 3.0 };
      int shelfMinX = 1000000;
      int shelfMaxX = 0;
      int toppleCount = 0;
```

//Arrays

```
      int[,] elev;
      int[,] randomElev;
      int[] histo;
      int[] bubbleSize;
      double[] bubbleStart;
      int[] bubbleGapCounter;
      int[] bubbleSizeDistribution;
      int[] bubbleSignal;
      bool[] bubbleFlag;
      int ncols, nrows;

      Random randy = new Random();
      Random randy2 = new Random();
      int bubblesWithin = 0;
      int decision = 0;
      int x, y;
      int bubbles = 0;
```

//Time step variables

```
      int iteration = 0; //completion of one scan (time in seconds it takes a 1 mm diameter to move 1 mm (1/282th of a
            second))
      double realTime = 0; //time in seconds
      double bubbleSpeed = 282.0; //in mm per second, equivalent to number of iterations in 1 second
      int bubbleProductionInOneSecond = 0; //number of bubbles produced in 1 second
      double bubbleTime = 0; //in iterations, how many bubbles are produced in 1 second
            (282/bubbleProductionInOneSecond)
```

```
double histoSamplingTimeStep = 0; //sampling time step in iterations
int imageCount = 0;
int pause = 0;
double bubbleIn, bubbleOut;
int bubbleOutTimeStep = 0;
int startHisto = 0;
int startSizeDist = 0;
int step = 0;
```

//Bubble variables

```
int quantity = 0;
int quantityDeepPeat = 0;
int quantityShallowPeat = 0;
int positionShallowPeatRow = 0;
int positionShallowPeatCol = 0;
int positionDeepPeatRow = 0;
int positionDeepPeatCol = 0;
int randomRow = 0;
int randomCol = 0;
int coordsGood = 0;
int sumTrap = 0;
double cellsize = 0;
double adjustedBubbleSpeed = 0;
```

//Graphical User Interface (GUI) variables

```
private System.Drawing.Bitmap m_objDrawingSurface;
int graphics_scale = 2;
public Form1()
{
    InitializeComponent(); //Loads graphical interface
}
```

1.3 Methods

//Method to initialize variables from user inputs from GUI

```
private void initialise()
{
    topple = 3; //hard code that avalanches will occur with a height of 3 pixels
    bubbleSpeed = System.Convert.ToDouble(bubbleSpeedtextBox20.Text);
    cellsize = System.Convert.ToDouble(cellSizetextBox20.Text);
    adjustedBubbleSpeed = Math.Round((bubbleSpeed / cellsize));//number of iteration to perform in 1 sec
    simDuration = System.Convert.ToDouble(simDurationTextBox.Text);
    bubbleProductionInOneSecond = System.Convert.ToInt32(textBoxBubbleTime.Text);
    bubbleTime = Math.Round((adjustedBubbleSpeed / bubbleProductionInOneSecond)); //interval in iterations that a
        bubble should be added
    histoSamplingTimeStep = (System.Convert.ToDouble(histoSamplingtextBox.Text)) * adjustedBubbleSpeed;
    elev = new int[nrows, ncols];
    histo = new int[10000];
    bubbleSize = new int[ncols];
    bubbleStart = new double[ncols];
    bubbleSizeDistribution = new int[10000];
    bubbleGapCounter = new int[ncols];
    bubbleFlag = new bool[ncols];
    bubbleSignal = new int[100000];
    step = System.Convert.ToInt32(steptextBox3.Text);
    quantity = System.Convert.ToInt32(quantitytextBox3.Text);
    quantityDeepPeat = System.Convert.ToInt32(textBoxQuantityDeep.Text);
    quantityShallowPeat = System.Convert.ToInt32(textBoxQuantityShallow.Text);
    bubbleChainGap = System.Convert.ToInt32(BubbleChainGaptextBox20.Text);
}
```

// Method to draw image of peat and bubbles on screen

```
void drawwater(int ncolsDraw, int nrowsDraw, int[,] arrayDraw)
{
    Graphics objGraphics;
    objGraphics = Graphics.FromImage(m_objDrawingSurface);
    objGraphics.Clear(SystemColors.Control);
    int redcol = 0, greencol = 0, bluecol = 0, alphacol = 255;
    int t = 0;
    t = graphics_scale;
    for (x = 1; x < nrowsDraw - 1; x++)
    {
        for (y = 1; y < ncolsDraw - 1; y++)
        {
            if (arrayDraw[x, y] == 0) //draws water
```

```
            {
                redcol = 0;// System.Convert.ToInt32(red * 255);
                greencol = 0;// System.Convert.ToInt32(green * 255);
                bluecol = 0;// System.Convert.ToInt32(blue * 255);
                alphacol = 255;
                SolidBrush brush = new SolidBrush(Color.FromArgb(alphacol, redcol, greencol, bluecol));
                objGraphics.FillRectangle(brush, (y) * t, (x) * t, t, t);
            }       // Close of Entire Grid Mask
            if ((arrayDraw[x, y] == 0) && (y % 2 == 0) && (guidesOnCheckbox.Checked == true)) // draws guide lines
            {
                redcol = 0;// System.Convert.ToInt32(red * 255);
                greencol = 0;// System.Convert.ToInt32(green * 255);
                bluecol = 255;// System.Convert.ToInt32(blue * 255);
                alphacol = 100;
                SolidBrush brush = new SolidBrush(Color.FromArgb(alphacol, redcol, greencol, bluecol));
                objGraphics.FillRectangle(brush, (y) * t, (x) * t, t, t);
            }       // Close of Entire Grid Mask
            if ((arrayDraw[x, y] == 10) && (y % 2 == 0))
            {
                redcol = 0;// System.Convert.ToInt32(red * 255);
                greencol = 255;// System.Convert.ToInt32(green * 255);
                bluecol = 0;// System.Convert.ToInt32(blue * 255);
                alphacol = 100;
                SolidBrush brush = new SolidBrush(Color.FromArgb(alphacol, redcol, greencol, bluecol));
                objGraphics.FillRectangle(brush, (y) * t, (x) * t, t, t);
            }
            if (arrayDraw[x, y] == 1) // draws bubbles
            {
                redcol = 255;// System.Convert.ToInt32(red * 255);
                greencol = 255;// System.Convert.ToInt32(green * 255);
                bluecol = 255;// System.Convert.ToInt32(blue * 255);
                alphacol = 255;
                SolidBrush brush = new SolidBrush(Color.FromArgb(alphacol, redcol, greencol, bluecol));
                objGraphics.FillRectangle(brush, (y) * t, (x) * t, t, t);
            }       // Close of Entire Grid Mask
            if ((arrayDraw[x, y] == 2) && (storageCheckBox.Checked != true)) // draws shelves
            {
                redcol = 255;// System.Convert.ToInt32(red * 255);
                greencol = 0;// System.Convert.ToInt32(green * 255);
                bluecol = 0;// System.Convert.ToInt32(blue * 255);
                alphacol = 255;
                SolidBrush brush = new SolidBrush(Color.FromArgb(alphacol, redcol, greencol, bluecol));
                objGraphics.FillRectangle(brush, (y) * t, (x) * t, t, t);
            }
        }                       // Close of Column Loop
    }                           // Close of Row Loop
    zoomPanImageBox1.Image = m_objDrawingSurface; //image is diplayed in pan/zoom image box
    objGraphics.Dispose();
}
```

// Method to start simulation

```
private void startSim()
{
    zoomPanImageBox1.Refresh();
    startButton.Enabled = false;
    //display information
    if ((autoSpinUpcheckBox.Checked == true) || (fixedSpinUpcheckBox1.Checked == true))
    {
        recordOutputTextBox4.Text = "spin-up in progress";
    }
    timer1.Enabled = true;
    bubbles = 1;
}
```

// Method to count and store length of bubble chains (bubble sizes)

```
void bubbleTrapTopple3(int x, int y) //records the bubble size distribution for topple 3 rule, only called after spinup
{
    //check if bubble exists in trap
    if ((elev[x, y] == 1) || (elev[x, y + 1] == 1)) //bubble exists
    {
        //record the bubble
        if (elev[x, y] == 1)
        {
            bubbleSize[y]++;
```

```
            //record the time the first bubble link was recorded
            if ((bubbleSize[y] == 1) && (bubbleTimeStampcheckBox1.Checked = true))
            {
               bubbleStart[y] = realTime; //time the beginning of bubble exits the top
            }
            if (bubbleGapCounter[y] > 0) //gap was previously found
            {
               bubbleGapCounter[y] = 0; //resets gap counter if new bubble found
            }
            bubbleFlag[y] = true; //open chain
            sumTrap = 1; //records if bubble is in trap
         }
         if (elev[x, y + 1] == 1)
         {
            bubbleSize[y]++;
            //record the time the first bubble link was recorded
            if ((bubbleSize[y] == 1) && (bubbleTimeStampcheckBox1.Checked = true))
            {
               bubbleStart[y] = realTime; //time the beginning of bubble exits the top
            }
            if (bubbleGapCounter[y] > 0) //gap was previously found
            {
               bubbleGapCounter[y] = 0; //resets gap counter if new bubble found
            }
            bubbleFlag[y] = true; //open chain
            sumTrap = 1; //records if bubble is in trap
         }
      }
      if ((elev[x, y] == 0) && (elev[x, y + 1] == 0)) //a gap
      {
         if (bubbleFlag[y] == true)
         {
            bubbleGapCounter[y]++; //keep track of gaps
            sumTrap = 1; //bubble possibly in trap, maybe a broken bubbble
            if (bubbleGapCounter[y] >= bubbleChainGap) //chain is over, close chain (e.g. 3mm gap)
            {
               bubbleSizeDistribution[bubbleSize[y]]++;
               //output to file to bubble size, start time, end time
               if (bubbleTimeStampcheckBox1.Checked == true)
               {
                  sr20.WriteLine(bubbleSize[y] + "," + bubbleStart[y] + "," + realTime + "," + iteration);
               }
               //reset counters
               bubbleSize[y] = 0;
               bubbleGapCounter[y] = 0;
               bubbleStart[y] = 0;
               bubbleFlag[y] = false;
            }
         }
      }
   }
```

// Method to topple 'sandpiles'

```
   void topplingRules()
   {
      //Exit top bubbles
      if ((x < 2) && (elev[x, y] == 1))
      {
         elev[x, y] = 0;
         bubbleOut++;
         if (startHisto == 1) //histogram output option is enabled
         {
            bubbleOutTimeStep++; //records bubble exiting
            bubbleOutContinous++; //contiously tallys the amount of release of bubbles
         }
      }
      if (slipperyCheckBox1.Checked == false) //Normal toppling rules
      {
         //Rule 1, bubble upward movement
         if ((elev[x, y] == 1) && (elev[x - 1, y] == 0))
         {
            elev[x - 1, y] = 1;
            elev[x, y] = 0;
```

```
    }
    //Rule2, 3 bubbles stacked upon each other with no bubbles on both sides of stack (freestanding)
    else if ((elev[x, y] == 1) && (elev[x - 1, y] == 1) && (elev[x - 2, y] == 1)
       && (elev[x, y - 1] == 0) && (elev[x - 1, y - 1] == 0) && (elev[x - 2, y - 1] == 0)
       && (elev[x, y - 2] == 0) && (elev[x, y + 1] == 0) && (elev[x - 1, y + 1] == 0) &&
       (elev[x - 2, y + 1] == 0) && (elev[x, y + 2] == 0))
    {
       decision = randy.Next(0, 2);
       if (decision == 0) //topple left
       {
          elev[x, y] = 0;
          elev[x - 1, y] = 0;
          elev[x - 1, y - 1] = 1;
          elev[x, y - 2] = 1;
          toppleCount++;
       }
       else
       {
          //topple right
          elev[x, y] = 0;
          elev[x - 1, y] = 0;
          elev[x - 1, y + 1] = 1;
          elev[x, y + 2] = 1;
          toppleCount++;
       }
    }
    //Rule3, 3 bubbles stacked upon each other space available to topple left
    else if ((elev[x, y] == 1) && (elev[x - 1, y] == 1) && (elev[x - 2, y] == 1)
       && (elev[x, y - 1] == 0) && (elev[x - 1, y - 1] == 0) && (elev[x - 2, y - 1] == 0) &&
       (elev[x, y - 2] == 0))
    {
       elev[x, y] = 0;
       elev[x - 1, y] = 0;
       elev[x - 1, y - 1] = 1;
       elev[x, y - 2] = 1;
       toppleCount++;
    }
    //Rule4, 3 bubbles stacked upon each other space available to topple right
    else if ((elev[x, y] == 1) && (elev[x - 1, y] == 1) && (elev[x - 2, y] == 1)
       && (elev[x, y + 1] == 0) && (elev[x - 1, y + 1] == 0) && (elev[x - 2, y + 1] == 0)
       && (elev[x, y + 2] == 0))
    {
       elev[x, y] = 0;
       elev[x - 1, y] = 0;
       elev[x - 1, y + 1] = 1;
       elev[x, y + 2] = 1;
       toppleCount++;
    }
    else
    {
       //do nothing
    }
}
else //slippery toppling rules, rules for 'sandpile' with less cohesiveness
{
    //Rule 1, bubble upward movement
    if ((elev[x, y] == 1) && (elev[x - 1, y] == 0))
    {
       elev[x - 1, y] = 1;
       elev[x, y] = 0;
    }
    //Rule2, 3 bubbles stacked upon each other with no bubbles on both sides of stack (freestanding)
    else if ((elev[x, y] == 1) && (elev[x - 1, y] == 1) && (elev[x - 2, y] == 1)
       && (elev[x, y - 1] == 0) && (elev[x - 1, y - 1] == 0)
       && (elev[x, y - 2] == 0) && (elev[x, y + 1] == 0) && (elev[x - 1, y + 1] == 0) &&
       (elev[x, y + 2] == 0))
    {
       decision = randy.Next(0, 2);
       if (decision == 0) //topple left
       {
          elev[x, y] = 0;
          elev[x - 1, y] = 0;
          elev[x - 1, y - 1] = 1;
```

```
                elev[x, y - 2] = 1;
                toppleCount++;
            }
            else
            {
                //topple right
                elev[x, y] = 0;
                elev[x - 1, y] = 0;
                elev[x - 1, y + 1] = 1;
                elev[x, y + 2] = 1;
                toppleCount++;
            }
        }
        //Rule3, 3 bubbles stacked upon each other space available to topple left
        else if ((elev[x, y] == 1) && (elev[x - 1, y] == 1) && (elev[x - 2, y] == 1)
            && (elev[x, y - 1] == 0) && (elev[x - 1, y - 1] == 0) &&
            (elev[x, y - 2] == 0))
        {
            elev[x, y] = 0;
            elev[x - 1, y] = 0;
            elev[x - 1, y - 1] = 1;
            elev[x, y - 2] = 1;
            toppleCount++;
        }
        //Rule4, 3 bubbles stacked upon each other space available to topple right
        else if ((elev[x, y] == 1) && (elev[x - 1, y] == 1) && (elev[x - 2, y] == 1)
            && (elev[x, y + 1] == 0) && (elev[x - 1, y + 1] == 0)
            && (elev[x, y + 2] == 0))
        {
            elev[x, y] = 0;
            elev[x - 1, y] = 0;
            elev[x - 1, y + 1] = 1;
            elev[x, y + 2] = 1;
            toppleCount++;
        }
        else
        {
            //do nothing
        }
    }
}
```

//Method to reset variables and arrays

```
private void zeroOutVariables()
{
    //reset variables
    histoSamplingTimeStep = 0;
    bubbleTime = 0;
    bubbleProductionInOneSecond = 0;
    rowTopmostShelf = 0;
    simDuration = 0;
    potentialMaxBubblesWithin = 0;
    shelfLength = 0;
    shelfCount = 0;
    ncolsRandomElev = 0;
    nrowsRandomElev = 0;
    histoSamplingTimeStep = 0;
    shelfMinX = 1000000;
    shelfMaxX = 0;
    toppleCount = 0;
    ncols = 0;
    nrows = 0;
    bubblesWithin = 0;
    decision = 0;
    bubbles = 0;
    realTime = 0;
    iteration = 0;
    imageCount = 0;
    pause = 0;
    bubbleIn = 0;
    bubbleOut = 0;
    bubbleOutTimeStep = 0;
    startHisto = 0;
```

```
        startSizeDist = 0;
        step = 0;
        quantity = 0;
        quantityDeepPeat = 0;
        quantityShallowPeat = 0;
        positionShallowPeatRow = 0;
        positionShallowPeatCol = 0;
        positionDeepPeatRow = 0;
        positionDeepPeatCol = 0;
        randomRow = 0;
        randomCol = 0;
        coordsGood = 0;
        //reset arrays
        for (x = 0; x < nrows; x++)
        {
            for (y = 0; y < ncols; y++)
            {
                elev[x, y] = 0;
                randomElev[x, y] = 0;
            }
        }
        for (int i = 0; i < bubbleSizeDistribution.Length; i++)
        {
            bubbleSizeDistribution[i] = 0;
            histo[i] = 0;
        }
        for (int i = 0; i < bubbleSize.Length; i++)
        {
            bubbleSize[i] = 0;
            bubbleGapCounter[i] = 0;
            bubbleFlag[i] = false;
            bubbleStart[i] = 0;
        }
        for (int i = 0; i < bubbleSignal.Length; i++)
        {
            bubbleSignal[i] = 0;
        }
    }
// Peat rupture method
    private void peatRupture()
    {
        int selectShelf = 0;
        bool shelfPicked = false;
        while (shelfPicked == false)
        {
            //choose a shelf randomly
            selectShelf = randy2.Next(0, shelfRuptureCoords.Length);
            if ((shelfRuptureCoords[selectShelf].ycoord != 0) && (shelfRuptureCoords[selectShelf].xcoord != 0))
            {
                shelfPicked = true;
            }
        }
        //delete center 2 center peat cells
        elev[shelfRuptureCoords[selectShelf].xcoord, shelfRuptureCoords[selectShelf].ycoord + shelfLength / 2] = 0;
        elev[shelfRuptureCoords[selectShelf].xcoord, shelfRuptureCoords[selectShelf].ycoord + shelfLength / 2 - 1] = 0;
        //remove shelf coordinates from list
        shelfRuptureCoords[selectShelf].ycoord = 0;
        shelfRuptureCoords[selectShelf].xcoord = 0;
    }
//Load shelf arrangement and parameters method
    private void loadData(int mySimCount)
    {
        if ((batchModecheckBox1.Checked == true))
        {
            //load first xml file
            loadXmlFile(mySimCount);
        }
        //read in peat file header to get ncols, nrows
        string FILE_NAME = this.loaddtextBox.Text;
        string FILE_NAME_BUBBLE_SIGNAL = this.bubbleSignalTextBox.Text;
        StreamReader sr = File.OpenText(FILE_NAME);
        if (bubbleSignalFilecheckBox1.Checked == true)
```

```
{
    sr200 = File.OpenText(FILE_NAME_BUBBLE_SIGNAL);
}
string[] lineArray2;
lineArray2 = sr.ReadLine().Split(new char[] { ',' }); //read ncols from header
ncols = System.Convert.ToInt32(lineArray2[1]);
lineArray2 = sr.ReadLine().Split(new char[] { ',' }); //read nrows from header
nrows = System.Convert.ToInt32(lineArray2[1]);
sr.Close();
initialise(); //initialise variables
//load peat array from file
int x, y = 1, xcounter;
String input, input2;
int tttt = 0;
y = 0;
bool firstShelfFound = false;
StreamReader sr10 = File.OpenText(FILE_NAME);
lineArray2 = sr10.ReadLine().Split(new char[] { ',' }); //read ncols from header
ncols = System.Convert.ToInt32(lineArray2[1]);
lineArray2 = sr10.ReadLine().Split(new char[] { ',' }); //read nrows from header
nrows = System.Convert.ToInt32(lineArray2[1]);
while ((input = sr10.ReadLine()) != null)
{
    string[] lineArray;
    lineArray = input.Split(new char[] { ' ' });
    xcounter = 1;
    for (x = 1; x <= (lineArray.Length - 1); x++)
    {
        if (lineArray[x] != "" && xcounter <= ncols)
        {
            tttt = int.Parse(lineArray[x]);
            elev[y, xcounter] = tttt;
            if (tttt == 2)
            {
                if (xcounter < shelfMinX)
                {
                    shelfMinX = xcounter;
                }
                if (xcounter > shelfMaxX)
                {
                    shelfMaxX = xcounter;
                }
            }
            xcounter++;
        }
    }
    y++;
}
sr10.Close();
//find out number of shelves and length
for (x = 0; x < nrows; x++)
{
    for (y = 0; y < ncols; y++)
    {
        if ((elev[x, y] == 2) && (firstShelfFound == false)) //calculates length of first shelf
        {
            shelfLength++;
            if (elev[x, y + 1] == 0)
            {
                firstShelfFound = true;
                rowTopmostShelf = x;
            }
        }
        if ((elev[x, y] == 2) && (elev[x, y + 1] == 0))
        {
            shelfCount++;
            rowBottommostShelf = x;
        }
    }
}
//read in bubble signal file
if (bubbleSignalFilecheckBox1.Checked == true)
{
```

```
            int counter = 0;
            while ((input2 = sr200.ReadLine()) != null)
            {
                bubbleSignal[counter] = System.Convert.ToInt32(input2);
                counter = counter + 1;
            }
            sr200.Close();
        }
        //initialise shelf variables
        shelfRuptureCoords = new point[shelfCount];
        point shelfBeginCoord = new point(0, 0);
        //calculate potential maximum amount of bubbles the peat can hold (bubbleWithin)
        potentialMaxBubblesWithin = Math.Ceiling(0.5 * (shelfLength * shelfLength) + shelfLength) * shelfCount;
        bubbleWithinMaxTextBox4.Text = potentialMaxBubblesWithin.ToString();
        //make drawing surface
        m_objDrawingSurface = new Bitmap((ncols) * graphics_scale,
            (nrows) * graphics_scale, System.Drawing.Imaging.PixelFormat.Format24bppRgb);
        //draw peat array
        drawwater(ncols, nrows, elev);
        //set zoom level of image box
        magnifyValue = zoomFactor[this.trackBar2.Value]; //magnification of peat
        zoomPanImageBox1.setZoom();
        shelfLengthTextBox3.Text = shelfLength.ToString();
        numShelvesTextBox3.Text = shelfCount.ToString();
        //create output files with unique names
        if (TimeScheckBox1.Checked == true)
        {
            sr3 = File.CreateText("releaseContinuousChopMethod_qty" + shelfCount + "_size" + shelfLength + "_topple" +
                    topple + ".csv");
            sr3.WriteLine("time,releaseQuantity"); //time series header
        }
        if (bubbleOutputCheckBox.Checked == true)
        {
            //create output file and header
            sr2 = File.CreateText("releaseDistribution" + histoSamplingtextBox.Text + "secs_qty" + shelfCount + "_size" +
                    shelfLength + "_topple" + topple + ".csv");
            sr2.WriteLine("releaseQuantity,frequency");
        }
        if (bubbleSizeDistCheckBox.Checked == true)
        {
            //create output files
            sr4 = File.CreateText("sizeDistribution_qty" + shelfCount + "_size" + shelfLength + "_topple" + topple + ".csv");
            sr4.WriteLine("bubbleSize,frequency");
        }
        if (bubbleTimeStampcheckBox1.Checked == true)
        {
            sr20 = File.CreateText("releaseContinuousStampMethod__qty" + shelfCount + "_size" + shelfLength + "_topple" +
                    topple + ".csv");
            sr20.WriteLine("bubbleSize,startTime,endTime,endIter"); //time series header
        }
        loadButton.Enabled = false;
        startButton.Enabled = true;
    }
// Method to write simulation parameters to configuration file
    private void writeXML(string configName, bool sensativity, string peatFileName)
    {
        XmlTextWriter xwriter;
        //Create a new XmlTextWriter
        xwriter = new XmlTextWriter(configName, System.Text.Encoding.UTF8);
        xwriter.Formatting = Formatting.Indented;
        xwriter.Indentation = 4;
        xwriter.WriteStartDocument(true);
        xwriter.WriteStartElement("Params");
        xwriter.WriteElementString("simDuration", simDurationTextBox.Text); //how long the sim is
        if (sensativity == false)
        {
            xwriter.WriteElementString("inputFile", loaddtextBox.Text); //filename read from input tab
        }
        else
        {
            xwriter.WriteElementString("inputFile", peatFileName); //filename read from data tab
        }
```

```
        xwriter.WriteElementString("BubbleProduction", textBoxBubbleTime.Text); //bubble production per input location
        xwriter.WriteElementString("bubbleProductionFromFile",
            XmlConvert.ToString(bubbleSignalFilecheckBox1.Checked));
        xwriter.WriteElementString("bubbleProductionFile", bubbleSignalTextBox.Text); //bubble production signal file
        xwriter.WriteElementString("focusBubblesCenter", XmlConvert.ToString(focuscheckBox1.Checked));
        xwriter.WriteElementString("focusBubblesMany", XmlConvert.ToString(focus2checkBox1.Checked));
        xwriter.WriteElementString("stepFocusBubblesMany", steptextBox3.Text);
        xwriter.WriteElementString("hardCodedBubbles", XmlConvert.ToString(hardCodecheckBox1.Checked));
        xwriter.WriteElementString("shallowDeepBubbles", XmlConvert.ToString(checkBoxShallowDeep.Checked));
        xwriter.WriteElementString("quantityShallowBubbles", textBoxQuantityShallow.Text);
        xwriter.WriteElementString("quantityDeepBubbles", textBoxQuantityDeep.Text);
        xwriter.WriteElementString("randomBubbles", XmlConvert.ToString(RandomcheckBox1.Checked));
        xwriter.WriteElementString("quantityRandomBubbles", quantitytextBox3.Text);
        xwriter.WriteElementString("autoSpinUp", XmlConvert.ToString(autoSpinUpcheckBox.Checked));
        xwriter.WriteElementString("fixedSpinUp", XmlConvert.ToString(fixedSpinUpcheckBox1.Checked));
        xwriter.WriteElementString("fixedSpinUpBubbleAmount", fixedSpinUptextBox.Text);
        xwriter.WriteElementString("bubbleOutputDist", XmlConvert.ToString(bubbleOutputCheckBox.Checked));
        xwriter.WriteElementString("histoSampling", histoSamplingtextBox.Text);
        xwriter.WriteElementString("bubbleSizeDist", XmlConvert.ToString(bubbleSizeDistCheckBox.Checked));
        xwriter.WriteElementString("timeSeriesChopMethod", XmlConvert.ToString(TimeScheckBox1.Checked));
        xwriter.WriteElementString("timeSeriesTimeStampMethod",
            XmlConvert.ToString(bubbleTimeStampcheckBox1.Checked));
        xwriter.WriteElementString("animate", XmlConvert.ToString(checkBox2.Checked));
        xwriter.WriteElementString("animateBubbleStorage", XmlConvert.ToString(storageCheckBox.Checked));
        xwriter.WriteEndElement();
        xwriter.Close();
    }
// Method to end simulation and save outputs
private void endSim()
    {
        //close all output files
        //close output histogram
        if ((startHisto == 1) && (bubbleOutputCheckBox.Checked == true))
        {
            for (x = 0; x < histo.Length; x++)
            {
                sr2.WriteLine(x + "," + histo[x]);
            }
            sr2.Close();
        }
        //close bubble size distribution
        if ((startSizeDist == 1) && (bubbleSizeDistCheckBox.Checked == true))
        {
            for (x = 0; x < bubbleSizeDistribution.Length; x++)
            {
                sr4.WriteLine(x + "," + bubbleSizeDistribution[x]);
            }
            sr4.Close();
        }
        //close time series
        if (TimeScheckBox1.Checked == true)
        {
            sr3.Close();
        }
        if (bubbleTimeStampcheckBox1.Checked == true)
        {
            sr20.Close();
        }
        //save final array to file
        string FILENAME = "storage_qty" + shelfCount + "_size" + shelfLength + "_topple" + topple + ".txt";
        using (StreamWriter sw = new StreamWriter(FILENAME))
        {
            sw.WriteLine("ncols," + ncols.ToString());
            sw.WriteLine("nrows," + nrows.ToString());
            for (x = 0; x < nrows; x++)
            {
                for (y = 0; y < ncols; y++)
                {
                    sw.Write(elev[x, y]);
                    sw.Write(" ");
                }
                sw.Write("\n");
```

```
            }
            sw.Close();
        }
        drawwater(ncols, nrows, elev);
        m_objDrawingSurface.Save("image_qty" + shelfCount + "_size" + shelfLength + "_topple" + topple + ".png",
            System.Drawing.Imaging.ImageFormat.Png);   //final screenshot
        if (simCount < (simNumb - 1))//number of sims according to number of xml files
        {
            //update simCount
            simCount++;
            //reset variabels and arrays
            zeroOutVariables();
            //reload new simulation
            loadData(simCount);
            startSim();
        }
    }
//Method to load batch mode simulations
    private void loadXmlFile(int fileNumber) //sequentially loads config files existing in a directory (batch mode)
    {
        //find all xml files in current directory
        FileInfo[] xmlFiles = di.GetFiles("*.xml"); //array with xml files in current directory
        simNumb = xmlFiles.Length;
        //read xml file
        XmlTextReader xreader;
        xreader = new XmlTextReader(current + "\\" + xmlFiles[fileNumber].ToString());
        xreader.ReadStartElement("Params");
        simDurationTextBox.Text = xreader.ReadElementString("simDuration");
        loaddtextBox.Text = xreader.ReadElementString("inputFile");
        textBoxBubbleTime.Text = xreader.ReadElementString("BubbleProduction");
        bubbleSignalFilecheckBox1.Checked =
            XmlConvert.ToBoolean(xreader.ReadElementString("bubbleProductionFromFile"));
        bubbleSignalTextBox.Text = xreader.ReadElementString("bubbleProductionFile");
        focuscheckBox1.Checked = XmlConvert.ToBoolean(xreader.ReadElementString("focusBubblesCenter"));
        focus2checkBox1.Checked = XmlConvert.ToBoolean(xreader.ReadElementString("focusBubblesMany"));
        steptextBox3.Text = xreader.ReadElementString("stepFocusBubblesMany");
        hardCodecheckBox1.Checked = XmlConvert.ToBoolean(xreader.ReadElementString("hardCodedBubbles"));
        checkBoxShallowDeep.Checked = XmlConvert.ToBoolean(xreader.ReadElementString("shallowDeepBubbles"));
        textBoxQuantityShallow.Text = xreader.ReadElementString("quantityShallowBubbles");
        textBoxQuantityDeep.Text = xreader.ReadElementString("quantityDeepBubbles");
        RandomcheckBox1.Checked = XmlConvert.ToBoolean(xreader.ReadElementString("randomBubbles"));
        quantitytextBox3.Text = xreader.ReadElementString("quantityRandomBubbles");
        autoSpinUpcheckBox.Checked = XmlConvert.ToBoolean(xreader.ReadElementString("autoSpinUp"));
        fixedSpinUpcheckBox1.Checked = XmlConvert.ToBoolean(xreader.ReadElementString("fixedSpinUp"));
        fixedSpinUptextBox.Text = xreader.ReadElementString("fixedSpinUpBubbleAmount");
        bubbleOutputCheckBox.Checked = XmlConvert.ToBoolean(xreader.ReadElementString("bubbleOutputDist"));
        histoSamplingtextBox.Text = xreader.ReadElementString("histoSampling");
        bubbleSizeDistCheckBox.Checked = XmlConvert.ToBoolean(xreader.ReadElementString("bubbleSizeDist"));
        TimeScheckBox1.Checked = XmlConvert.ToBoolean(xreader.ReadElementString("timeSeriesChopMethod"));
        bubbleTimeStampcheckBox1.Checked =
            XmlConvert.ToBoolean(xreader.ReadElementString("timeSeriesTimeStampMethod"));
        checkBox2.Checked = XmlConvert.ToBoolean(xreader.ReadElementString("animate"));
        storageCheckBox.Checked = XmlConvert.ToBoolean(xreader.ReadElementString("animateBubbleStorage"));
        xreader.ReadEndElement();
        xreader.Close();
    }
// Method to add bubbles to shelf arrangements
    void addBubble()
    {
        //Add a bubble
        if (bubbles == 1) //bubbles activated
        {
            if (iteration % bubbleTime == 0) //new bubble every n iterations
            {
                if (focuscheckBox1.Checked == true)  //add single stream of bubbles from below at bisection of shelf
                        arrangement
                {
                    elev[nrows - 2, ncols / 2] = 1; //fixed bubbles
                    bubbleIn++;
                }
                if (focus2checkBox1.Checked == true) )  //add many streams of bubbles at set intervals (columns) across
                        the shelf arrangement
```

```
{
   for (int i = step; i < ncols; i = i + step)
   {
      if ((i >= shelfMinX) && (i <= shelfMaxX))
      {
         elev[nrows - 2, i] = 1;
         bubbleIn++;
      }
   }
}
if (RandomcheckBox1.Checked == true) //add bubbles anywhere within the shelf arrangement  at random
         locations
{
   for (int i = 0; i < quantity; i++)
   {
      while (coordsGood == 0)
      {
         randomCol = randy.Next(shelfMinX + 1, shelfMaxX - 1);
         randomRow = nrows - 2;
         if (elev[randomRow, randomCol] != 1) //peat or bubble in location
         {
            coordsGood = 1;
         }
      }
      //add bubble
      elev[randomRow, randomCol] = 1;
      bubbleIn++;
      coordsGood = 0;
   }
}
if (checkBoxShallowDeep.Checked == true) // adds bubbles in random locations within 2 layers of peat
         (shallow and deep)
{
   //deep peat (lower half) bubbles random locations from bottom
   for (int i = 0; i < quantityDeepPeat; i++)
   {
      while (coordsGood == 0)
      {
         positionDeepPeatCol = randy.Next(shelfMinX + 1, shelfMaxX - 1);
         positionDeepPeatRow = nrows - 2;
         if (elev[positionDeepPeatRow, positionDeepPeatCol] != 1)  //peat or bubble in location
         {
            coordsGood = 1;
         }
      }
      //add bubble
      elev[positionDeepPeatRow, positionDeepPeatCol] = 1;
      bubbleIn++;
      coordsGood = 0;
   }
   //shallow peat bubbles random locations
   for (int i = 0; i < quantityShallowPeat; i++)
   {
      while (coordsGood == 0)
      {
         positionShallowPeatCol = randy.Next(shelfMinX + 1, shelfMaxX - 1);
         positionShallowPeatRow = randy.Next(rowTopmostShelf, rowBottommostShelf);
         if ((elev[positionShallowPeatRow, positionShallowPeatCol] != 1) && (elev[positionShallowPeatRow,
                  positionShallowPeatCol] != 2)) //peat or bubble in location
         {
            coordsGood = 1;
         }
      }
      //add bubble
      elev[positionShallowPeatRow, positionShallowPeatCol] = 1;
      bubbleIn++;
      coordsGood = 0;
   }
}
if (hardCodecheckBox1.Checked == true) //adds bubbles at hardcoded locations
{
   {
      //bubble prototype input locations
```

```
                elev[nrows - 2, 58] = 1;
                bubbleIn++;
                elev[nrows - 2, 81] = 1;
                bubbleIn++;
                elev[nrows - 2, 106] = 1;
                bubbleIn++;
                elev[nrows - 2, 130] = 1;
                bubbleIn++;
                elev[nrows - 2, 155] = 1;
                bubbleIn++;
                elev[nrows - 2, 179] = 1;
                bubbleIn++;
                elev[nrows - 2, 204] = 1;
                bubbleIn++;
            }
        }
        //quantitiy of bubbles determined  from file
        //add bubbles from a time series text file, at x random locations
        if (bubbleSignalFilecheckBox1.Checked == true)
        {
            for (int i = 0; i < bubbleSignal[Convert.ToInt16(Math.Truncate(realTime))]; i++)//determine number of
                locations from array using truncated time
            {
                while (coordsGood == 0)
                {
                    randomCol = randy.Next(shelfMinX + 1, shelfMaxX - 1);
                    randomRow = nrows - 2;
                    if (elev[randomRow, randomCol] != 1) //peat or bubble in location
                    {
                        coordsGood = 1;
                    }
                }
                //add bubble
                elev[randomRow, randomCol] = 1;
                bubbleIn++;
                coordsGood = 0;
            }
        }
    }
  }
}
```

1.4 Events

//Run through 'main loop' of program repeatedly until end of simulation

```
private void timer1_Tick(object sender, EventArgs e)
{
    main_loop(sender, e);
}
```

// Visualization

```
private void Form1_Load(object sender, EventArgs e)
{
    zoomPanImageBox1.Visible = true; //loads image box when form is loaded
}
private void trackBar2_Scroll(object sender, EventArgs e) //zoom part
{
    magnifyValue = zoomFactor[this.trackBar2.Value]; //magnification of peat
    zoomPanImageBox1.setZoom();
}
```

//*********Main loop of program********

```
private void main_loop(object sender, EventArgs e) //the main loop of the program
{
    if (randy.Next(0, 2) == 0) //decide scan the shelf arrangement  left to right or right to left
    {
```

//Scan shelf arrangement (left to right)

```
        if (graphicsCheckBox.Checked == true)
        {
            drawwater(ncols, nrows, elev); //call method to draw shelf arrangement
        }
```

//Move bubbles

```
            for (x = 1; x < nrows - 1; x++)
            {
               for (y = 1; y < ncols - 1; y++)
               {
                  topplingRules(); //call toppling rule method
               }
            }
//Measure bubble sizes
            if (startSizeDist == 1) //only trap bubbles if bubble sizes are being collected
            {
               sumTrap = 0;
               for (y = 0; y <= ncols - 1; y++) //scan across bubble trap
               {
                  if (y % 2 == 0) //bubble trap
                  {
                     bubbleTrapTopple3(5, y); //bubble trap is on
                  }
               }
               if (sumTrap == 0) //no bubbles in trap, zero release
               {
                  sr20.WriteLine("0," + realTime + "," + realTime + "," + iteration);
               }
            }
//Add bubbles to shelf arrangement
            addBubble(); //call method to add bubbles to shelf arrangment
//Record bubble release
            if (startHisto == 1) //check if release histogram option is enabled
            {
               if ((iteration % histoSamplingTimeStep == 0) & (iteration != 0)) //time to record bubble release
               {
                  histo[bubbleOutTimeStep] = histo[bubbleOutTimeStep] + 1;
                  bubbleOutTimeStep = 0;
               }
               if (TimeScheckBox1.Checked == true) //record time series output
               {
                  sr3.WriteLine(realTime.ToString() + "," + bubbleOutContinous.ToString());
                  bubbleOutContinous = 0;
               }
            }
         }
         else
         {
//Scan shelf arrangement (right to left)
            if (graphicsCheckBox.Checked == true)
            {
               drawwater(ncols, nrows, elev);
            }
//Move bubbles
            for (x = 1; x < nrows - 1; x++)
            {
               for (y = ncols - 1; y > 1; y--)
               {
                  topplingRules();
               }
            }
//Measure bubble sizes
            if (startSizeDist == 1)  //only trap bubbles if bubble sizes are being collected
            {
               sumTrap = 0;
               for (y = 0; y <= ncols - 1; y++) //scan across bubble trap
               {
                  if (y % 2 == 0) //bubble trap
                  {
                     bubbleTrapTopple3(5, y); //bubble trap is on row 5
                  }
               }
               if (sumTrap == 0)//no bubbles in trap, zero release
               {
                  sr20.WriteLine("0," + realTime + "," + realTime + "," + iteration);
               }
            }
```

```
//Add bubbles to shelf arrangement
        addBubble();
//Record bubble release
        if (startHisto == 1) //check if release histogram option is enabled
        {
            if ((iteration % histoSamplingTimeStep == 0) & (iteration != 0)) //time to record bubble release
            {
                histo[bubbleOutTimeStep] = histo[bubbleOutTimeStep] + 1;
                bubbleOutTimeStep = 0;
            }
            if (TimeScheckBox1.Checked == true) //record time series output
            {
                sr3.WriteLine(realTime.ToString() + "," + bubbleOutContinous.ToString());
                bubbleOutContinous = 0;
            }
        }
    }
    iteration++;
    realTime = iteration / adjustedBubbleSpeed; //iteration = 1/282 sec
    //calculate number of bubbles within
    if (iteration % adjustedBubbleSpeed == 0)
    {
        bubblesWithin = 0;
        for (x = 1; x < nrows - 1; x++)
        {
            for (y = ncols - 1; y > 1; y--)
            {
                if (elev[x, y] == 1)
                {
                    bubblesWithin++;
                }
            }
        }
    }
//Spin-up options
    //OPTION 1:if autospin activated, then collect output after bubbles added exceeds precalculated maximum
      bubbles within shelf arrangement
    if ((autoSpinUpcheckBox.Checked == true) && (bubbleIn > potentialMaxBubblesWithin))
    {
        //reset all time
        realTime = 0; //reset time after spin up takes place
        iteration = 0;
        //reset bubble trap, just in case
        for (int i = 0; i < bubbleSizeDistribution.Length; i++)
        {
            bubbleSizeDistribution[i] = 0;
        }
        for (y = 0; y <= ncols - 1; y++) //scan across bubble trap
        {
            bubbleSize[y] = 0;
            bubbleGapCounter[y] = 0;
            bubbleFlag[y] = false;
            bubbleStart[y] = 0;
        }
        //reset histogram out, just in case
        for (int i = 0; i < histo.Length; i++)
        {
            histo[i] = 0;
        }
        //reset bubble in and out
        bubbleOut = 0;
        bubbleIn = 0;
        //start recording bubble out histogram
        startHisto = 1;
        //start recording bubble size distribution
        startSizeDist = 1;
        recordOutputTextBox4.Text = "output to file";
        recordOutputTextBox4.Refresh();
        //turn off auto spin off option
        autoSpinUpcheckBox.Checked = false;
        autoSpinUpcheckBox.Enabled = false;
    }
```

```
        //OPTION 2:fixed amount of bubbles are added into system before recording outputs
        if ((fixedSpinUpcheckBox1.Checked == true) && (bubbleIn > System.Convert.ToInt32(fixedSpinUptextBox.Text)))
        {
            //reset time
            realTime = 0; //reset time after spin up takes place
            iteration = 0;
            //reset bubble trap
            for (int i = 0; i < bubbleSizeDistribution.Length; i++)
            {
                bubbleSizeDistribution[i] = 0;
            }
            for (y = 0; y <= ncols - 1; y++) //scan across bubble trap
            {
                bubbleSize[y] = 0;
                bubbleGapCounter[y] = 0;
                bubbleFlag[y] = false;
                bubbleStart[y] = 0;
            }
            //reset histogram out
            for (int i = 0; i < histo.Length; i++)
            {
                histo[i] = 0;
            }
            //reset bubble in and out
            bubbleOut = 0;
            bubbleIn = 0;
            //start recording bubble out histogram
            startHisto = 1;
            //start recording bubble size distribution
            startSizeDist = 1;
            recordOutputTextBox4.Text = "output to file";
            recordOutputTextBox4.Refresh();
            //turn off spin option
            fixedSpinUpcheckBox1.Checked = false;
            fixedSpinUpcheckBox1.Enabled = false;
        }
        //OPTION 3: no spin up
        if ((autoSpinUpcheckBox.Checked == false) && (fixedSpinUpcheckBox1.Checked == false))//no autospin collect
            data immediately
        {
            //start recording bubble out histogram
            startHisto = 1;
            //start recording bubble size distribution
            startSizeDist = 1;
            recordOutputTextBox4.Text = "output to file";
        }
        timeBox.Text = realTime.ToString(); //update time continuously
        //update status bar every 1 second
        if (iteration % adjustedBubbleSpeed == 0)
        {
            bubbleIntextBox.Text = bubbleIn.ToString();
            bubbleWithintextBox4.Text = bubblesWithin.ToString();
            bubbleOuttextBox.Text = bubbleOut.ToString();
        }
        imageCount++;
//Produce animation of bubbles
        if ((imageCount % adjustedBubbleSpeed == 0) && (checkBox2.Checked == true) && (startHisto == 1)) //record
            image every second
        {
            drawwater(ncols, nrows, elev);
            Graphics g = Graphics.FromImage(m_objDrawingSurface);
            string t = "t=" + Math.Round(realTime, 0);
            g.DrawString(t, new Font("Tahoma", 10), Brushes.White, new PointF(0, 0));
            m_objDrawingSurface.Save((imageCount / adjustedBubbleSpeed) + ".png",
System.Drawing.Imaging.ImageFormat.Png);
        }
        //shelf storage part, only draws bubbles not shelves
        if ((imageCount % adjustedBubbleSpeed == 0) && (storageCheckBox.Checked == true) && (startHisto == 1))//record
image every second
        {
            drawwater(ncols, nrows, elev);
            Graphics g = Graphics.FromImage(m_objDrawingSurface);
```

```
            m_objDrawingSurface.Save((imageCount / adjustedBubbleSpeed) + ".png",
System.Drawing.Imaging.ImageFormat.Png);
        }
 //Stop simulation
        if (realTime > simDuration)//simuation has reached the end
        {
            timer1.Stop();
            endSim();
        }
    }

//********End of main loop of program********

//Events related to buttons and dropdown menu on GUI
// Start button
    private void button2_Click(object sender, EventArgs e)//start button
    {
        startSim();
    }
//Add bubbles button
    private void button1_Click(object sender, EventArgs e)//begin to add bubbles
    {
        if (bubbles == 0)
        {
            bubbles = 1;
        }
        else
        {
            bubbles = 0;
        }
    }
//Clear shelf arrangement button
    private void button2_Click_1(object sender, EventArgs e)//clear all peat and bubbles
    {
        for (x = 1; x < nrows - 1; x++)
        {
            for (y = 1; y < ncols - 1; y++)
            {
                elev[x, y] = 0;
            }
        }
        if (startHisto == 1) //resets output histogram
        {
            for (x = 0; x < 499; x++)
            {
                histo[x] = 0;
            }
        }
        bubbleOut = 0;
        bubbleIn = 0;
        bubbleOutTimeStep = 0;
        bubbleIntextBox.Text = bubbleIn.ToString();
        bubbleOuttextBox.Text = bubbleOut.ToString();
    }
//Pause simulation button
    private void button3_Click(object sender, EventArgs e)//pause the simulation
    {
        if (pause == 0)
        {
            timer1.Stop();
            pause = 1;
            button5.Enabled = true;
        }
        else
        {
            timer1.Start();
            pause = 0;
            button5.Enabled = false;
        }
    }
//Advance the simulation one time step button
```

```
    private void button5_Click(object sender, EventArgs e)
    {
        main_loop(sender, e);
    }
//Load shelf arrangement and parameters button
    private void LoadPeatButton_Click(object sender, EventArgs e)
    {
        string FILE_NAME = this.loaddtextBox.Text;
        int x, y = 1, xcounter;
        String input;
        int tttt = 0;
        StreamReader sr = File.OpenText(FILE_NAME);
        y = 0;
        string[] lineArray2;
        lineArray2 = sr.ReadLine().Split(new char[] { ',' }); //read ncols from header
        ncols = System.Convert.ToInt32(lineArray2[1]);
        lineArray2 = sr.ReadLine().Split(new char[] { ',' }); //read nrows from header
        nrows = System.Convert.ToInt32(lineArray2[1]);
        while ((input = sr.ReadLine()) != null)
        {
            string[] lineArray;
            lineArray = input.Split(new char[] { ' ' });
            xcounter = 1;
            for (x = 1; x <= (lineArray.Length - 1); x++)
            {
                if (lineArray[x] != "" && xcounter <= ncols)
                {
                    tttt = int.Parse(lineArray[x]);
                    elev[y, xcounter] = tttt;
                    if (tttt == 1)
                    {
                        bubbleIn++;
                    }
                    if (tttt == 2)
                    {
                        if (xcounter < shelfMinX)
                        {
                            shelfMinX = xcounter; //finds leftmost col with shelf
                        }
                        if (xcounter > shelfMaxX)
                        {
                            shelfMaxX = xcounter; //finds rightmost col with shelf
                        }
                    }
                    xcounter++;
                }
            }
            y++;
        }
        sr.Close();
        bubbleIntextBox.Text = bubbleIn.ToString();
    }
//Produce screenshot of shelf arrangement button
    private void button7_Click(object sender, EventArgs e) //take screenshot
    {
        drawwater(ncols, nrows, elev);
        m_objDrawingSurface.Save("image_qty" + shelfCount + "_size" + shelfLength + "_topple" + topple + ".png",
            System.Drawing.Imaging.ImageFormat.Png);
    }
//Clear shelf arrangement button
    private void clearPbutton8_Click(object sender, EventArgs e) //clear peat
    {
        for (x = 1; x < nrows - 1; x++)
        {
            for (y = 1; y < ncols - 1; y++)
            {
                if (elev[x, y] == 2)
                {
                    elev[x, y] = 0;
                }
            }
        }
```

```
    }
//Clear all stored bubbles button
    private void button10_Click(object sender, EventArgs e) //clear bubbles
    {
        for (x = 1; x < nrows - 1; x++)
        {
            for (y = 1; y < ncols - 1; y++)
            {
                if (elev[x, y] == 1)
                {
                    elev[x, y] = 0;
                }
            }
        }
    }
//Refresh graphics button
    private void refreshGraphics_Click(object sender, EventArgs e) //refresh the graphics
    {
        drawwater(ncols, nrows, elev);
    }
//Make shelf arrangements button
    private void makeShelvesButton_Click(object sender, EventArgs e)
    //because of bubble trap shelves must start on even columns and end on odd columns
    //therefore shelves can only be even length
    {
        //local variables made and initialized
        int rowsEmpty, rowsEmptyAbove, xBuffer, yBuffer, shelfQuantity, shelfSize, shelfRowOrigin = 0;
        int shelfColOrigin = 0;
        int shelfCounter = 0;
        bool evenOrigin = false;
        bool shelfExists = false;
        rowsEmpty = System.Convert.ToInt32(rowsEmptyTextBox20.Text);
        rowsEmptyAbove = System.Convert.ToInt32(rowAboveEmptytextBox20.Text) + 20; //20 rows ensures that shelf
            not to close bubble trap on row 5
        shelfQuantity = System.Convert.ToInt32(quantityShelvesTextBox.Text);
        shelfSize = System.Convert.ToInt32(sizeShelvesTextBox.Text);
        xBuffer = System.Convert.ToInt32(xBufferTextBox.Text);
        yBuffer = System.Convert.ToInt32(yBufferTextBox.Text);
        //define array where shelves will be made
        ncolsRandomElev = System.Convert.ToInt32(ncolsTextBox.Text);
        nrowsRandomElev = System.Convert.ToInt32(nrowsTextBox.Text);
        randomElev = new int[nrowsRandomElev, ncolsRandomElev];  //random shelf array
        //make blank image
        m_objDrawingSurface = new Bitmap((ncolsRandomElev) * graphics_scale,
            (nrowsRandomElev) * graphics_scale, System.Drawing.Imaging.PixelFormat.Format24bppRgb);
        Random randNum = new Random();
        while (shelfCounter < shelfQuantity)
        {
            //randomly select a pixel on an even column
            while (evenOrigin == false)
            {
                shelfColOrigin = randNum.Next(10, (ncolsRandomElev - shelfSize - 10)); //avoid edges
                if (shelfColOrigin % 2 == 0)
                {
                    evenOrigin = true;
                }
            }
            evenOrigin = false;
            //randomly select row
            shelfRowOrigin = randNum.Next(rowsEmptyAbove, nrowsRandomElev - (shelfSize + 2 + rowsEmpty));
            //check area around proposed shelf
            for (int shelfRow = (shelfRowOrigin - yBuffer); shelfRow < (shelfRowOrigin + yBuffer); shelfRow++)
            {
                for (int shelfCol = (shelfColOrigin - xBuffer); shelfCol < (shelfColOrigin + shelfSize + xBuffer); shelfCol++)
                {
                    if (randomElev[shelfRow, shelfCol] == 2)
                    {
                        shelfExists = true;
                    }
                }
            }
            //record shelf if clear
```

```
            if (shelfExists == false)
            {
                //make shelf
                for (int shelfDraw = 0; shelfDraw < shelfSize; shelfDraw++)
                {
                    randomElev[shelfRowOrigin, (shelfColOrigin + shelfDraw)] = 2;
                }
                shelfCounter++;
                shelvesMadeTextBox.Text = shelfCounter.ToString();
                shelvesMadeTextBox.Refresh();
            }
            if (shelfExists == true)
            {
                shelfExists = false;
            }
        }
        //draw the shelves onscreen
        drawwater(ncolsRandomElev, nrowsRandomElev, randomElev);
        //set zoom level of image box
        magnifyValue = zoomFactor[this.trackBar2.Value]; //magnification of peat
        zoomPanImageBox1.setZoom();
    }
//Load data button
    private void loadButton_Click(object sender, EventArgs e)
    {
        loadData(simCount);
    }
//Save shelf arrangement button
    private void saveRandomPeatbutton_Click(object sender, EventArgs e)
    {
        //save random peat array to file
        string FILENAME = saveShelftextBox.Text;
        using (StreamWriter sw = new StreamWriter(FILENAME))
        {
            sw.WriteLine("ncols," + ncolsRandomElev.ToString());
            sw.WriteLine("nrows," + nrowsRandomElev.ToString());
            for (x = 0; x < nrowsRandomElev; x++)
            {
                for (y = 0; y < ncolsRandomElev; y++)
                {
                    sw.Write(randomElev[x, y]);
                    sw.Write(" ");
                }
                sw.Write("\n");
            }
            sw.Close();
        }
    }
//Peat rupture button
    private void peatRuptureButton8_Click(object sender, EventArgs e)
    {
        peatRupture(); //experimental
    }
//Load parameters from configuration file
    private void openToolStripMenuItem_Click(object sender, EventArgs e)
    {
        XmlTextReader xreader;
        OpenFileDialog openFileDialog1 = new OpenFileDialog();
        openFileDialog1.InitialDirectory = current;
        openFileDialog1.Filter = "cfg files (*.xml)|*.xml|All files (*.*)|*.*";
        openFileDialog1.FilterIndex = 1;
        openFileDialog1.RestoreDirectory = false;
        if (openFileDialog1.ShowDialog() == DialogResult.OK)
        {
            cfgname = openFileDialog1.FileName;
            xreader = new XmlTextReader(cfgname);
            //Read the file
            if (xreader != null)
            {
                xreader.ReadStartElement("Params");
                simDurationTextBox.Text = xreader.ReadElementString("simDuration");
                loaddtextBox.Text = xreader.ReadElementString("inputFile");
```

```
            textBoxBubbleTime.Text = xreader.ReadElementString("BubbleProduction");
            bubbleSignalFilecheckBox1.Checked =
                XmlConvert.ToBoolean(xreader.ReadElementString("bubbleProductionFromFile"));
            bubbleSignalTextBox.Text = xreader.ReadElementString("bubbleProductionFile");
            focuscheckBox1.Checked = XmlConvert.ToBoolean(xreader.ReadElementString("focusBubblesCenter"));
            focus2checkBox1.Checked = XmlConvert.ToBoolean(xreader.ReadElementString("focusBubblesMany"));
            steptextBox3.Text = xreader.ReadElementString("stepFocusBubblesMany");
            hardCodecheckBox1.Checked = XmlConvert.ToBoolean(xreader.ReadElementString("hardCodedBubbles"));
            checkBoxShallowDeep.Checked =
                XmlConvert.ToBoolean(xreader.ReadElementString("shallowDeepBubbles"));
            textBoxQuantityShallow.Text = xreader.ReadElementString("quantityShallowBubbles");
            textBoxQuantityDeep.Text = xreader.ReadElementString("quantityDeepBubbles");
            RandomcheckBox1.Checked = XmlConvert.ToBoolean(xreader.ReadElementString("randomBubbles"));
            quantitytextBox3.Text = xreader.ReadElementString("quantityRandomBubbles");
            autoSpinUpcheckBox.Checked = XmlConvert.ToBoolean(xreader.ReadElementString("autoSpinUp"));
            fixedSpinUpcheckBox1.Checked = XmlConvert.ToBoolean(xreader.ReadElementString("fixedSpinUp"));
            fixedSpinUptextBox.Text = xreader.ReadElementString("fixedSpinUpBubbleAmount");
            bubbleOutputCheckBox.Checked = XmlConvert.ToBoolean(xreader.ReadElementString("bubbleOutputDist"));
            histoSamplingtextBox.Text = xreader.ReadElementString("histoSampling");
            bubbleSizeDistCheckBox.Checked = XmlConvert.ToBoolean(xreader.ReadElementString("bubbleSizeDist"));
            TimeScheckBox1.Checked = XmlConvert.ToBoolean(xreader.ReadElementString("timeSeriesChopMethod"));
            bubbleTimeStampcheckBox1.Checked =
                XmlConvert.ToBoolean(xreader.ReadElementString("timeSeriesTimeStampMethod"));
            checkBox2.Checked = XmlConvert.ToBoolean(xreader.ReadElementString("animate"));
            storageCheckBox.Checked = XmlConvert.ToBoolean(xreader.ReadElementString("animateBubbleStorage"));
            xreader.ReadEndElement();
            xreader.Close();
        }
    }
}
```

//Save parameters to configuration file

```
private void saveToolStripMenuItem_Click(object sender, EventArgs e)
{
    SaveFileDialog saveFileDialog1 = new SaveFileDialog();
    saveFileDialog1.InitialDirectory = current;
    saveFileDialog1.Filter = "cfg files (*.xml)|*.xml|All files (*.*)|*.*";
    saveFileDialog1.FilterIndex = 1;
    saveFileDialog1.RestoreDirectory = false;
    if (saveFileDialog1.ShowDialog() == DialogResult.OK)
    {
        cfgname = saveFileDialog1.FileName;
    }
    writeXML(cfgname, false, "");
}
```

//Quit simulation button

```
private void quitSaveButton6_Click(object sender, EventArgs e) //quit and save button
{
    if (realTime < simDuration)//save files mid-simulation
    {
        endSim();
        this.Close();
    }
    else
    {
        this.Close();
    }
}
```

//Makes confguartion files for batch mode simulation

```
private void makeConfigFilebutton4_Click_1(object sender, EventArgs e)
{
    string[] sensaShelfQty;//array that holds all the shlef sizes
    sensaShelfQty = sensaShelfQtytextBox.Text.Split(new char[] { ',' }); //shelf sizes
    int shelfSize;
    for (int index = 0; index < sensaShelfQty.Length; index++) //number of shelf quantity specified
    {
        //local variables made and initialized
        int rowsEmpty, rowsEmptyAbove, xBuffer, yBuffer, shelfQuantity, shelfRowOrigin = 0;
        int shelfColOrigin = 0;
        int shelfCounter = 0;
        bool evenOrigin = false;
        bool shelfExists = false;
        shelfQuantity = System.Convert.ToInt32(sensaShelfQty[index]); //shelf quantity
```

```
    rowsEmpty = System.Convert.ToInt32(rowsEmptyTextBox20.Text);
    rowsEmptyAbove = System.Convert.ToInt32(rowAboveEmptytextBox20.Text) + 20;
    shelfSize = System.Convert.ToInt32(sizeShelvesTextBox.Text);
    xBuffer = System.Convert.ToInt32(xBufferTextBox.Text);
    yBuffer = System.Convert.ToInt32(yBufferTextBox.Text);
    //define array where shelves will be made
    ncolsRandomElev = System.Convert.ToInt32(ncolsTextBox.Text);
    nrowsRandomElev = System.Convert.ToInt32(nrowsTextBox.Text);
    randomElev = new int[nrowsRandomElev, ncolsRandomElev];  //random shelf array
    Random randNum = new Random();
    while (shelfCounter < shelfQuantity)
    {
        //randomly select a pixel on an even column
        while (evenOrigin == false)
        {
            shelfColOrigin = randNum.Next(10, (ncolsRandomElev - shelfSize - 10)); //avoid edges
            if (shelfColOrigin % 2 == 0)
            {
                evenOrigin = true;
            }
        }
        evenOrigin = false;
        //randomly select row
        shelfRowOrigin = randNum.Next(rowsEmptyAbove, nrowsRandomElev - (shelfSize + 2 + rowsEmpty));
        //check area around proposed shelf
        for (int shelfRow = (shelfRowOrigin - yBuffer); shelfRow < (shelfRowOrigin + yBuffer); shelfRow++)
        {
            for (int shelfCol = (shelfColOrigin - xBuffer); shelfCol < (shelfColOrigin + shelfSize + xBuffer); shelfCol++)
            {
                if (randomElev[shelfRow, shelfCol] == 2)
                {
                    shelfExists = true;
                }
            }
        }
        //record shelf if clear
        if (shelfExists == false)
        {
            //make shelf
            for (int shelfDraw = 0; shelfDraw < shelfSize; shelfDraw++)
            {
                randomElev[shelfRowOrigin, (shelfColOrigin + shelfDraw)] = 2;
            }
            shelfCounter++;
            shelvesMadeTextBox.Text = shelfCounter.ToString();
            shelvesMadeTextBox.Refresh();
        }
        if (shelfExists == true)
        {
            shelfExists = false;
        }
    }
    //save the peat matrix with unique name
    string FILENAME = "peat_qty" + shelfQuantity + "_size" + shelfSize + ".txt";
    using (StreamWriter sw = new StreamWriter(FILENAME))
    {
        sw.WriteLine("ncols," + ncolsRandomElev.ToString());
        sw.WriteLine("nrows," + nrowsRandomElev.ToString());
        for (x = 0; x < nrowsRandomElev; x++)
        {
            for (y = 0; y < ncolsRandomElev; y++)
            {
                sw.Write(randomElev[x, y]);
                sw.Write(" ");
            }
            sw.Write("\n");
        }
        sw.Close();
    }
    //make a config file
    string FILENAME2 = "peat_qty" + shelfQuantity + "_size" + shelfSize + ".xml";
    writeXML(FILENAME2, true, FILENAME);
}
```

```
            recordOutputTextBox4.Text = "finished config files";
        }
    }
}
```

Table 2. Development history of MEGA.

model version	changes to model
1.0	Basic inverted sandpile model. Algorithm for generating random shelf arrangements.
2.0	Time step added to model, and bubbles have velocity.
2.1	Parallelization implemented by using C# Parallel.For loops to scan shelf arrangement. Flux is measured in chambers at the peat surface. Shelf arrangement shelf sizes randomly selected using gamma and normal distributions.
2.2	Bubble production can represent environmental forcing through production signal. Performance improvement by scanning shelf arrangement only when bubbles are in movement.
3.0	Model streamlined by removing code.
4.0	Bubble production is represented as three signals added to the peat at three depths.
5.0	Porosity of peat can be set differently for shallow and deep peat layers. Placement of shelves is restricted by template that is derived from a fractal pattern. Placement of shelves is dictated by two gradients (vertical and horizontal direction).

The development history of MEGA is summarized in Table 2. The major technical model developments were a parallel method for scanning the shelf arrangement (v2.1), and scanning the shelf arrangement when bubbles were only in movement (v2.2). These developments improved the computational performance of the model significantly and made it possible to model plot scale shelf arrangements. Parallelization was implemented by using C# built-in Parallel.For method to scan the 2D array that represents the shelf arrangement. Scanning the shelf arrangement is the most computational expensive part of MEGA, and requires a nested for loops to access the array locations that represent the shelf arrangement or bubbles. One loop is required to iterate through the indices of the array rows,

and a second loop is needed to iterate through the indices of the array columns. In MEGA a Parallel.For was used in the outer loop of the nested loop. Further improvements to the model performance included the development of an algorithm to scan the shelf arrangement only when bubbles are in movement (e.g. avalanches). When no bubble movement is detected or no toppling rules are executed the model does not scan the shelf arrangement, but advances time until new bubbles are added to the shelf arrangement through bubble production.

2. Shelf bubble machine (SBM) development

Three prototypes of the shelf bubble machine were constructed before the final version of the SBM used in Chapter 3. The first bubble machine prototype consisted of a plastic graduated cylinder with the base removed and was inserted within a beaker filled with water. Within the graduated cylinder metal rods were suspended from above at different heights, and attached to the end of each rod was a piece of corrugated plastic that represented a shelf. Bubbles were produced manually with a syringe attached to tubing that was attached to the base of the graduated cylinder. From this first prototype it was noticed that gas storage underneath a 'bare' plastic shelf was low, and greater amounts of surface tension were needed to have larger amounts of gas storage, as in MEGA.

A second shelf bubble machine prototype was constructed using two sheets of clear plastic with pieces of high density foam to separate the plastic sheets (Figure 60a). These two sheets of plastic were bolted together and a sufficient amount of pressure was applied to the sheets of plastic to suspend shelves constructed out of PVC wrapped with rubber bands. This prototype was submerged within a beaker filled with water. To increase the roughness of the shelves, sections of scouring

pad were attached to the underside of each shelf, and a background for the prototype was made out of paper. Bubbles for the prototype were produced using a fish pump connected to tubing with several pin sized holes, and the section of perforated tubing was placed at the base of the beaker below the shelf arrangement.

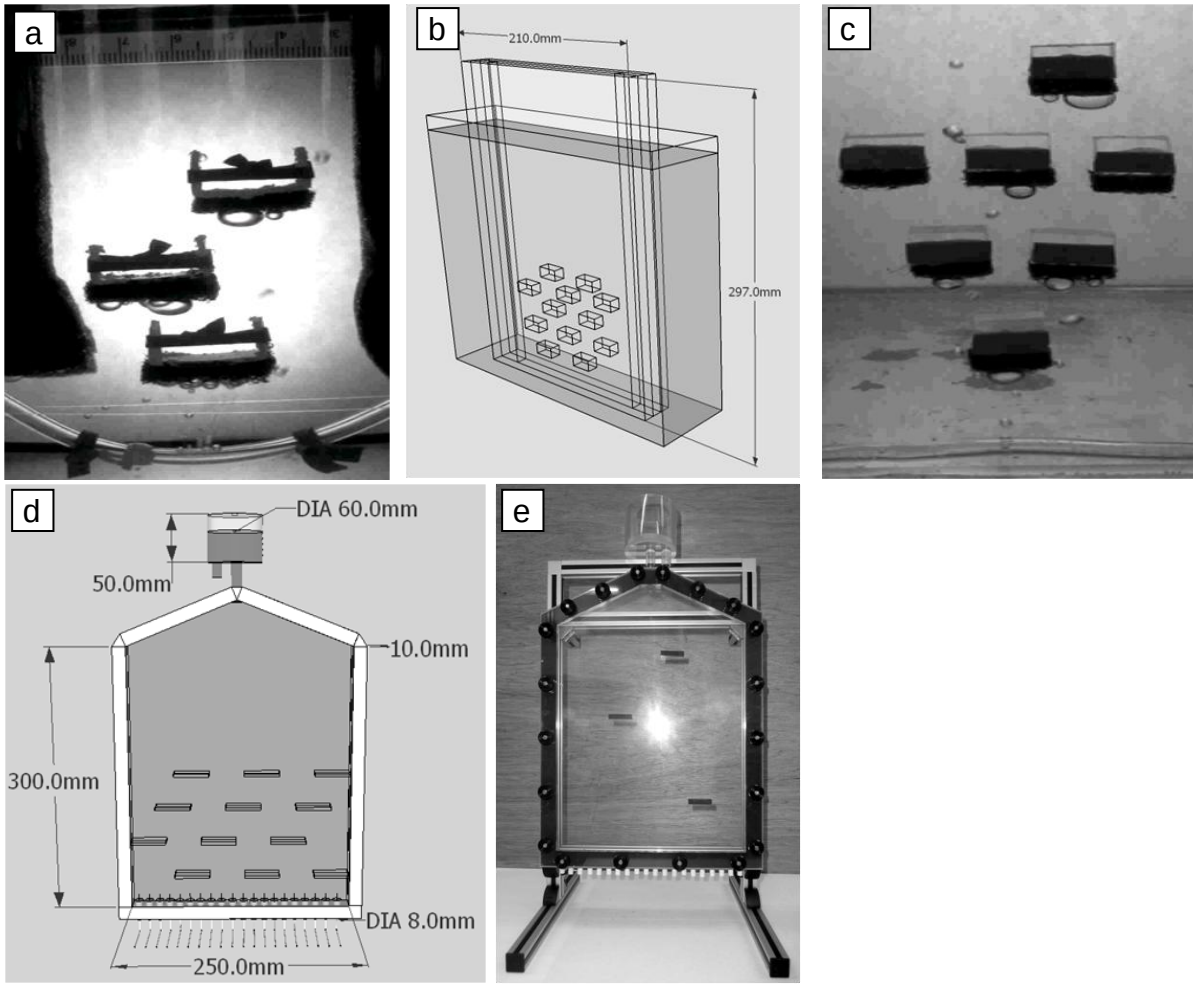

Figure 60. (a,b,c) Shelf bubble machine prototypes, (d,e) and the shelf bubble machine.

Filming the bubbles from this second prototype, and converting the video to images revealed that bubbles were blurry and may move too fast to be filmed with the video camera obtained (Sony HDR-SR10E). Changes were made to improve the contrast between bubbles and water, by trying different types of lighting and

lighting positions. This included backlighting the prototype with a standard incandescent light bulb, fluorescent lamp, light-emitting diode lamps (LED), and a halogen lamp. Lighting from the halogen lamp provided improvements to the quality of the video, but bubbles continued to be blurry in appearance. Assuming that the speed of the bubbles produced the blurriness, attempts were made to reduce the speed of the bubbles by operating the prototype in vegetable oil. Operating the prototype with oil was abandoned due to the cleanup effort required at the end of the experiment. A solution to the bubble blurriness was provided by converting the video to images using freeware DOS program called FFmpeg (http://www.ffmpeg.org/). Erroneously it was assumed that bubble speed caused the bubble blurriness, instead the video had to be deinterlaced prior to conversion to images (sample code provided below). After deinterlacing the video the images of bubbles were significantly better and measurement of bubble sizes was possible.

```
C:\> ffmpeg -i bubbleMovie.m2ts   -r 1   -deinterlace   -s 1920x1080 image−%d.jpg
          ↑                       ↑          ↑             ↑              ↑
     input movie            frames per sec  deinterlace  frame size   output
                            to extract      option                    frame name
```

A third prototype of the SBM was similar in design to the second prototype but constructed entirely out of Perspex. This prototype consisted of two panes (210 mm x 297 mm) of Perspex separated enough (10 mm) to accommodate shelves made out of Perspex (Figure 60b,c). As in the previous prototype, shelves were fitted with scouring pad to increase surface roughness. The entire Perspex structure was immersed in a fish tank filled with water. This prototype was used to

decide the dimensions of the final SBM (250 mm x 300 mm), and the sizes of the shelves in the final SBM (20 mm and 60 mm). Additionally from this prototype the amount of area required to film bubbles exiting the shelf arrangement for measurement of bubble sizes in the SBM was estimated.

Blueprints of the final SBM were drafted using Google SketchUp (Figure 60d) and construction of the SBM (Figure 60e) was performed by the Instrument Workshop in the University of Leeds School of Earth and Environment. Throughout the construction of the SBM bi-weekly meetings with the workshop manager were held to discuss alterations to the SBM design. After receiving delivery of the SBM many trials were performed to produce a steady quantity of bubbles with individual bubbles of an approximate diameter of 1 mm or less. First, ceramic and wooden fish tank aerators connected to a fish pump were tried, but the dimensions of the aerators were too large to fit within the SBM. Next syringes connected to tygon tubing were fitted with needles with different point types (e.g. bevelled, blunt) and gauges (e.g. 22, 30, 32 gauge). These different needles were inserted into the base of the SBM, filled with water, and bubble sizes produced by each needle type were measured. After inspecting the bubble sizes, it was decided that a 30 Gauge one inch blunt dispensing needle consistently produced bubbles required for the SBM experiments. Furthermore, it was decided that syringe pumps would be employed to deliver a steady production of bubbles.

Additional trials with the final SBM included determining the distance that the video cameras should be placed to produce the sharpest video when filming bubble sizes (distance from SBM, 75 cm) and storage (distance from SBM, 100 cm). Initially a

paper background was used as a background for the SBM. After image analysis of initial bubble size video, it was decided that the paper background contained imperfections that made bubble extraction difficult. To rectify this, a frosted plastic sheet of plastic was used as a background for the SBM. Lastly, tests of the SBM found that bubbles that exit the shelf arrangement could become attached to the sloping roof of the SBM. If the bubbles were to accumulate on the roof the SBM, this could affect bubble flux measurements in the SBM gas trap. Efforts were made to prevent bubble attachment by making the roof of the SBM smoother with plumber's tape and increasing the angle of the SBM roof. All of these attempts failed, and the solution was to thoroughly clean the roof of the SBM with mineralised methylated spirits. By cleaning the roof of the SBM, nucleation sites were removed, and bubbles did not attach to the roof of the SBM.

3. Cylindrical bubble machine (CBM) development

No prototypes of the CBM were constructed, but due to the similarities with the SBM in operation, many of the methods developed for the SBM were applied to the CBM. Blueprints of the CBM were drawn in Google SketchUp (Figure 61a) and construction of the CBM (Figure 61b) was performed by the Instrument Workshop in the University of Leeds School of Earth and Environment. As with the SBM, throughout the construction of the CBM bi-weekly meetings with the workshop manager were held to discuss alterations to the CBM design.

Test samples of peat were used in the CBM to determine the experimental setup required. At first, peat samples were directly placed within the main tank of the CBM, but this method was abandoned because removal of the sample from the CBM damaged the peat structure. Instead peat samples were trimmed to fit

permanently within an acrylic tube that served as module that could be inserted within the CBM. The first modules were not transparent, but it was decided that the final modules would be transparent to observe if gas movement occurred along the interior surface of the module that is in contact with the peat. Due to the buoyancy of the peat, the modules within the CBM floated to the top of the CBM. Efforts were unsuccessfully made to anchor the module to the bottom of the CBM with weights. Instead modules were fitted with foam collars that applied sufficient pressure against the main tank of the CBM to hold the module in place at the base of the CBM.

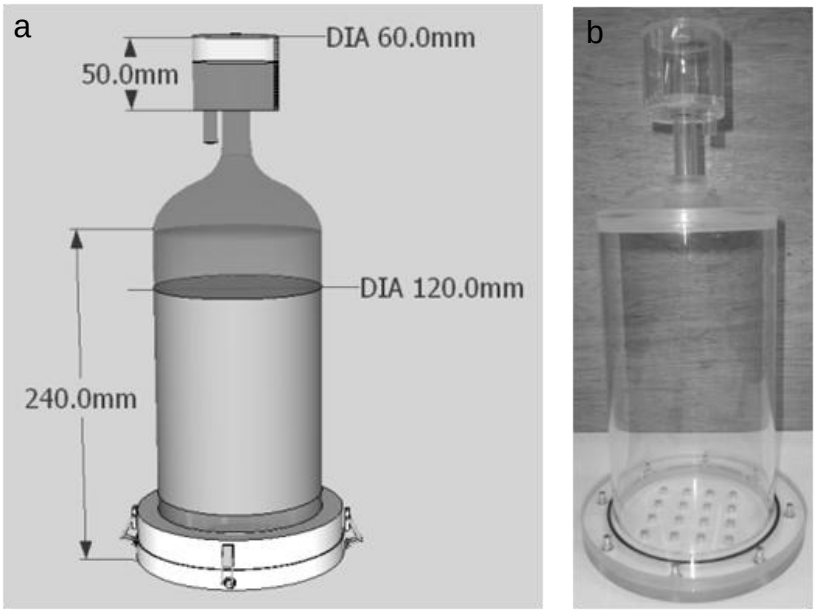

Figure 61. (a) Blueprints of CBM, (b) and the CBM.

4. Image analysis of bubble storage, size, and release

Meauruements of bubble size and release within the SBM and CBM were first performed manually from images extracted from video. Bubble size measurements involved drawing a grid on the image and counting the number of

grid cells that a bubble occupies. Measuremnts of bubble release, from both bubble machines, requires a measurement of the water level within the gas trap. Initially this was also manually estimated by superimposing horizontal lines on images of the gas trap and estimating the change in water level. Due to the number of bubble sizes measurements (10,000s) and bubble releases measurements (100s) per bubble machine experiment it was necessary to develop a computationally efficient method to analyze images extracted from video. A soulution was provided by the freeware image proceesing software ImageJ (http://rsb.info.nih.gov/ij/). Using ImageJ's macro language a series of ImageJ commands could be run automatically to measure bubble storage, size, and release. Below are example image processing scripts for frames of shelf arrangement from the SBM consisting of three shelves of length 60 mm.

```
//Bubble storage image analysis script for shelf arrangement of 3 shelves of 60mm length
//set variables and parameters
dir1 = "D:\\THIS_WEEK2\\bubbleAlgorithmCalibrations\\bubbleStorage60mm3Shelves\\";
dir2 =  "D:\\THIS_WEEK2\\bubbleAlgorithmCalibrations\\bubbleStorage60mm3Shelves\\output\\";
start = 1;
finish = 100;
numbFiles = finish;
run("Input/Output...", "jpeg=100 gif=255 file=.csv copy");
run("Set Measurements...", "area redirect=None decimal=3");
run("Options...", "iterations=1 count=1 pad edm=Overwrite");
setPasteMode("Transparent-white");

//set scale
open(dir1+ "foo-"+start+".jpeg");
makeLine(254, 131, 507, 131);
run("Set Scale...", "distance=253 known=60 pixel=1 unit=unit global");
close();

for (j=start;j<=numbFiles; j++)
{
        open(dir1+ "foo-"+j+".jpeg");
        saveAs("Jpeg",dir2+"orig_"+"foo-"+j+".jpg");

        //threshold image
        run("Variance...", "radius=2");
        run("Make Binary");
        run("Dilate");
        run("Fill Holes");
        run("Erode");
        run("Erode");
        run("Erode");
        run("Erode");

        //shelf 1 analysis
```

```
makePolygon(747,89,757,96,770,97,789,96,801,95,816,96,825,95,840,95,858,95,872,92,879,91,894,92,915,93,9
35,91,949,93,976,93,999,92,1021,145,735,146);
run("Analyze Particles...", "size=0-Infinity circularity=0.00-1.00 show=Nothing");
saveAs("Measurements", dir2+"\\Results_shelf1_"+j+".txt");
run("Outline");
run("Dilate");
run("Clear Results");
run("Select None");

//shelf2 analysis
makePolygon(255,180,287,182,300,180,327,180,345,183,374,184,395,182,416,181,439,183,479,182,513,181,52
2,229,244,229);
run("Analyze Particles...", "size=0-Infinity circularity=0.00-1.00 show=Nothing");
saveAs("Measurements", dir2+"\\Results_shelf2_"+j+".txt");
run("Outline");
run("Dilate");
run("Clear Results");
run("Select None");

//shelf3 analysis
makePolygon(434,441,438,446,442,446,449,449,459,450,470,449,481,449,492,451,502,450,515,450,531,449,54
6,451,561,450,581,451,602,452,620,450,635,450,653,449,675,450,683,451,691,443,698,524,420,524);
run("Analyze Particles...", "size=0-Infinity circularity=0.00-1.00 show=Nothing");
saveAs("Measurements", dir2+"\\Results_shelf3_"+j+".txt");
run("Outline");
run("Dilate");
run("Clear Results");
run("Select None");

//outline of stoarage
saveAs("Jpeg",dir2+"shelfs_foo-"+j+".jpg");

//overlay image and outline of storage for double checking
open(dir2+"orig_foo-"+j+".jpg");
selectWindow("shelfs_foo-"+j+".jpg");
run("Copy");
selectWindow("orig_foo-"+j+".jpg");
run("Paste");
saveAs("Jpeg", dir2+"overlay"+"foo-"+j+".jpg");
close();
close();
}
```

```
//Bubble size image analysis script for shelf arrangement of 3 shelves of 60mm length
//set variables and parameters
dir1 = "D:\\THIS_WEEK2\\bubbleAlgorithmCalibrations\\sizes\\BubbleSize3shelves60mm\\";
dir2 = "D:\\THIS_WEEK2\\bubbleAlgorithmCalibrations\\sizes\\BubbleSize3shelves60mm\\output\\";
startImage =1;
endImage =1000;
run("Input/Output...", "jpeg=100 gif=255 file=.csv copy");
run("Set Measurements...", "area redirect=None decimal=3");
run("Options...", "iterations=1 count=1 pad edm=Overwrite");
setPasteMode("Transparent-white");

//set scale
open(dir1+ "foo-"+startImage+".jpeg");
makeLine(479, 976, 807, 969);
run("Set Scale...", "distance=328.07 known=60 pixel=1 unit=unit global");
close();

for (i=startImage; i<=endImage; i++)
{
        //orignal image cropped
        open(dir1+"foo-"+i+".jpeg");
        run("Deinterlace ");
        makeRectangle(82, 304, 1682, 538);
        run("Crop");
        makeRectangle(237, 76, 1199, 326);
        run("Crop");
        saveAs("Jpeg",dir2+"orig_"+"foo-"+i+".jpg");
```

```
        close();

        //threshold  bubbles
        open(dir1+"foo-"+i+".jpeg");
        run("Deinterlace ");
        makeRectangle(82, 304, 1682, 538);
        run("Crop");
        run("Despeckle");
        run("Find Edges");
        run("Sharpen");
        run("Make Binary");
        run("Dilate");
        run("Find Edges");
        run("Dilate");
        makeRectangle(237, 76, 1199, 326);
        run("Crop");
        run("Fill Border Holes");
        run("BinaryKillBorders ", "top right bottom left white");
        run("Erode");
        run("Erode");
        run("Erode");
        run("Erode");
        run("Erode");

        // Analyze particles
        run("Analyze Particles...", "size=0-Infinity circularity=0.00-1.00 show=Nothing");
        saveAs("Measurements", dir2+"\\Results_"+i+".txt");
        run("Clear Results");
        //save processed image
        run("Outline");
        saveAs("Jpeg",dir2+"processed_"+"foo-"+i+".jpg");

        //overlay for double checking
        selectWindow("processed_foo-"+i+".jpg");
        run("Copy");
        open(dir2+"orig_foo-"+i+".jpg");
        selectWindow("orig_foo-"+i+".jpg");
        run("Paste");
        saveAs("Jpeg", dir2+"overlay"+"foo-"+i+".jpg");
        close();
        close();
}
```

```
//Bubble release image analysis script for shelf arrangement of 3 shelves of 60mm length
//set variables and parameters
dir1 = "D:\\THIS_WEEK2\\bubbleAlgorithmCalibrations\\release\\bubbleRelease3shelves60mm\\";
dir2 = "D:\\THIS_WEEK2\\bubbleAlgorithmCalibrations\\release\\bubbleRelease3shelves60mm\\output\\";
start = 1;
end = 1000;
run("Input/Output...", "jpeg=100 gif=255 file=.csv copy");
run("Set Measurements...", "area redirect=None decimal=3");
run("Options...", "iterations=1 count=1 pad edm=Overwrite");
setPasteMode("Transparent-zero");

//set scale
open(dir1+ "foo-"+start+".jpeg");
makeLine(994, 886, 1006, 202);
run("Set Scale...", "distance=684.11 known=50 pixel=1 unit=unit global");
close();

for (j=start;j<=end; j++)
{
        //crop orginal image
        open(dir1+"foo-"+j+".jpeg");
        run("Deinterlace ");
        makeRectangle(544, 188, 890, 718);
        run("Crop");
        saveAs("Jpeg",dir2+"orig_"+"foo-"+j+".jpg");
        close();
```

```
//color threshold
open(dir1+"foo-"+j+".jpeg");
run("Deinterlace ");
//makeRectangle(494, 180, 830, 736);
makeRectangle(544, 188, 890, 718);
run("Crop");
// Color Thresholder 1.44o
min=newArray(3);
max=newArray(3);
filter=newArray(3);
a=getTitle();
run("HSB Stack");
run("Convert Stack to Images");
selectWindow("Hue");
rename("0");
selectWindow("Saturation");
rename("1");
selectWindow("Brightness");
rename("2");
min[0]=52;
max[0]=255;
filter[0]="pass";
min[1]=0;
max[1]=255;
filter[1]="pass";
min[2]=0;
max[2]=255;
filter[2]="pass";
for (i=0;i<3;i++){
  selectWindow(""+i);
  setThreshold(min[i], max[i]);
  run("Convert to Mask");
  if (filter[i]=="stop")  run("Invert");
}
imageCalculator("AND create", "0","1");
imageCalculator("AND create", "Result of 0","2");
for (i=0;i<3;i++){
  selectWindow(""+i);
  close();
}
selectWindow("Result of 0");
close();
selectWindow("Result of Result of 0");
rename(a);
run("Fill Holes");
run("Erode");
run("Erode");
run("Erode");
run("Dilate");
run("Dilate");
run("Dilate");
run("Dilate");
run("Dilate");
run("Dilate");

// Analyze particles
run("Analyze Particles...", "size=0-Infinity circularity=0.00-1.00 show=Nothing");
saveAs("Measurements", dir2+"\\Results_"+j+".txt");
run("Clear Results");

//save processed image
run("Outline");
run("Dilate");
run("Invert");
saveAs("Jpeg",dir2+"processed_"+"foo-"+j+".jpg");

//overlay for double checking
selectWindow("processed_foo-"+j+".jpg");
run("Copy");
open(dir2+"orig_foo-"+j+".jpg");
selectWindow("orig_foo-"+j+".jpg");
```

```
            run("Paste");
            saveAs("Jpeg", dir2+"overlay"+"foo-"+j+".jpg");
            close();
            close();
}
```

5. Slicing peat core and analysis

Several methods to slice a peat core were dicussed and tried before deciding to slice the peat using the method in Chapter 4. The first method discussed would require the use of a bandsaw to slice through the frozen peat sample. This method was not tried because it was thought that friction produced by the bandsaw blade would begin to melt the peat core and the pore structure of the melting peat could easily be destroyed. It was decided that a manual method would be needed to slice the peat core, as a manual method would not melt the peat and preserve the pore structure. Using a frozen peat test core, several saws and knives were trialled for slicing. A hacksaw could not easily cut through the peat sample, and the blade broke midway through the core. A tenon saw became stuck midway through the core, and could not be moved. A 20 cm blade knife could not cut easily through the frozen core and the time required to cut through the core allowed the core to thaw and the pore structure to change. Lastly, a fine cut saw was tired and a slice through the peat core was easily performed with no visible damage to the peat.

Analysis of the peat slices was first performed using a colour thresholding technique within the image processing software ImageJ. Colour thresholding required setting thresholds for red, green, and blue (RGB) image values to isolate pixels that correspond to pores. In this analysis threshold values were set manually by observing which image locations were selected with different conbinations of RGB threshold values. This method was abandoned after it was

decided that a significant amount of bias could be introduced by manually setting threshold values. For this reason an automated method was selected to classify the images using a Euclidean distance classification method (ISODATA).

References

Akaike, H. (1974), A new look at the statistical model identification, *Automatic Control, IEEE Transactions on*, *19*(6), 716-723.

Albano, E. V. (1995), Spreading analysis and finite-size scaling study of the critical-behavior of a forest-fire model with immune trees, *Physica A*, *216*(3), 213-226.

Amos, R. T., and K. U. Mayer (2006), Investigating the role of gas bubble formation and entrapment in contaminated aquifers: Reactive transport modelling, *Journal of Contaminant Hydrology*, *87*(1-2), 123-154.

Anderson, B., K. B. Bartlett, S. Frolking, K. Hayhoe, J. Jenkins, and W. Salas (2010), Methane and nitrous oxide emissions from natural sources United States Environmental Protection Agency, Washington, DC.

Arneth, A., S. P. Harrison, S. Zaehle, K. Tsigaridis, S. Menon, P. J. Bartlein, J. Feichter, A. Korhola, M. Kulmala, D. O'Donnell, G. Schurgers, S. Sorvari, and T. Vesala (2010), Terrestrial biogeochemical feedbacks in the climate system, *Nature Geoscience*, *3*(8), 525-532.

Baird, A. J., and S. Waldron (2003), Shallow horizontal groundwater flow in peatlands is reduced by bacteriogenic gas production, *Geophysical Research Letters*, *30*(20).

Baird, A. J., C. W. Beckwith, S. Waldron, and J. M. Waddington (2004), Ebullition of methane-containing gas bubbles from near-surface *Sphagnum* peat, *Geophysical Research Letters*, *31*(21).

Bak, P., C. Tang, and K. Wiesenfeld (1987), Self-organized criticality: An explanation of the 1/f noise, *Physical Review Letters*, *59*(4), 381-384.

Bak, P., and C. Tang (1989), Earthquakes as a self-organized critical phenomena, *Journal of Geophysical Research-Solid Earth and Planets*, *94*(B11), 15635-15637.

Ball, G. H., and D. J. Hall (1965), ISODATA, a novel method of data analysis and pattern classification, DTIC Document.

Bao, J., and L. Schaefer (2013), Lattice Boltzmann equation model for multi-component multi-phase flow with high density ratios, *Applied Mathematical Modelling*, *37*(4), 1860-1871.

Belyea, L. R. (1996), Separating the effects of litter quality and microenvironment on decomposition rates in a patterned peatland, *Oikos*, *77*(3), 529-539.

Belyea, L. R., and R. Clymo (2001), Feedback control of the rate of peat formation, *Proceedings of the Royal Society of London. Series B: Biological Sciences*, *268*(1473), 1315-1321.

Birovljev, A., G. Wagner, P. Meakin, J. Feder, and T. Jøssang (1995), Migration and fragmentation of invasion percolation clusters in two-dimensional porous media, *Physical Review E*, *51*(6), 5911.

Bland, J. M., and D. G. Altman (1995), Multiple significance tests: the Bonferroni method, *British Medical Journal*, *310*(6973), 170.

Blunt, M. J., M. D. Jackson, M. Piri, and P. H. Valvatne (2002), Detailed physics, predictive capabilities and macroscopic consequences for pore-network models of multiphase flow, *Advances in Water Resources*, *25*(8-12), 1069-1089.

Blunt, M. J., B. Bijeljic, H. Dong, O. Gharbi, S. Iglauer, P. Mostaghimi, A. Paluszny, and C. Pentland (2013), Pore-scale imaging and modelling, *Advances in Water Resources*, *51*, 197-216.

Boelter, D. H. (1965), Hydraulic conductivity of peats, *Soil Science*, *100*(4), 227-231.

Boelter, D. H. (1969), Physical properties of peats as related to degree of decomposition, *Soil Science Society of America Proceedings*, *33*(4), 606-609.

Bourgeat, A., M. Jurak, and F. Smaï (2009), Two-phase, partially miscible flow and transport modeling in porous media; application to gas migration in a nuclear waste repository, *Computational Geosciences*, *13*(1), 29-42.

Box, G. E., and N. R. Draper (1987), *Empirical model-building and response surfaces*, John Wiley & Sons.

Bridgham, S. D., H. Cadillo-Quiroz, J. K. Keller, and Q. Zhuang (2013), Methane emissions from wetlands: biogeochemical, microbial, and modeling perspectives from local to global scales, *Global Change Biology*, *19*(5), 1325-1346.

Bubier, J., A. Costello, T. R. Moore, N. T. Roulet, and K. Savage (1993a), Microtopography and methane flux in boreal peatlands, northern Ontario, Canada, *Canadian Journal of Botany-Revue Canadienne De Botanique*, *71*(8), 1056-1063.

Bubier, J. L., T. R. Moore, and N. T. Roulet (1993b), Methane emissions from wetlands in the midboreal region of Northern Ontario, Canada, *Ecology*, *74*(8), 2240-2254.

Bubier, J. L., and T. R. Moore (1994), An ecological perspective on methane emissions from northern wetlands, *Trends in Ecology & Evolution*, *9*(12), 460-464.

Bubier, J. L., T. R. Moore, L. Bellisario, N. T. Comer, and P. M. Crill (1995), Ecological controls on methane emissions from a Northern Peatland Complex in the zone of discontinuous permafrost, Manitoba, Canada, *Global Biogeochemical Cycles*, *9*(4), 455-470.

Burrows, E., J. Bubier, A. Mosedale, G. Cobb, and P. Crill (2005), Net ecosystem exchange of carbon dioxide in a temperate poor fen: A comparison of automated and manual chamber techniques, *Biogeochemistry*, *76*(1), 21-45.

Buwa, V. V., and V. V. Ranade (2002), Dynamics of gas-liquid flow in a rectangular bubble column: experiments and single/multi-group CFD simulations, *Chemical Engineering Science*, *57*(22), 4715-4736.

Cao, M. K., S. Marshall, and K. Gregson (1996), Global carbon exchange and methane emissions from natural wetlands: Application of a process-based model, *Journal of Geophysical Research-Atmospheres*, *101*(D9), 14399-14414.

Chappellaz, J., T. Bluniert, D. Raynaud, J. M. Barnola, J. Schwander, and B. Stauffert (1993), Synchronous changes in atmospheric CH_4 and Greenland climate between 40 and 8 kyr BP, *Nature*, *366*(6454), 443-445.

Chen, S., and G. D. Doolen (1998), Lattice Boltzmann method for fluid flows, *Annual Review of Fluid Mechanics*, *30*(1), 329-364.

Christensen, T. R., N. Panikov, M. Mastepanov, A. Joabsson, A. Stewart, M. Öquist, M. Sommerkorn, S. Reynaud, and B. Svensson (2003), Biotic controls on CO_2 and CH_4 exchange in wetlands: a closed environment study, *Biogeochemistry*, *64*(3), 337-354.

Cihan, A., and M. Y. Corapcioglu (2008), Effect of compressibility on the rise velocity of an air bubble in porous media, *Water Resources Research*, *44*(4), W04409.

Clauset, A., C. R. Shalizi, and M. E. J. Newman (2009), Power-law distributions in empirical data, *SIAM Reviews*, *51*(4), 661-703.

Clymo, R. S. (1984), The limits to peat bog growth, *Philosophical Transactions of the Royal Society of London Series B-Biological Sciences*, *303*(1117), 605-654.

Clymo, R. S., and D. M. E. Pearce (1995), Methane and carbon dioxide production in, transport through, and efflux from a peatland, *Philosophical Transactions of the Royal Society of London Series A -Mathematical Physical and Engineering Sciences*, *351*(1696), 249-259.

Comas, X., and L. Slater (2007), Evolution of biogenic gases in peat blocks inferred from noninvasive dielectric permittivity measurements, *Water Resources Research*, *43*(5).

Comas, X., L. Slater, and A. Reeve (2008), Seasonal geophysical monitoring of biogenic gases in a northern peatland: Implications for temporal and spatial variability in free phase gas production rates, *Journal of Geophysical Research: Biogeosciences*, *113*(G1).

Comas, X., L. Slater, and A. S. Reeve (2011), Atmospheric pressure drives changes in the vertical distribution of biogenic free-phase gas in a northern peatland, *Journal of Geophysical Research*, *116*(G4), G04014.

Comas, X., and W. Wright (2012), Heterogeneity of biogenic gas ebullition in subtropical peat soils is revealed using time-lapse cameras, *Water Resources Research*, *48*(4).

Corapcioglu, M. Y., A. Cihan, and M. Drazenovic (2004), Rise velocity of an air bubble in porous media: Theoretical studies, *Water Resources Research*, *40*(4), 9.

Coulthard, T., A. J. Baird, J. Ramirez, and J. M. Waddington (2009), Modeling methane dynamics in peat: future prospects, in *Northern Peatlands and Carbon Cycling*, edited by A. J. Baird, et al., p. 299, American Geophysical Union, Washington D. C.

Davidson, E. A., and I. A. Janssens (2006), Temperature sensitivity of soil carbon decomposition and feedbacks to climate change, *Nature*, *440*(7081), 165-173.

Delnoij, E., J. Kuipers, and W. Van Swaaij (1999), A three-dimensional CFD model for gas-liquid bubble columns, *Chemical Engineering Science*, *54*(13), 2217-2226.

Dise, N. B., E. Gorham, and E. S. Verry (1993), Environmental factors controlling methane emissions from peatlands in northern Minnesota, *Journal of Geophysical Research-Atmospheres*, *98*(D6), 10583-10594.

Dlugokencky, E. J., L. Bruhwiler, J. W. C. White, L. K. Emmons, P. C. Novelli, S. A. Montzka, K. A. Masarie, P. M. Lang, A. M. Crotwell, J. B. Miller, and L. V. Gatti (2009), Observational constraints on recent increases in the atmospheric CH_4 burden, *Geophysical Research Letters*, *36*(18), L18803.

Drossel, B., and F. Schwabl (1992), Self-organized critical forest-fire model, *Physical Review Letters*, *69*(11), 1629-1632.

Duineveld, P. C. (1995), The rise velocity and shape of bubbles in pure water at high Reynolds number, *Journal of Fluid Mechanics*, *292*, 325-332.

Dunfield, P., R. Knowles, R. Dumont, and T. R. Moore (1993), Methane production and consumption in temperate and subarctic peatsoils: Response to temperature and pH, *Soil Biology & Biochemistry*, *25*(3), 321-326.

Efron, B. (1979), Bootstrap methods: another look at the jackknife, *The Annals of Statistics*, 1-26.

Fechner-Levy, E. J., and H. F. Hemond (1996), Trapped methane volume and potential effects on methane ebullition in a northern peatland, *Limnology and Oceanography*, *41*(7), 1375-1383.

Fechner, E. J., and H. F. Hemond (1992), Methane transport and oxidation in the unsaturated zone of a *Sphagnum* peatland, *Global Biogeochemical Cycles*, *6*(1), 33-44.

Forster, P., V. Ramaswamy, P. Artaxo, T. Berntsen, R. Betts, D. W. Fahey, J. Haywood, J. Lean, D. C. Lowe, G. Myhre, J. Nganga, R. Prinn, G. Raga, M. Schulz, and R. Van Dorland (2007), Changes in atmospheric constituents and in radiative forcing., in *Climate Change 2007: The Physical Science Basis. Contribution of Working Group I to the Fourth Assessment Report of the Intergovernmental Panel on Climate Change* edited by S. Solomon, et al., Cambridge University Press, Cambridge and New York.

Frenzel, P., and J. Rudolph (1998), Methane emission from a wetland plant: the role of CH_4 oxidation in *Eriophorum*, *Plant and Soil*, *202*(1), 27-32.

Frenzel, P., and E. Karofeld (2000), CH_4 emission from a hollow-ridge complex in a raised bog: The role of CH_4 production and oxidation, *Biogeochemistry*, *51*(1), 91-112.

Frisch, U., B. Hasslacher, and Y. Pomeau (1986), Lattice-gas automata for the Navier-Stokes equation, *Physical Review Letters*, *56*(14), 1505-1508.

Frolking, S., and N. T. Roulet (2007), Holocene radiative forcing impact of northern peatland carbon accumulation and methane emissions, *Global Change Biology*, *13*(5), 1079-1088.

Gedney, N., P. M. Cox, and C. Huntingford (2004), Climate feedback from wetland methane emissions, *Geophysical Research Letters*, *31*(20).

Geiger, S., K. S. Schmid, and Y. Zaretskiy (2012), Mathematical analysis and numerical simulation of multi-phase multi-component flow in heterogeneous porous media, *Current Opinion in Colloid & Interface Science*, *17*(3), 147-155.

Glaser, P. H., J. P. Chanton, P. Morin, D. O. Rosenberry, D. I. Siegel, O. Ruud, L. I. Chasar, and A. S. Reeve (2004), Surface deformations as indicators of deep ebullition fluxes in a large northern peatland, *Global Biogeochemical Cycles*, *18*(1), GB1003.

Gonzalez, R., and R. Woods (1992), *Digital Image Processing*, Addison Wesley.

Gonzalez, R. C., and R. E. Woods (2011), *Digital Image Processing*, Pearson Education.

Goodrich, J. P., R. K. Varner, S. Frolking, B. N. Duncan, and P. M. Crill (2011), High-frequency measurements of methane ebullition over a growing season at a temperate peatland site, *Geophysical Research Letters*, *38*(7), L07404.

Gorham, E. (1991), Northern peatlands: Role in the carbon cycle and probable responses to climatic warming, *Ecological Applications*, *1*(2), 182-195.

Green, S. M., and A. J. Baird (2011), A mesocosm study of the role of the sedge *Eriophorum angustifolium* in the efflux of methane-including that due to episodic ebullition-from peatlands, *Plant and Soil*, *351*(1-2), 207-218.

Green, S. M., and A. J. Baird (2013), The importance of episodic ebullition methane losses from three peatland microhabitats: a controlled-environment study, *European Journal of Soil Science*, *64*(1), 27-36.

Grimm, V., K. Frank, F. Jeltsch, R. Brandl, J. Uchmanski, and C. Wissel (1996), Pattern-oriented modelling in population ecology, *Science of the Total Environment*, *183*(1), 151-166.

Grimm, V., E. Revilla, U. Berger, F. Jeltsch, W. M. Mooij, S. F. Railsback, H. H. Thulke, J. Weiner, T. Wiegand, and D. L. DeAngelis (2005), Pattern-oriented modeling of agent-based complex systems: Lessons from ecology, *Science*, *310*(5750), 987-991.

Haberman, W., and R. Morton (1953), An experimental investigation of the drag and shape of air bubbles rising in various liquids, DTIC Document.

Heimann, M. (2010), How stable is the methane cycle?, *Science*, *327*(5970), 1211-1212.

Helmig, R., B. Flemisch, M. Wolff, A. Ebigbo, and H. Class (2013), Model coupling for multiphase flow in porous media, *Advances in Water Resources*, *51*(0), 52-66.

Hirt, C. W., and B. D. Nichols (1981), Volume of fluid (VOF) method for the dynamics of free boundaries, *Journal of Computational Physics*, *39*(1), 201-225.

Hoang, D. A., V. Steijn van, L. M. Portela, M. T. Kreutzer, and C. R. Kleijn (2013), Benchmark numerical simulations of segmented two-phase flows in microchannels using the Volume of Fluid method, *Computers & Fluids*, *86*(5), 28-36.

Inamuro, T., and T. Ogata (2004), A lattice kinetic scheme for bubble flows, *Philosophical Transactions: Mathematical, Physical and Engineering Sciences*, *362*(1821), 1735-1743.

Inamuro, T., T. Ogata, S. Tajima, and N. Konishi (2004), A lattice Boltzmann method for incompressible two-phase flows with large density differences, *Journal of Computational Physics*, *198*(2), 628-644.

Isaksen, I. S. A., M. Gauss, G. Myhre, K. M. W. Anthony, and C. Ruppel (2011), Strong atmospheric chemistry feedback to climate warming from Arctic methane emissions, *Global Biogeochemical Cycles*, *25*.

Ito, A., and M. Inatomi (2012), Use of a process-based model for assessing the methane budgets of global terrestrial ecosystems and evaluation of uncertainty, *Biogeosciences*, *9*(2), 759-773.

Ito, K., and M. Matsuzaki (1990), Earthquakes as a self-organized critical phenomena, *Journal of Geophysical Research-Solid Earth and Planets*, *95*(B5), 6853-6860.

Jerolmack, D. J., and C. Paola (2010), Shredding of environmental signals by sediment transport, *Geophysical Research Letters*, *37*(19), L19401.

Ji, W., A. Dahmani, D. P. Ahlfeld, J. D. Lin, and E. Hill (1993), Laboratory study of air sparging: Air flow visualization, *Ground Water Monitoring & Remediation*, *13*(4), 115-126.

Joabsson, A., T. R. Christensen, and B. Wallen (1999), Vascular plant controls on methane emissions from northern peatforming wetlands, *Trends in Ecology & Evolution*, *14*(10), 385-388.

Jobbagy, E. G., and R. B. Jackson (2000), The vertical distribution of soil organic carbon and its relation to climate and vegetation, *Ecological Applications*, *10*(2), 423-436.

Judd, A. G. (2004), Natural seabed gas seeps as sources of atmospheric methane, *Environmental Geology*, *46*(8), 988-996.

Kellner, E., A. J. Baird, M. Oosterwoud, K. Harrison, and J. M. Waddington (2006), Effect of temperature and atmospheric pressure on methane ebullition from near-surface peats, *Geophysical Research Letters*, *33*(18).

Kettridge, N., and A. Binley (2008), X-ray computed tomography of pent soils: Measuring gas content and peat structure, *Hydrological Processes*, *22*(25), 4827-4837.

Kettridge, N., and A. Binley (2011), Characterization of peat structure using X-ray computed tomography and its control on the ebullition of biogenic gas bubbles, *Journal of Geophysical Research*, *116*(G1), G01024.

Kettridge, N., A. Binley, S. M. Green, and A. J. Baird (2011), Ebullition events monitored from northern peatlands using electrical imaging, *Journal of Geophysical Research: Biogeosciences*, *116*(G4), G04004.

Kirk, D. B., and W.-m. W. Hwu (2010), *Programming Massively Parallel Processors: A Hands-on Approach*, 280 pp., Morgan Kaufmann Publishers Inc.

Kong, X.-Z., W. Kinzelbach, and F. Stauffer (2010), Morphodynamics during air injection into water-saturated movable spherical granulates, *Chemical Engineering Science*, *65*(16), 4652-4660.

Lai, D. (2009), Modelling the effects of climate change on methane emission from a northern ombrotrophic bog in Canada, *Environmental Geology*, *58*(6), 1197-1206.

Laine, A., D. Wilson, G. Kiely, and K. A. Byrne (2007), Methane flux dynamics in an Irish lowland blanket bog, *Plant and Soil*, *299*(1-2), 181-193.

Liu, Z., J. Xu, and K. Shi (2013), Self-organized criticality of climate change, *Theoretical and Applied Climatology*, 1-7.

Ludington, W. B., K. A. Wemmer, K. F. Lechtreck, G. B. Witman, and W. F. Marshall (2013), Avalanche-like behavior in ciliary import, *Proceedings of the National Academy of Sciences*, *110*(10), 3925-3930.

MacDonald, G. M., D. W. Beilman, K. V. Kremenetski, Y. Sheng, L. C. Smith, and A. A. Velichko (2006), Rapid early development of circumarctic peatlands and atmospheric CH_4 and CO_2 variations, *Science*, *314*(5797), 285-288.

Matthews, E., and I. Y. Fung (1987), Methane emission from natural wetlands global distribution, area, and environmental characteristics of sources, *Global Biogeochemical Cycles*, *1*(1), 61-86.

McCray, J. E., and R. W. Falta (1997), Numerical simulation of air sparging for remediation of NAPL contamination, *Ground Water*, *35*(1), 99-110.

Meakin, P., and A. M. Tartakovsky (2009), Modeling and simulation of pore-scale multiphase fluid flow and reactive transport in fractured and porous media, *Reviews of Geophysics*, *47*(3), RG3002.

Meier, J. A., J. S. Jewell, C. E. Brennen, and J. Imberger (2011), Bubbles emerging from a submerged granular bed, *Journal of Fluid Mechanics*, *666*, 189-203.

Moore, T. R., and N. T. Roulet (1993), Methane flux: Water table relations in northern wetlands, *Geophysical Research Letters*, *20*(7), 587-590.

Moore, T. R., J. L. Bubier, and L. Bledzki (2007), Litter decomposition in temperate peatland ecosystems: the effect of substrate and site, *Ecosystems*, *10*(6), 949-963.

Morris, P. J., J. M. Waddington, B. W. Benscoter, and M. R. Turetsky (2011), Conceptual frameworks in peatland ecohydrology: Looking beyond the two-layered (acrotelm-catotelm) model, *Ecohydrology*, *4*(1), 1-11.

Mulligan, M., and J. Wainwright (2013), Modelling and Model Building, in *Environmental Modelling*, edited by J. Wainwright and M. Mulligan, pp. 7-26, John Wiley & Sons, Ltd.

Mumford, K. G., J. E. Smith, and S. E. Dickson (2010), The effect of spontaneous gas expansion and mobilization on the aqueous-phase concentrations above a dense non-aqueous phase liquid pool, *Advances in Water Resources*, *33*(4), 504-513.

Oldenburg, C. M., and J. L. Lewicki (2006), On leakage and seepage of CO_2 from geologic storage sites into surface water, *Environmental Geology*, *50*(5), 691-705.

Paczuski, M., S. Maslov, and P. Bak (1996), Avalanche dynamics in evolution, growth, and depinning models, *Physical Review E*, *53*(1), 414-443.

Panikov, N. S., M. A. Mastepanov, and T. R. Christensen (2007), Membrane probe array: Technique development and observation of CO_2 and CH_4 diurnal oscillations in peat profile, *Soil Biology & Biochemistry*, *39*(7), 1712-1723.

Parsekian, A. D., X. Comas, L. Slater, and P. H. Glaser (2011), Geophysical evidence for the lateral distribution of free phase gas at the peat basin scale in a large northern peatland, *Journal of Geophysical Research: Biogeosciences*, *116*(G3), G03008.

Parsekian, A. D., L. Slater, and D. Gimenez (2012), Application of ground-penetrating radar to measure near-saturation soil water content in peat soils, *Water Resources Research*, *48*.

Pelletier, L., T. R. Moore, N. T. Roulet, M. Garneau, and V. Beaulieu-Audy (2007), Methane fluxes from three peatlands in the La Grande Riviere watershed, James Bay lowland, Canada, *Journal of Geophysical Research-Biogeosciences*, *112*(G1).

Petit, J. R., J. Jouzel, D. Raynaud, N. I. Barkov, J. M. Barnola, I. Basile, M. Bender, J. Chappellaz, M. Davis, G. Delaygue, M. Delmotte, V. M. Kotlyakov, M. Legrand, V. Y. Lipenkov, C. Lorius, L. Pepin, C. Ritz, E. Saltzman, and M. Stievenard (1999), Climate and atmospheric history of the past 420,000 years from the Vostok ice core, Antarctica, *Nature*, *399*(6735), 429-436.

Quinton, W. L., D. M. Gray, and P. Marsh (2000), Subsurface drainage from hummock-covered hillslopes in the Arctic tundra, *Journal of Hydrology*, *237*(1-2), 113-125.

Quinton, W. L., M. Hayashi, and S. K. Carey (2008), Peat hydraulic conductivity in cold regions and its relation to pore size and geometry, *Hydrological Processes*, *22*(15), 2829-2837.

Quinton, W. L., T. Elliot, J. S. Price, F. Rezanezhad, and R. Heck (2009), Measuring physical and hydraulic properties of peat from X-ray tomography, *Geoderma*, *153*(1-2), 269-277.

Rezanezhad, F., W. L. Quinton, J. S. Price, D. Elrick, T. R. Elliot, and R. J. Heck (2009), Examining the effect of pore size distribution and shape on flow through unsaturated peat using 3-D computed tomography, *Hydrology and Earth System Sciences*, *13*(10), 1993-2002.

Rezanezhad, F., W. L. Quinton, J. S. Price, T. R. Elliot, D. Elrick, and K. R. Shook (2010), Influence of pore size and geometry on peat unsaturated hydraulic conductivity computed from 3D computed tomography image analysis, *Hydrological Processes*, *24*(21), 2983-2994.

Rhodes, M. E., B. Bijeljic, and M. J. Blunt (2008), Pore-to-field simulation of single-phase transport using continuous time random walks, *Advances in Water Resources*, *31*(12), 1527-1539.

Roosevelt, S. E., and M. Y. Corapcioglu (1998), Air bubble migration in a granular porous medium: Experimental studies, *Water Resources Research*, *34*(5), 1131-1142.

Rosenberry, D. O., P. H. Glaser, D. I. Siegel, and E. P. Weeks (2003), Use of hydraulic head to estimate volumetric gas content and ebullition flux in northern peatlands, *Water Resources Research*, *39*(3).

Rosenberry, D. O., P. H. Glaser, and D. I. Siegel (2006), The hydrology of northern peatlands as affected by biogenic gas: current developments and research needs, *Hydrological Processes*, *20*(17), 3601-3610.

Rothman, D. H., and S. Zaleski (2004), *Lattice-gas cellular automata: Simple models of complex hydrodynamics*, Cambridge University Press.

Roulet, N. T., R. Ash, W. Quinton, and T. Moore (1993), Methane flux from drained northern peatlands: Effect of a persistent water table lowering on flux, *Global Biogeochemical Cycles*, *7*(4), 749-769.

Roulet, N. T., P. M. Lafleur, P. J. H. Richard, T. R. Moore, E. R. Humphreys, and J. Bubier (2007), Contemporary carbon balance and late Holocene carbon accumulation in a northern peatland, *Global Change Biology*, *13*(2), 397-411.

Rydin, H., and J. Jeglum (2006), *The biology of peatlands*, Oxford University Press, New York.

Schneider, C. A., W. S. Rasband, and K. W. Eliceiri (2012), NIH Image to ImageJ: 25 years of image analysis, *Nature Methods*, *9*(7), 671-675.

Shakhova, N., I. Semiletov, A. Salyuk, V. Yusupov, D. Kosmach, and Ö. Gustafsson (2010), Extensive methane venting to the atmosphere from sediments of the east Siberian Arctic shelf, *Science*, *327*(5970), 1246-1250.

Shannon, R. D., J. R. White, J. E. Lawson, and B. S. Gilmour (1996), Methane efflux from emergent vegetation in peatlands, *Journal of Ecology*, *84*(2), 239-246.

Shi, K., and C.-Q. Liu (2009), Self-organized criticality of air pollution, *Atmospheric Environment*, *43*(21), 3301-3304.

Shurpali, N. J., S. B. Verma, R. J. Clement, and D. P. Billesbach (1993), Seasonal distribution of methane flux in a Minnesota peatland measured by eddy-correlation, *Journal of Geophysical Research-Atmospheres*, *98*(D11), 20649-20655.

Smith, L. C., G. M. MacDonald, A. A. Velichko, D. W. Beilman, O. K. Borisova, K. E. Frey, K. V. Kremenetski, and Y. Sheng (2004), Siberian peatlands a net carbon sink and global methane source since the early Holocene, *Science*, *303*(5656), 353-356.

Sohrabi, M., A. Danesh, D. Tehrani, and M. Jamiolahmady (2008), Microscopic mechanisms of oil recovery by near-miscible gas injection, *Transport in Porous Media*, *72*(3), 351-367.

Sokal, R. R., and F. J. Rohlf (1995), *Biometry*, W. H. Freeman, New York.

Stamp, I., A. J. Baird, and C. M. Heppell (2013), The importance of ebullition as a mechanism of methane (CH_4) loss to the atmosphere in northern peatlands, *Geophysical Research Letters*, *40*(10), 2087-2090.

Strack, M., E. Kellner, and J. M. Waddington (2005), Dynamics of biogenic gas bubbles in peat and their effects on peatland biogeochemistry, *Global Biogeochemical Cycles*, *19*(1).

Strack, M., E. Kellner, and J. M. Waddington (2006), Effect of entrapped gas on peatland surface level fluctuations, *Hydrological Processes*, *20*(17), 3611-3622.

Strack, M., and J. M. Waddington (2007), Response of peatland carbon dioxide and methane fluxes to a water table drawdown experiment, *Global Biogeochemical Cycles*, *21*(1).

Strack, M., and J. M. Waddington (2008), Spatiotemporal variability in peatland subsurface methane dynamics, *Journal of Geophysical Research*, *113*(G2), G02010.

Strack, M., J. M. Waddington, M. Turetsky, N. T. Roulet, and K. A. Byrne (2008), Peatlands and climate change, in *Northern peatlands, greenhouse gas exchange and climate change.*, edited by M. Strack, International Peat Society, Jyväskylä.

Strack, M., and T. Mierau (2010), Evaluating spatial variability of free-phase gas in peat using ground-penetrating radar and direct measurement, *Journal of Geophysical Research: Biogeosciences*, *115*(G2).

Sundh, I., M. Nilsson, G. Granberg, and B. H. Svensson (1994), Depth distribution of microbial production and oxidation of methane in northern boreal peatlands, *Microbial Ecology*, *27*(3), 253-265.

Sussman, M., P. Smereka, and S. Osher (1994), *A level set approach for computing solutions to incompressible two-phase flow*, Department of Mathematics, University of California, Los Angeles.

Thomson, D. J. (1982), Spectrum estimation and harmonic-analysis, *Proceedings of the Institute of Electrical and Electronics Engineers*, *70*(9), 1055-1096.

Thomson, D. J. (1990), Time-series analysis of Holocene climate data, *Philosophical Transactions of the Royal Society A -Mathematical Physical and Engineering Sciences*, *330*(1615), 601-616.

Thomson, N., and R. Johnson (2000), Air distribution during in situ air sparging: an overview of mathematical modeling, *Journal of Hazardous Materials*, *72*(2), 265-282.

Tokida, T., T. Miyazaki, and M. Mizoguchi (2005a), Ebullition of methane from peat with falling atmospheric pressure, *Geophysical Research Letters*, *32*(13).

Tokida, T., T. Miyazaki, M. Mizoguchi, and K. Seki (2005b), In situ accumulation of methane bubbles in a natural wetland soil, *European Journal of Soil Science*, *56*(3), 389-396.

Tokida, T., T. Miyazaki, M. Mizoguchi, O. Nagata, F. Takakai, A. Kagemoto, and R. Hatano (2007), Falling atmospheric pressure as a trigger for methane ebullition from peatland, *Global Biogeochemical Cycles*, *21*(2).

Tokida, T., T. Miyazaki, and M. Mizoguchi (2009), Physical controls on ebullition losses of methane from peatlands, in *Carbon Cycling in Northern Peatlands*, edited by A. J. Baird, et al., pp. 219-228, American Geophysical Union, Washington D. C.

Torn, M. S., and J. Harte (2006), Missing feedbacks, asymmetric uncertainties, and the underestimation of future warming, *Geophysical Research Letters*, *33*(10).

Turcotte, D. L. (2001), Self-organized criticality: Does it have anything to do with criticality and is it useful?, *Nonlinear Processes in Geophysics*, *8*(4-5), 193-196.

Unverdi, S. O., and G. t. Tryggvason (1992), A front-tracking method for viscous, incompressible, multi-fluid flows, *Journal of Computational Physics*, *100*(1), 25-37.

Valentine, D. W., E. A. Holland, and D. S. Schimel (1994), Ecosystem and physiological controls over methane production in northern wetlands, *Journal of Geophysical Research-Atmospheres*, *99*(D1), 1563-1571.

Waddington, J. M., N. T. Roulet, and R. V. Swanson (1996), Water table control of methane emission enhancement by vascular plants in boreal peatlands, *Journal of Geophysical Research-Atmospheres*, *101*(D17), 22775-22785.

Waddington, J. M., K. Harrison, E. Kellner, and A. J. Baird (2009), Effect of atmospheric pressure and temperature on entrapped gas content in peat, *Hydrological Processes*, *23*(20), 2970-2980.

Walter, B. P., M. Heimann, R. D. Shannon, and J. R. White (1996), A process-based model to derive methane emissions from natural wetlands, *Geophysical Research Letters*, *23*(25), 3731-3734.

Walter, K. M., S. A. Zimov, J. P. Chanton, D. Verbyla, and F. S. Chapin (2006), Methane bubbling from Siberian thaw lakes as a positive feedback to climate warming, *Nature*, *443*(7107), 71-75.

Whalen, S. C., and W. S. Reeburgh (2000), Methane oxidation, production, and emission at contrasting sites in a boreal bog, *Geomicrobiology Journal*, *17*(3), 237-251.

Whittington, P. N., and J. S. Price (2006), The effects of water table draw-down (as a surrogate for climate change) on the hydrology of a fen peatland, Canada, *Hydrological Processes*, *20*(17), 3589-3600.

Yang, G. Q., B. Du, and L. S. Fan (2007), Bubble formation and dynamics in gas-liquid-solid fluidization- A review, *Chemical Engineering Science*, *62*(1-2), 2-27.

Yavitt, J., G. Lang, and D. Downey (1988), Potential methane production and methane oxidation rates in peatland ecosystems of the Appalachian mountains United States *,Global Biogeochemical Cycles*, *2*(3), 253-268.

Yavitt, J. B., C. J. Williams, and R. K. Wieder (1997), Production of methane and carbon dioxide in peatland ecosystems across north America: Effects of temperature, aeration, and organic chemistry of pent, *Geomicrobiology Journal*, *14*(4), 299-316.

Yeoh, G. H., and J. Tu (2010), *Computational Techniques for Multi-Phase Flows*, 1-643 pp., Butterworth-Heinemann.

Yu, Z., J. Loisel, D. P. Brosseau, D. W. Beilman, and S. J. Hunt (2010), Global peatland dynamics since the Last Glacial Maximum, *Geophysical Research Letters*, *37*(13), L13402.

Zhao, W., and M. A. Ioannidis (2011), Gas exsolution and flow during supersaturated water injection in porous media: I. Pore network modeling, *Advances in Water Resources*, *34*(1), 2-14.

Zheng, H. W., C. Shu, and Y. T. Chew (2006), A lattice Boltzmann model for multiphase flows with large density ratio, *Journal of Computational Physics*, *218*(1), 353-371.

Zhuang, Q., J. M. Melillo, D. W. Kicklighter, R. G. Prinn, A. D. McGuire, P. A. Steudler, B. S. Felzer, and S. Hu (2004), Methane fluxes between terrestrial ecosystems and the atmosphere at northern high latitudes during the past century: A retrospective analysis with a process-based biogeochemistry model, *Global Biogeochemical Cycles*, *18*(3).